Emanoelle Diz Acosta

BORON MODIFIED SILICON CARBIDE BY PDC ROUTE: DENSE AND POROUS CERAMICS

Florianópolis
2019

Emanoelle Diz Acosta

BORON MODIFIED SILICON CARBIDE BY PDC ROUTE: DENSE AND POROUS CERAMICS

Tese de Doutorado submetida ao Programa de Pós-Graduação em Engenharia Química da Universidade Federal de Santa Catarina, como requisito à obtenção do grau de Doutora em Engenharia Química.
Orientador: Prof. Dr. Ricardo Antonio Francisco Machado
Co-orientador: Dr. Samuel Bernard

Florianópolis
2019

Boron Modified Silicon Carbide by Polymer Derived Ceramic Route: dense and porous ceramics

por
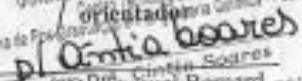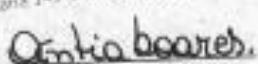
Emanoelle Diz Acosta

Tese julgada para obtenção do título de **Doutor em Engenharia Química**, na área de Concentração de **Desenvolvimento de Processos Químicos e Biotecnológicos** e aprovada em sua forma final pelo Programa de Pós-graduação em Engenharia Química da Universidade Federal de Santa Catarina.
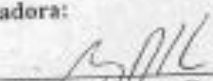
Prof. Dr. Ricardo Antonio Francisco Machado
orientador

Prof. Dr. Samuel Bernard
coorientador

Prof.ª Dr.ª Cintia Soares
coordenadora

Banca Examinadora:

Prof. Dr. Agenor De Noni Junior

Prof.ª Dr.ª Cristiane da Costa

Dr.ª Estela de Oliveira Nunes (videoconferência)

Florianópolis, 27 de março de 2019.

À Olivia Schlichting, tia Preta, com todo meu amor.

Resumo

O presente trabalho aborda a química e o processamento de precursores, a transformação polímero-cerâmica e a evolução microestrutural da cerâmica a altas temperaturas. Assim como, o design de peças cerâmicas densas e porosas e sua caracterização. Essas cerâmicas foram produzidas pela transformação térmica de precursores específicos para tal aplicação, os quais foram sintetizados pela modificação química do polímero précerâmico AHPCS (allylhydridopolycarbosilane) com o dimetilsulfeto de boro (BDMS). Esta modificação química foi investigada em detalhes por RMN de estado sólido, FTIR e análises elementares. As ligações entre o boro e os grupos do AHPCS atuaram como unidades de reticulação, estendendo a faixa de processabilidade do AHPCS e suprimindo a destilação de fragmentos oligoméricos durante o regime de pirólise. Este conhecimento serviu para otimizar o processamento do precursor cerâmico para produzir peças cerâmicas densas e porosas de carbeto de sílicio por prensagem a quente. Cerâmica densa com dureza de 26,73 GPa e densidade de 2,45 g.cm^{-3} foi obtida a 1000 ^{o}C. As cerâmicas macroporosas (espumas) foram produzidas com a decomposição por tratamento térmico do agente sacrificial PMMA (funcionalizado com prata) de aproximadamente 25 μm e 350 nm, resultando em uma estrutura com poros bastante interconectados. A espuma produzida com PMMA comercial ($\sim$ 25μm) foi eficientemente funcionalizada com uma camada mesoporosa. Esta camada mesoporosa foi elaborada utilizando solução de AHPCS e copolímero em bloco (BCP), este último como agente direcionador de estrutura. Os BCPs em cerâmica porosa não-óxida permitem a construção de materiais nanoestruturados, através de métodos mais acessíveis, quando comparados, por exemplo, a *nanocasting*. A nanoestrutura e a microestrutura das cerâmicas finais à base de SiC estão intimamente ligadas ao teor de boro dos polímeros de partida. Além disso, demonstrouse que a incorporação do boro tem efeito positivo sobre a densificação do SiC, o que pode ser observado em todos os processos deste trabalho, que inclui também a aplicação da técnica de

Rapid Hot Pressing (RHP), onde pós cerâmicos amorfos foram sinterizados, resultando em cerâmicas densas e isentas de trincas, com densidade de aproximadamente 2,86 g.cm^{-3} e condutividade elétrica de 3.096,25 S.m^{-1} para amostras tratadas em argônio a 1800 ^{o}C.

Palavras-chave: Cerâmicas Derivadas de Polímero, AHPCS hidroborado, Cerâmicas Porosas e Densas.

Resumo expandido

Introdução

A história de compostos de carbeto de silício (SiC) começou
há mais de um século com a síntese desenvolvida por Edward
Goodrich Acheson. As propriedades apresentadas por cerâmicas
covalentes, como o carbeto de silício, qualificam-nas para apli-
cações nas quais são necessárias alta resistência mecânica, ao
desgaste e à oxidação, além de significativa estabilidade térmica
e química. Após a descoberta inicial, várias abordagens alternati-
vas para o processamento de SiC foram realizadas com benefícios
e limitações específicas em cada caso, dado que o processamento
cerâmico convencional nem sempre fornece a pureza adequada
e características morfológicas que as aplicações de "alto nível"
requerem. Um processo alternativo para obter cerâmicas é a for-
mação de materiais a partir de precursores inorgânicos pela rota
PDC (Cerâmica Derivada de Polímero). Este método ganhou
muito destaque nas últimas quatro décadas devido ao seu grande
potencial para a produção de materiais de alto desempenho com
composição, forma e porosidade controladas. A rota PDC tem
várias vantagens, tais como: a capacidade de alterar a estru-
tura molecular do material de partida (polímero pré-cerâmico);
potencial para moldar o material em filmes/camadas, pós, es-
pumas, fibras, etc., para uso em diferentes aplicações; controle
sob a porosidade, entre outras especificações. Pode-se dizer que
as propriedades químicas e físicas do PDC podem ser adaptadas
pelo *design* adequado do precursor molecular inicial. Estes pre-
cursores são convertidos em materiais cerâmicos amorfos cova-
lentes a temperaturas inferiores a 1000 ^{o}C. Durante a pirólise,
entretanto, há significativa retração, perda de peso, formação
de porosidade e fragmentação do material, que são obstáculos
consideráveis à produção de peças cerâmicas derivadas de SiC,
obtidas através do polímero pré-cerâmico. Portanto, uma al-
ternativa para controlar as modificações estruturais desses pre-
cursores é o aprimoramento químico do precursor inorgânico.
A modificação química adequada do precursor leva à formação
de precursores de fonte única (SSPs). Estas abordagens quími-

cas baseadas em SSPs oferecem controle sobre as composições químicas, microestrutura, temperatura de processamento e maior versatilidade em termos de processabilidade (SCHMIDT et al., 2017). Neste trabalho, Allylhydridopolycarbosilane (AHPCS) (nome comercial SMP-10) foi usado como precursor químico, aprimorado com um precursor de boro (Borane Dimethy Sulfide - BDMS), para produzir cerâmica Si(B)C. A adição de boro foi realizada para promover a densificação, com o objetivo de reduzir a retração volumétrica, melhorar a processabilidade e aumentar o rendimento da cerâmica, dado o seu potencial para aumentar o grau de reticulação do precursor cerâmico. O principal objetivo deste trabalho foi demonstrar a viabilidade da rota PDC, a partir da modificação do precursor cerâmico com boro para a preparação de estruturas densas e porosas. O processamento termoplástico direcionou o trabalho, com o uso de poliborocarbossilano selecionado (SMP-10 modificado com BMDS) e sua conversão por prensagem a quente e posterior pirólise. Embora o potencial do processamento termoplástico e subsequente pirólise de polímeros pré-cerâmicos para a produção de cerâmicas amorfas e nanoestruturadas seja bem reconhecido, a abordagem é frequentemente associada à alta porosidade em cerâmica, tornando este método ineficaz em cerâmicas densas. Uma alternativa a esse método foi o uso da técnica de Rapid Hot Pressing (RHP) para produzir peças cerâmicas 3D de SiC com baixa porosidade residual (densa). O objetivo da aplicação do RHP foi verificar as propriedades mecânicas, propriedades térmicas e elétricas do AHPCS hidroborado, permitindo novos desafios, principalmente com a aplicação de um pré-tratamento com gás amônia do precursor cerâmico utilizado neste trabalho. Além disso, materiais de alta porosidade (espumas) foram elaborados e discutidos, como outro assunto central deste trabalho. As espumas cerâmicas apresentam um elevado número de poros interconectados, o que resulta em baixa densidade, alta resistência térmica, alta área específica, baixa condutividade térmica e alta permeabilidade a fluidos (MOREIRA; INNOCENTINI; COURY, 2004; SHE; OHJI; DENG, 2002; ORTEGA et al., 2003; SALAZAR et al., 2006). Esses materiais porosos foram obtidos pela incorporação

de microesferas de PMMA como agente de sacrifício, sintetizado e funcionalizado com prata. Bem como, foram realizadas estratégias para produzir material mesoporoso usando copolímeros em bloco (BCPs) de estireno e butadieno (SBS) como materiais direcionadores de porosidade. Os polímeros orgânicos usados como material material de sacrifício permitem poros uniformemente distribuídos em várias escalas, obtendo então um produto com características ótimas para alguns tipos de cerâmicas, tais como: membranas de separação, biomateriais, materiais catalíticos, materiais estruturais leves, filtros de alto desempenho para tratamento de água e resíduos, entre outros. Assim, o bom desempenho pode ser aliado ao baixo custo desses materiais criadores de porosidade, como no caso do PMMA utilizado neste trabalho, com inúmeras possibilidades de funcionalização, como exemplo da prata, que apresenta forte ação bactericida.

Objetivos

Este trabalho tem como objetivo principal a obtenção e caracterização de materiais cerâmicos Si(B)C, a partir de precursores cerâmicos. Os objetivos específicos foram: (a) modificação da estrutura molecular do precursor AHPCS (SMP-10) com a adição de boro, afim de melhorar características relativas ao processamento do polímero e sua conversão em cerâmica;(b) obtenção de cerâmica densa, utilizando rota PDC, partindo precursor cerâmico hidroborado e sua caracterização; (c) produção de estruturas densas, pelo método de *Rapid Hot Pressing* (RHP), partindo do AHPCS hidroborado e estudo das suas características térmicas, elétricas e da densidade; (d) avaliar a contribuição da pré-pirolise em amônia durante a termólise do precursor cerâmico; (e) sintetizar agente de sacrifício PMMA de tamanhos específicos, utilizando atécnicas de polimerização em emulsão e funcionalizá-los com prata nanométrica; (f) elaborar composições de PMMA/ AHPCS hidroborado, a fim de produzir por prensagem a quente peças de Si-(B)-C, com porosidade aberta e interconectada e caracterizar este material; (g) avaliar o comportamento dos copolímeros em bloco em mistura com AHPCS hidroborado e sua aplicação para produção de camada mesoporosa.

Metodologia

Para a realização deste trabalho foi produzido, na primeira etapa (1), o precursor cerâmico modificado com boro (AHPCS hidroborado), com duas diferentes quantidades de boro (PCS_B30 e PCS_B60). Para tanto, todas as sínteses foram realizadas em atmosfera inerte de argônio, com manipulação de reagentes e materiais intermediários em glovebox ou *Schlenk line*. Partindo do precursor hidroborado, foi dada a sequência, na segunda etapa (2), da produção das cerâmicas densas de Si(B)C por duas estratégias diferentes: prensagem a quente (*warm-pressing*) e sinterização rápida (RHP). Na terceira etapa da metodologia (3), foi elaborada cerâmica porosa de Si(B)C, começando com a síntese do agente de sacrifício PMMA, sendo importante apontar que o PMMA foi funcionalizado com nanopartículas de prata (Ag) durante sua síntese. Ainda, na etapa (3), destaca-se a metodologia utilizada para funcionalização das estruturas cerâmicas porosas obtidas por prensagem a quente com coatings mesoporosos (utilizando copolímero em bloco pelo método *templating*). Como última abordagem (4), outras estratégias foram utilizadas para a produção de pós cerâmicos através de aditivos (peróxido de dicumila e benzoato de prata).

Resultados e Discussão

O objetivo de inserir grupos reativos foi de reduzir a temperatura de reticulação, tornando o processamento do polímero em cerâmica mais viável, este resultado pôde ser atingido com a adição molecular de boro. Além disso, o boro aumenta o rendimento cerâmico e permite a obtenção de β-SiC em temperaturas superiores a 1200 ^{o}C. Na presença de gás de amônia, notou-se a possível formação de bandas de infravermelho (FTIR) em relação às cerâmicas de Si(B)CN. Entretanto, mais análises são necessárias para confirmar os efeitos do gás amônia na estrutura formada com tratamento intermediário, bem como na estrutura final. A metodologia RHP mostrou-se viável para produzir, em curtos períodos (15 min em 1750 ou 1800 ^{o}C), materiais de alta condutividade elétrica. O SiC poroso derivado de PCS_B30 foi reproduzido sem iniciação crítica de rachaduras. Este resul-

tado somente foi atingido, quando o polímero pré-cerâmico foi suficientemente comprimido com o PMMA bem distribuído, formando uma estrutura pré-pirolise resistente. A estrutura porosa contribui para uma emissão de gases de forma mais eficiente e uma redução de volume uniforme durante a pirólise do polímero, reduzindo a pressão interna e o estresse térmico, evitando as rachaduras. Também é relevante destacar a presença de prata na cerâmica porosa com PMMA funcionalizado, confirmada por HRTEM.

Considerações Finais

Este trabalho de pesquisa possibilitou a elaboração de estruturas densas e porosas. No caso das estruturas porosas contendo prata, torna-se necessário estudar o comportamento dos agentes sacrificiais funcionalizados e do material cerâmico, para que seja possível avaliar o efeito da prata nanométrica como agente bactericida e seu impacto ambiental. Os tratamentos térmicos em amônia aplicando altas temperaturas, servem de grande incentivo para estudos futuros, dada a inovação técnica frente às publicações existentes. Além disso, outros métodos podem ser desenvolvidos no futuro, visando a melhoria das estruturas 3D obtidas neste trabalho, a fim de adaptar a técnica para grandes escalas, visto os resultados promissores quanto às propriedades mecânicas e elétricas.

Palavras-chave: Cerâmicas Derivadas de Polímero, AHPCS hidroborado, Cerâmicas Porosas e Densas.

Abstract

The present work addresses the precursor chemistry and processing, the polymer-to-ceramic transformation and the ceramic microstructural evolution at high temperatures. As well as, the design of 3D dense and porous ceramics pieces and its characterization. These ceramics were produced by the thermal transformation of tailor-made single-source-precursors, which were synthesized by the chemical modification of the preceramic polymer allylhydridopolycarbosilane (AHPCS) with borane dimethylsulfide (BDMS). This chemical modification was investigated in details by solid-state NMR, FTIR and elemental analyses. The bonds between boron and the groups from AHPCS acted as crosslinking units, extending the processability range of AHPCS and suppressing the distillation of oligomeric fragments during the pyrolysis regime. This knowledge served to optimize the processing of the preceramic polymeric precursor to produce dense and porous SiC-based 3D ceramics pieces by warm pressing. Dense 3D ceramic with hardness of 26.73 GPa and density of 2.45 g.cm^{-3} was obtained at 1000 ^{o}C. Macroporous ceramics (foams) were produced with the decomposition by thermal treatment of sacrificial agent PMMA (functionalized with silver) of approximately 25 μm and 350 nm, resulting in a very interconnected structure of pores. The foam produced with commercial PMMA ($\sim$25 μm) was efficiently functionalized with a mesoporous layer. This mesoporous layer was coated on the foam using a solution of AHPCS and block copolymer (BCP) as structure direct agents. The BCP in porous non-oxide ceramics allows for the construction of high temperature nanostructure materials through easier methods, with less steps when compared, for example to nanocasting. The nanostructure and the microstructure of the final SiC-based ceramics are intimately linked to the boron content of the polymers. Moreover, it was shown that the incorporation of boron has a positive effect on the densification behavior of SiC, which can be observed in all the processes of this work, which also includes the application of the Rapid Hot Pressing (RHP) technique, where the amorphous ceramic pow-

ders were sintered, resulting in dense, crack-free ceramics, with density of approximately 2.86 g.cm^{-3} and electrical conductivity of 3096.25 S.m^{-1} for samples treated in argon at 1800 ^{o}C.

List of Figures

List of Tables

List of abbreviations

AFM Atomic Force Microscopy

AHPCS Allylhydridopolycarbosilane

BCP Block copolymer

BDMS Borane dimethyl sulfide

EFE Emulsifier-free emulsion polymerization

EGDMA Ethylene glycol dimethacrylate)

FTIR Fourier-transform infrared spectroscopy

F25A Foams produced with PAg25 and PCS_B30

F25 Foams produced with P25 and PCS_B30

F350 Foams produced with PAg350 and PCS_B30

MMA Methyl methacrylate

NMR Nuclear magnetic resonance spectroscopy

PAg25 Silver functionalized PMMA microspheres of 25 μm

PAg350 Silver functionalized PMMA nanospheres of 360 nm

P25 Commercial PMMA of 25 μm

PMMA Poly(methyl methacrylate)

PTFE Poly(tetrafluoroethene)

PVA Poly(vinyl acetate)

RHP Rapid Hot Pressing

SA Sacrificial Agents

SBS Styrene-butadiene-styrene block copolymer

SDA Structure Direct Agents

SiC Silicon Carbide

TGA Thermogravimetric Analysis

XRD X-ray diffraction analysis

Contents

1 Introduction

Covalently bonded compound silicon carbide's (SiC) history started more than a century ago with the synthesis developed by Edward Goodrich Acheson which is still used today. The properties presented by covalent ceramics, such as silicon carbide, qualify them for applications for which high mechanical, wear and oxidation resistance are required, as well as significant thermal and chemical stability.

Following the initial discovery, several alternative approaches for processing SiC have been attempted with specific benefits and limitations in each case, given that the conventional ceramic processing not always provides the adequate purity and morphological characteristics that "high level" applications require.

An alternative process to obtain ceramics is the formation of materials from polymeric precursors through the Polymer Derived Ceramics (PDC) route. This method gained a lot of highlight over the last four decades due to its great potential for the production of high performance materials with controlled composition, shape and porosity. The PDC route has several advantages, such as: the ability to change the molecular structure of the starting material (preceramic polymer); potential to shape the material as films/layers, powders, foams, fibers, etc., to use in different applications; the porosity/pore size can be controlled according to the synthesis and calcination temperature, among other specifications.

It may be said that the chemical and physical properties of PDC may be adapted by the adequate design of the initial molecular precursor. These precursors are converted into covalent amorphous ceramic materials at temperatures below 1000 ^{o}C. During pyrolysis, however, there is significant retraction, weight loss, porosity formation and material fragmentation, which are considerable obstacles to the production of SiC-derived ceramic pieces, obtained through the preceramic polymer.

Therefore, an alternative to control the structural modifications of these precursors is the chemical enhancement of the preceramic precursor. Adequate chemical modification of the preceramic precursor leads to the formation of single-source-precursors (SSPs). These chemical approaches based on SSPs offer control over the chemical compositions, microstructure, processing temperature and greater versatility in terms of processability (SCHMIDT et al., 2017).

In this work, allylhydridopolycarbosilane (AHPCS) (commercial name SMP-10) was used as chemical precursor to produce ceramics, which was chemically enhanced with a boron precursor (Borane Dimethy Sulfide - BDMS) to produce a polyborocarbosilane Si-(B)-C.

The addition of boron has been performed to promote the densification (with the aim to achieve low SiC shrinkage), improved processability and ceramic yield increase, given its potential to increase the crosslinking degree of the preceramic precursor.

The main objective of this work was to demonstrate the feasibility of PDC route, starting from the modification of the ceramic precursor with boron for the preparation of dense 3D structures and foams. It involved the development and optimization of the processing technique to produce dense and porous SiC ceramic pieces. Thermoplastic processing directed the work, with the use of selected polyborocarbosilane (SMP-10 modified with BMDS) and its conversion through warm pressing and posterior pyrolysis.

Although the potential of thermoplastic processing and subsequent pyrolysis of preceramic polymers for the production of amorphous and nanostructured ceramics is well recognized, the approach is often associated with high porosity in ceramics, making this method ineffective for use in high volume ceramics.

An alternative to this method was the use of the rapid hot pressing technique (RHP) to produce 3D ceramic pieces of SiC with very low residual porosity (denses). The goal of the application of RHP was to verify the chemical behavior, mechanical properties, thermal and electrical proprieties of the hydroborated

AHPCS, allowing new challenges, mainly with the application of a pre-heat treatment with gas ammonia of the SSP considered in this work.

Moreover, high porosity materials (foams) were elaborated and discussed, as another central subject of this work. Ceramic foams can be characterized as linked networks of irregularly shaped open or closed cell polyhedrons. There is the possibility that foams can be partly open and partly closed. These porous network structures, present a high number of interconnected pores, which results in low density, high thermal resistance, high specific area, low thermal conductivity and high flow and fluids permeability (MOREIRA; INNOCENTINI; COURY, 2004; SHE; OHJI; DENG, 2002; ORTEGA et al., 2003; SALAZAR et al., 2006).

In this way, insight was obtained on the fabrication of SiC foams, by incorporating sacrificial pore-forming plastic powder, PMMA microbeads, synthesized and functionalized with silver. As well as, a strategy to produce mesoporous material using block copolymers (BCPs), applying styrene and butadiene (SBS) as the sacrificial materials.

The organic polymers used as a sacrificial material allow for uniformly distributed pores on various scales, obtaining then a product with optimal characteristics for the task-specific ceramics, such as: separation membranes, bio-materials, catalytic materials, lightweight structural materials, high performance filters for water and waste treatment, among others.

Thus, the good performance can be allied with the low cost of these materials, which can also be synthesized in laboratory, as in the case of PMMA used in this work, with countless possibilities of functionalization, which in this case was the use of nanometric silver that presents strong bactericide action.

1.1 Objectives

1.1.1 General objective

Study, obtain and characterize Si-(B)-C ceramic materials from single-source precursor.

1.1.2 Specific objectives

- Modificate the molecular structure of the preceramic polymer AHPCS (SMP-10) with the addition of boron, in order to improve characteristics regarding the processing of the polymer and its conversion into ceramics.

- Obtain dense 3D ceramic pieces by PDC route, starting from the hydroborated preceramic polymer (single-source-precursor) and its characterization.

- Produce 3D ceramic dense structures by the Rapid Hot Pressing (RHP) method, starting from the hydroborated AHPCS and studying its thermal/electrical characteristics and variation in densities.

- Evaluate the contribution of ammonia as atmosphere in the low temperature regime of the pyrolysis process.

- Synthesize specific sizes of sacrifical agent PMMA particles functionalized with nanometric silver through emulsion polymerization technique for the production of macroporous ceramics.

- Elaborate PMMA/Hydroborated AHPCS compositions in order to produce by warm pressing 3D porous Si-(B)-C structure, with open and interconnected porosity and to characterize this material.

- Evaluate the behavior of the block copolymers in mixture with hydroborated AHPCS and their application to the mesoporous layer.

2 Literature Review

2.1 Silicon Carbide based Ceramics- an overview

Silicon Carbide (SiC), is a non generic name for an important non-oxide ceramic material which has been intensively investigated over the last decades and produced through several processing routes that result in a series of different micro-structures and hence a wide range of properties.

These properties, such as elevated hardness and strength, chemical and thermal stability, high meting point, resistance to oxidation and erosion (ABDERRAZAK; HMIDA, 2011), lead to vast applicability of SiC in the industry, including the fields of aerospace and aviation, electronics, energy, military, healthcare and others. Examples of these applications can be seen in recent publications, with attempts to increase the scale and increment the productivity and efficiency of its manufacture, with yields of lower weight and volume and increased power and reliability.

Such characteristics are clearly important for applications such as micro-electronics, where circuits, semiconductors, diodes and transistors based on SiC are being developed for high temperature, power and or radiation conditions, which demand for extremely pure materials and a perfect crystal lattice (ZETTER-LING, 2012; ELASSER et al., 2003; KAMINSKI, 2018).

Recent works have been studying SiC for bio applications (ROSENBLOOM et al., 2004; FAN; CHU, 2010; ZEUNER et al., 2018) as it can be light, tough, chemically inert and suitable for biomedical implants and coatings. A combination of excellent mechanical properties and low density renders them good base materials in biomedical devices such as alternative dental and orthopedic implants, bioeletronic devices, etc. (GREIL; LIFKA; KAINDL, 1998; YAKIMOVA et al., 2007).

Among numerous works with the most diverse applications with SiC as initial material, membrane production is of great importance. Several works focus on this material in applications

for water treatment, desalination and gas separation (hydrogen from steam, for example), among other filtration processes such as: nanofiltration, ultrafiltration, microfiltration, reverse osmosis and conventional particle filtration. Figure 1 presents different types of membrane filtration and the particles removed for specific pore sizes (KöNIG et al., 2014; LEE; ELAM; DARLING, 2016; ZSIRAI et al., 2016; SEA et al., 1998).

Figure 1: Schematic illustration of membrane filtration spectrum. The differentiation of the applicability and the type of membrane is mainly made by the average pore diameter of the membranes. The reverse osmosis membranes are so dense that the pores are considered as non-porous.
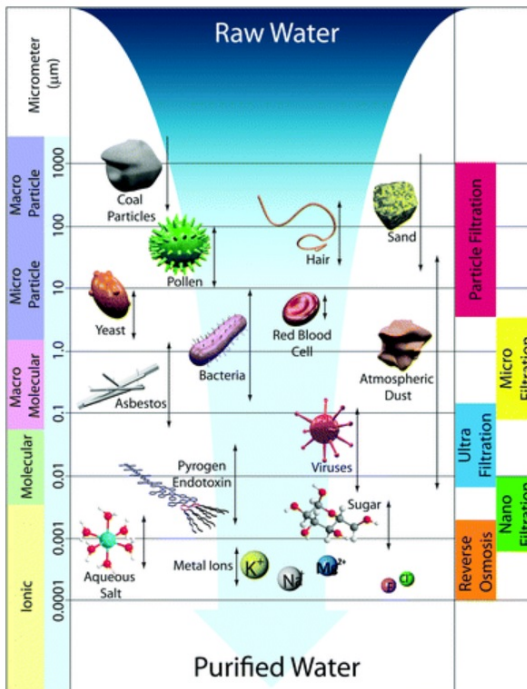
Source: Lee, Elam e Darling (2016).

SiC is frequently used in inorganic membrane production due to its resistance to thermal shock and to acidic and alkaline environments, as well as, being biocompatible (ELYASSI; SAHIMI; TSOTSIS, 2007). Inorganic membranes, and more specifically Silicon Carbide, has an important role for clean and safe water supply. According to Fard et al. (2018), based on the Scopus database, when "inorganic membranes" was used as the keyword, the publications in the application of inorganic membranes for water treatment and desalination increased from less than 21% in 2000 to about 40% in 2016.

The first known method for the fabrication of SiC was the Acheson process, named after its creator, E.G. Acheson, in 1891 and which enabled the commercialization of this compound.

SiC was already known from natural occurrences, as very small amounts can be found in meteorites (which was not suitable for industrial applications), and small quantities had been produced in laboratory scale. Acheson recognized the commercial potential of his method and further developed the "primitive" electric furnace he created for SiC production for industrial applications (GUICHELAAR, 1997; ZETTERLING; ENGINEERS, 2002; SOMIYA; INOMATA, 2012).

The process is performed in an Acheson furnace (Figure 2), when a mixture of the carbon material (usually petroleum coke), silica or quartz sand chemically react in high temperatures between 1700 and 2500 ^{o}C, hence forming α-SiC after the main reaction (carbothermal reduction method resulting in SiC powders).

Figure 2: The Acheson furnace and the crude silicon carbide product.
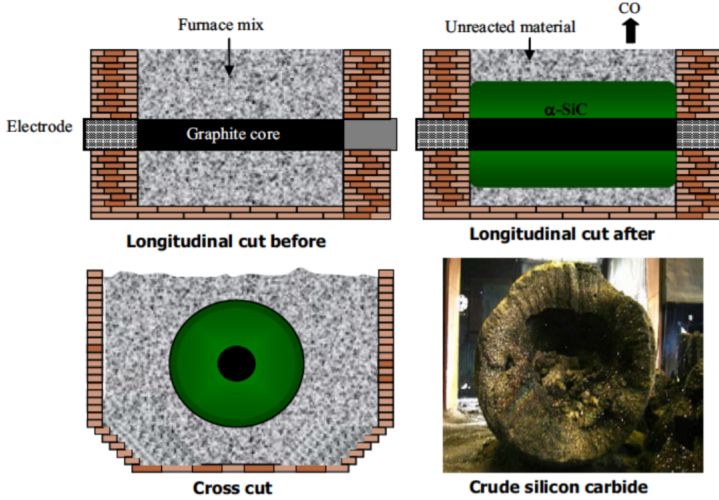
Source: Foreland (2012).

The global reaction of this process is described by the following Formula 2.1:

$$SiO_2(s) + 3C(s) \rightarrow SiC(s) + 2CO(g) \qquad (2.1)$$
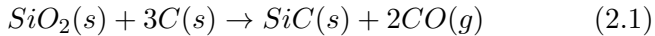
However, the output of this process is not pure. A condensation layer of silicon dioxide and other oxide impurities, non reacted material, firesand and large SiC blocks, which need to be reduced to obtain powder with the appropriate particle size, is found. In addition to this, impurities reduce the quality of the obtained powder. The main challenge of growing large SiC crystals of sufficient quality is the elevated energy expenditure necessary for this synthesis (MAGNANI et al., 2016; DIJEN; METSELAAR, 1991).

An interesting SiC feature is its politipism, which leads to a large number of structural variations for the material composition, affecting its properties (Table 1 presents some SiC

properties). Si and C atoms form a very strong tetrahedral covalent bonds through sharing sp^3 hybrid orbitals, whose structure may be SiC$_4$ or CSi$_4$. Although a great variety of SiC polytypes is known, it has become accepted practice to refer to the cubic polytype as β - SiC, and to all non-cubic structures (hexagonal and rombohedral) collectively as α - Silicon Carbide (IZHEVSKYI et al., 2000).

Table 1: General properties of Silicon Carbide.

SiC Properties	Values
Density	3.21 g/cm^3
Hardness	21-25 GPa (solidade state sintered)
	19-22 GPa (Liquid state sintered)
Thermal conductivity	3.6 W cm^{-1}K^{-1} (β-SiC)
	4.9 W cm^{-1}K^{-1} (α-SiC)
Oxidation resistance	up to 1600 ^{o}C
Dissociation temperature	2850 ^{o}C

Source: Wu et al. (2011), Abderrazak e Hmida (2011).

Nonetheless, it is clear that the fabrication of highly pure stoichiometric SiC is extremely challenging. Hence, for the production of high performance, purity and powder quality SiC ceramic, several alternative synthesis methods have been developed and proposed over the last decades, as it will be shown on Section 2.1.1.

2.1.1   Preparatives methods of SiC

Acheson's method allows for the production of powders with different grades of purity with particle size greater than 5 μm. An alternative, albeit effective, process, is combustion synthesis. This method requires highly exothermic reactions to be self sustainable. Combustion synthesis can happen through two modes: self propagating high temperature (SHS) and volu-

me combustion synthesis (VCS). In both cases, the reagents may
be in the form of a powder mixture or a pressed pellet. These
samples are then heated with an external source, such as laser
irradiation, radiant flux, resistance heating coil, spark and che-
mical oil, locally (for SHS) or uniformly (for VCS) to initiate the
exothermic reaction.

The combustion synthesis yield is, in general, porous, ty-
pically 50% of the theoretical density. Hot pressing, isostatic hot
pressing and shockwaves have been employed to make the pro-
ducts denser (BHADURI; BHADURI, 1999; COMBUSTION...,
2002).

Some characteristics of the SiC particle, such as size, shape
and surface chemistry, are very important for the subsequent den-
sification, which is effectively reached with nanoscale particles. In
general, it is believed that nanoscale SiC powder may allow for
a significant reduction of the pyrolyzing temperature and in the
time taken to produce high density/low porosity ceramic. Such
SiC particles may be obtained through different methods, as, for
example, the sol-gel process, chemical vapor deposition (CVD),
polymer pyrolysis, among other ceramic fabrication techniques
which have been directed to obtain features such as homoge-
neous dispersion of phases, as well as making the ceramic purer
and denser.

Chemical vapor deposition (CVD) involves the deposition
of a solid material on a surface either activated or heated by
reaction with a gaseous phase. In the preparation of SiC powders
by CVD, the main approach is to use chemical reactions between
the silicon source gas (SiC_4, SiH_4, etc.) and the carbon source
gas (CH_4, C_2H_4, etc.) (CHEN; GOTO; HIRAI, 1990). Besides
being used to create ceramic coatings, CVD can also be applied
to produce ceramic powders and monolithic ceramics (GOELA;
TAYLOR, 1988; ZUNJARRAO, 2008).

Naturally, all these techniques have been further developed
and improved with the evolution and necessities of new materials,
as well as, in many cases, they are incorporated to include other
techniques, with the goal of producing advanced high quality
ceramics.

Another very effective process is the pyrolysis of polymeric precursors, where these are converted into amorphous ceramics materials at temperatures below 1000 ^{o}C. Despite the relatively low organic-inorganic transformation temperature, polymer derived ceramic were shown to be stable at high temperatures (RAJ; RIEDEL; SORARU, 2001). The methodology, or route, known as Polymer Derived Ceramic (PDC) route, where, between other intermediate processes, the inorganic precursor is converted into advanced ceramic, will be used as principle of synthesis of this research work, and hence further discussed in Section 2.2.

2.2 Polymer Derived Ceramic (PDC) route

Development of organoelement chemistry has attracted significant attention to pre-ceramic polymers and precursors, which contain Silicon (Si) at its backbone, which after pyrolysis are transformed in ceramic materials. Ceramic obtained from these precursors are known as PDCs (BORCHARDT et al., 2012). The route to obtain PDCs is an effective method to produce advanced ceramics, specially in non oxide systems, with compositional and structural homogeneity (BERNARD; MIELE, 2014b).

The PDCs route is an emerging chemical process as attested by the increasingly commercial development of preceramic polymers to produce near-net shapes in a way not known from other techniques. It is important to highlight that the overall process for fabrication of PDCs involves three major steps: (i) Synthesis of preceramic polymers starting from suitable monomers; (ii) Polymer crosslinking at moderated temperatures (100 to 400 ^{o}C) and (iii) ceramization process (pyrolysis) of the crosslinked polymer which are converted into inorganic materials by heat treatment.

Another important stage, however, may be included for shape ceramics, which may be considered a key factor in utilizing the PDC route over other conventional powder production methods. This is the possibility of using plastic-forming techniques (warm pressing, injection, fiber spinning, etc.). These techniques will generate green bodies which will be transformed

in shaped components to be heat treated at above 800 °C.

Figure 3 presents the simplified scheme of this PDC route. These pathways for high throughput production of ceramics will be further explained in the next items.

Figure 3: General overview of PDC route.
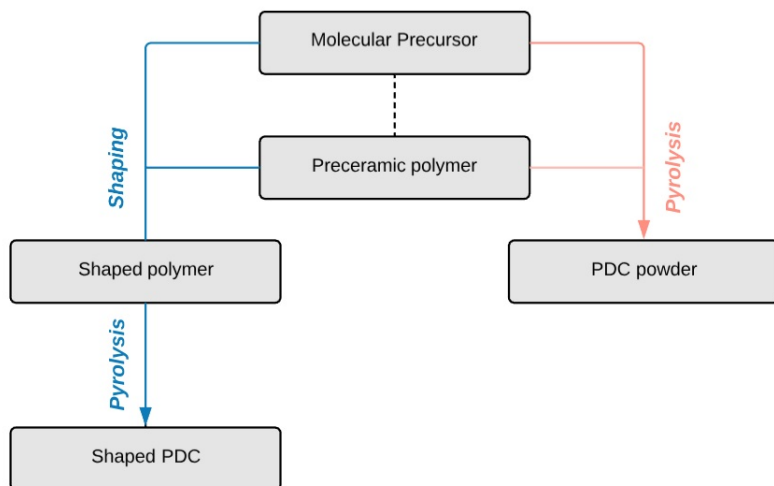
2.2.1   Preceramic polymers: polycarbosilane as SiC precursor

Preceramic polymers were over the last decades subject of ample research and development and are still compounds of high commercial value due to the quality of the ceramics obtained from them. Ceramic precursor research was accelerated by the creation of Nicalon ^{TM} fiber by Yuijima on the 70s, confirming a new method to produce ceramic at significantly low temperatures (800-1500 °C).

Ceramic precursors posses a chemical structure containing Si in its main chains in addition to other atoms that define the classes of silicon based polymers, as it can be seen in Figure 4.

Figure 4: General simplified formula of silicon-based preceramic polymers.
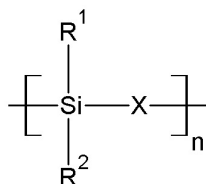
The nature of X is probably the most important variable, since it determines the class of the final polymer: Si–Si backbone defines the polysilanes class, while Si–O, Si–NH, Si–CH$_2$ and Si–N=C=N define the polysiloxanes, polysilazanes, polycarbosilanes and polysilylcarbodiimides, respectively (PARCIANELLO, 2012).

Substituents R1 and R2, which are both hydrogen, aliphatic compounds and lateral aromatic groups (e.g. allyl, vinyl, etc.) control the solubility, viscosity and thermal stability of the polymers. The carbon content of the final ceramic can be adjusted by lateral organic groups (COLOMBO et al., 2010). Besides the main ceramic precursors classes, a large number of them may be obtained through appropriate synthesis methods. In Figure 5 a wide variety of preceramic polymers may be seen.

Figure 5: Classes of Si-based preceramic polymers.
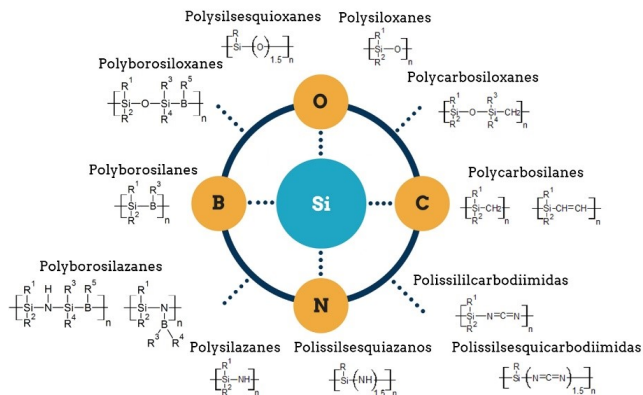
Polycarbosilanes (PCS) represents one of the most interesting and technologically relevant classes of preceramic polymers (FIOCCO, 2016). PCS was the first precursor applied to the production of SiC fiber (Nicalon^{TM}) by Nippon Carbon Co., and Tyranno^{TM} by UBE industries, by the first and most famous approach proposed by Yajima (Figure 6).

Figure 6: Yajima process for the synthesis of silicon carbide (SiC) ceramic fibers.
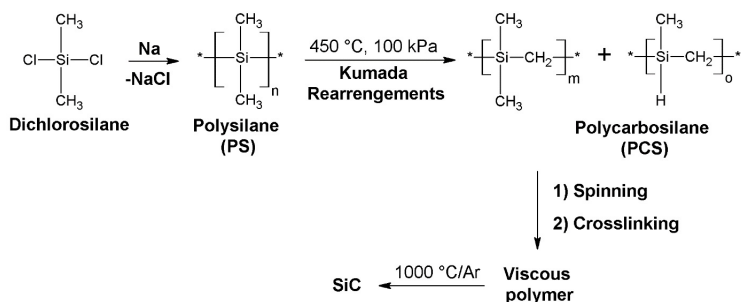
Yajima and co-workers prepared silicon carbide by pyrolysis of polycarbosilane PCS obtained from polydimethylsilane, which was synthesized by alkali-metal-promoted dehalocoupling of chlorosilanes (Wurtz coupling). The conversion of polysilane (PS) into PCS is often called "Kumada rearrangement" (as shown in Figure 6)(FIOCCO, 2016; KAUR, 2016; MORI; SUGAHARA, 2006).

With resulting polymers, green fibers were produced and the cure of these fibers were performed by either thermal oxidation in air at temperature of 100-200 ^{o}C by electron beam (EB) irradiation by Helium gas followed by a thermal treatment in an inert gas (SARKAR, 2010).

In thermal oxidation, green fibers became infusible by the cross-linkage via Si-O-Si and Si-O-C bonds with 7 % of oxygen increase in the fibers. In comparison, EB crosslinked the Si−H, −CH$_2$− or −CH$_3$ groups that introduced less than 1 % oxygen in the fibers (SARKAR, 2010; SUGIMOTO et al., 1995). This technology was used later by Nicalon^{TM} to produce continuous

SiC prepared by oxidation curing loses carbon and oxygen as CO by a carbothermal reduction. This SiC material tends to grow into larger crystals (β-SiC) at high temperature. Which can be a complication, as the grain coarsening and the crystal growth as well as the release of gases cause the loss of structural integrity (SARKAR, 2010).

Many other synthetic routes have been used to develop SiC preceramic polymers, for example: ring-opening polymerization, polycarbosilane synthesis via hydrosilylation, polysilane synthesis by dehydrocoupling reactions, and displacement and redistribution reactions of chlorosilanes (LAINE; BABONNEAU, 1993).

The chemistry of the PCS can be tailored by the type of the substituents attached to the silicon atom. For example, replacement of alkyl-group by allyl-group enhances the reactivity and crosslinking degree of PCS (KAUR, 2016).

Interrante et al. (1994) describes two different routes for the synthesis and applications of HPCS as a source of SiC coatings and its allyl-derivative, AHPCS, as a matrix source for SiC- and C-fiber reinforced composites. The first one has a very high cost, which makes it impractical right now as a SiC matrix source. The second one involves methyltrichlorosilane, a sub-product of the silicon industry and its conversion into Cl_3CH_2SiCl, which serves as the monomer for the Grignard coupling process (due to the trifunctional nature of the Si atom in this monomer unit).

This reaction yields a highly branched poly(chlorocarbosilane) of the approximate composition "$SiCl_2CH_2$". The chloropolymer could be reduced to a "SiH_2CH_2" polymer which they called hydridopolycarbosilane (HPCS), however, the ceramic yield was approximately 55 % (INTERRANTE et al., 1994; FROEHLING, 1993; ZHONG et al., 2017; KAUR, 2016).

Figure 7: Reaction mechanism for the formation of HPCS.
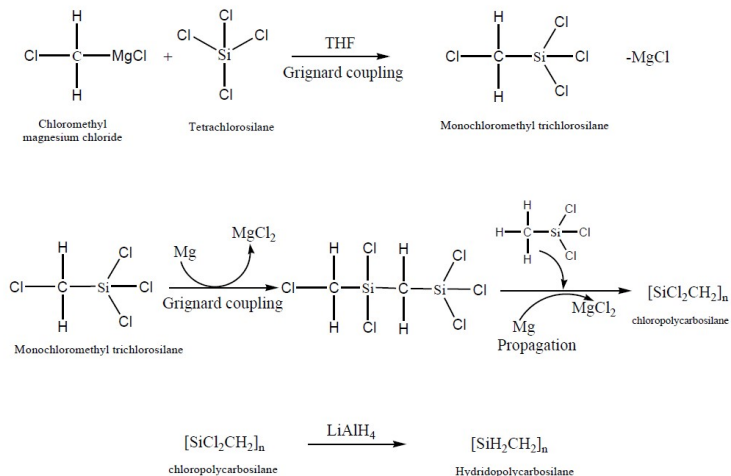
Source: Kaur (2016).

The last reaction shown in Figure 7 is the synthesis of HPCS. The intermediate poly(dichlorocarbosilane) was not actually isolated, but instead was converted directly to the corresponding hydridopolycarbosilane by addition of LiAlH (lithium aluminium hydride), as reported first by Whitmarsh e Interrante (1991).

Interestingly, poly(chlorocarbosilane) from the intermediate stage of HPCS preparation can be substituted with a small amount of olefinic functionality (such as vinyl or allyl) prior to reduction of the remaining Si-Cl groups to Si-H [XHPCS; where X = A (allyl) or V (vinyl)] (INTERRANTE et al., 1994).

The polymeric precursor modified by oleofine (allyl), of interest in this work, is Allyl-hydridopolycarbosilane (AHPCS). It is a light yellow colored liquid polymer of structure: - $[Si(CH_2CH=CH_2)_2CH_2]_{0.1}[SiH_2CH_2]_{0.9}$.

AHPCS has been used as the matrix for ceramic compounds due to, among other characteristics, its relative stability in air, being liquid at room temperature and its low viscosity,

which allows for a better infiltration/penetration on the applied materials. The selection of AHPCS precursor is interesting due to this polymer exhibiting the functional allyl group favors reaction mechanisms of this architecture type (this will be made clearer in Section 2.2.2) (KAUR; RIEDEL; IONESCU, 2014a; ZUNJARRAO; SINGH; SINGH, 2006).

According to its provider, Starfire Systems (Malta, NY), AHPCS is derived from high yield ceramic. Amorphous (glassy) SiC forms at 850–1200 ^{o}C with 72-78 % ceramic yield. Nanocrystalline β-SiC forms at 1250-1700 ^{o}C. The ceramics formed are stable at 1800 ^{o}C in air and till 2200 ^{o}C in inert atmosphere.

Even though it is a high yield process for advanced ceramics, it is known that poor control of shrinkage and structural integrity of the products obtained throughout the polymer-to-ceramic transformation is a critical problem in the PDC route using purely polymeric precursors (VIARD et al., 2017).

The polymer-ceramic transformation process implies the elimination of the oligomers or organic parts of a polymer (e.g., methyl groups attached to the Si atoms), with consequent significant gas release (CH_4, CO_2, C_2H_4 and C_3H_7, for example) and shrinkage. The usage of additives, such as boron, allows for the densification, processability and significant reduction of grain growth. This will be further discussed on the following section.

2.2.2 Boron modified AHPCS

Inorganic polymer, preceramic polymer or ceramic precursor possess strong commercial potential due to the end ceramic's "fine" final properties, which ends up emerging as one of the main sources of new high performance materials.

In general, materials with properties projected at molecular level using precursors are purer and more homogeneous due to the structural control. It also enables to directly process these compounds as coatings, fibers, porous materials, films, etc., which may not be obtained through traditional routes.

Many methods have been used aiming at including the chemical modification of the polymer in order to get a single-

source-precursor with differentiated characteristics. One of the alternatives to obtain ceramic with better structural characteristics is the addition, at molecular level, of compounds like boron.

Recently, single-source polymeric precursors to boron-modified SiC has been receiving more attention due to the improved homogeneity, sintering and ceramic density of the final ceramic. Boron, therefore, acts as a crosslinking element, which offers the possibility to extend the processability of preceramic polymers as AHPCS (BERNARD et al., 2005; YU et al., 2010; SCHMIDT et al., 2017).

Polymers with low boron contents may be easily processed, where in solution may be used for impregnation, coatings, films, etc. Polymers with high boron content are more appropriate for solid-state processing where it is possible to produce mechanically robust structures with monolith-type macroporous and dense structures after pyrolysis (VIARD et al., 2017). Moreover, boron carbide represents an attractive densification process.

Sneddon and coworkers were the first to report the hydroboration reactions of the AHPCS allyl groups with $BH_3 \cdot THF$ (Borane–tetrahydrofuran) and $BH_3 \cdot SMe_2$ (Borane Dimethyl Sulfide - BDMS) leading hydroborated polymers (PUERTA et al., 2003).

Despite the good initial results with allyl group hydroboration of AHPCS with these boron based compounds, the polymer were extensively reticulated, and, therefore, stopped being processable.

Hydroboration is performed by the grouping of AHPCS allyl molecules, similar to the B-H grouping from BDMS, non region selective, as it can be seen in Figure 8.

Moreover, Puerta et al. (2003) demonstrated that when pyrolyzed at 1000 ^{o}C under argon, AHPCS has shown to give high yields of amorphous SiC with only a slight excess of carbon, and the ceramic yields of the hydroborated polymer (called AHPCS-9-BBN) were significantly higher than that of AHPCS due to an additional crosslinking reaction involving the borane substituent (which can be observed in Figure 9).

Figure 8: Hydroboration of AHPCS using BDMS as boron source.
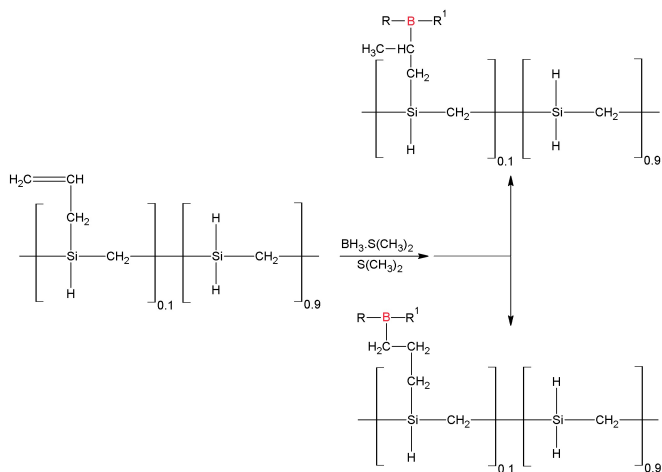
Figure 9: TGA (Thermal Gravimetric Analysis) studies showing the weight loss up to 1300 ^{o}C under argon of the AHPCS and AHPCS-9-BBN-4.
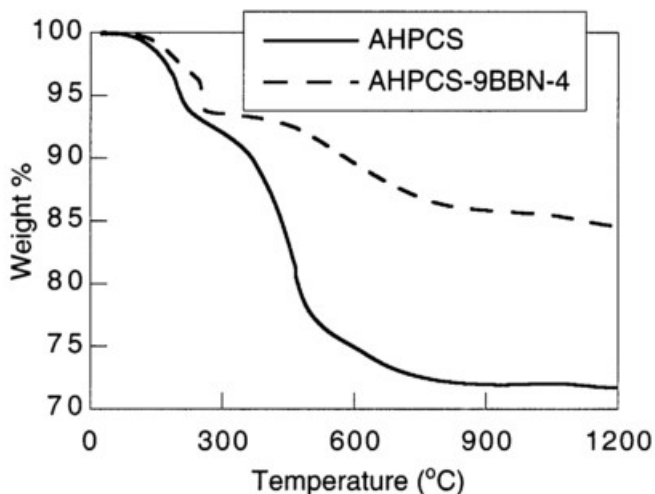
Source: Puerta et al. (2003)

Recently, Schmidt et al. (2017) investigated with more detail high temperature structural transformations of AHPCS modified with borane dimethyl sulfide (BDMS). Among other important results, it was observed that hydroborated AHPCS ceramic yield (with AHPCS molecular variations with the addition of different boron quantities) is significantly greater than pure AHPCS, as it is depicted in Figure 10.

Figure 10: TGA curves recorded for AHPCS and PBCS200, PBCS60 and PBCS30. Where PBCSX is AHPCS with different amounts of BDMS and X is Si:B ratio ranging from 200 to 30, varying with the quantity of BDMS added to the AHPCS solution.
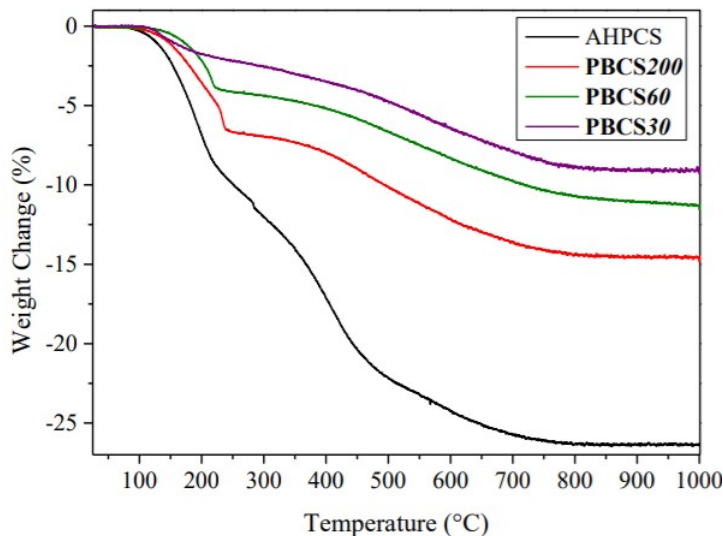
Source: Schmidt et al. (2017)

In addition to this, the remaining results from Puerta et al. (2003) showed that with a presence of only a small amount of boron, there was a significant increase in the density of the 1800 ^{o}C and 2000 ^{o}C ceramics derived from the 9-BBN (9 borabicylo[3.3.1]nonane) modified materials compared to those of the

unmodified ceramics.

Thus, the overall process for the fabrication of boron-containing silicon carbide based ceramic parts by PDC route, which can be seen in Figure 11, involves four major steps:

1. Synthesis of the single-source-precursor (SSP) from AH-PCS and BDMS;

2. Shaping using techniques as coating, casting, spinning, pressing, and others;

3. Crosslinking of the SSP;

4. Ceramization process (pyrolysis) of the shaped green bodies upon heat treatment.

Figure 11: PDC route of boron-containing silicon carbide based ceramic.
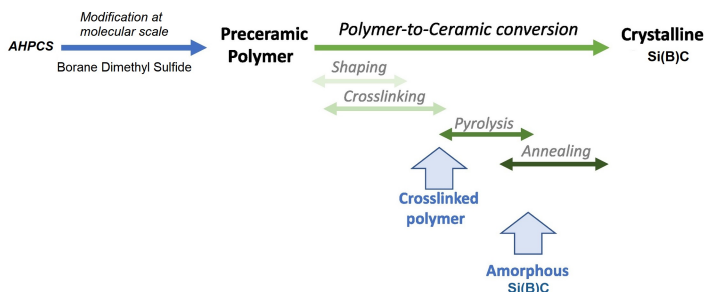
Therefore, this motivates the usage of boron as a molecular additive to improve the process of production of precursor for SiC ceramic in this work. The next step on the PDC route is the shaping of polymeric precursors and it will be discussed in the next section.

2.2.3   Shaping of preceramic polymers

A large range of forming methods are used to obtaining green bodies and consequently shaped ceramics. All the common and well-known plastic forming technologies can be applied to preceramic polymers, compaction method by uniaxial, isostatic and warm pressing (the last one which will be used in this work), coating of substrates by spraying, dip coating, spin coating or chemical vapour deposition (CVD), fiber drawing, preformed scaffolds for ceramic matrix composites (CMCs), casting, among other methods. Figure 12 shows some of the most relevant shaping techniques.

Figure 12: Shaping techniques for polymer derived ceramics manufacturing.
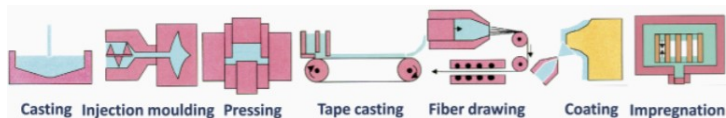
Source: Colombo et al. (2010).

With regard to polymers with molecular addition of boron, there are precursors with low boron content that display the appropriate requirements for facile processing in solution leading, for example, to the design of monoliths with hierarchical porosity, significant pore volume and high specific surface area after pyrolysis. And also polymers with high boron contents which are more appropriate for preparing dense ceramics by direct solid shaping (as pressing techniques, for example) and pyrolysis.

Hence, samples with low boron contents are liquid compounds with a higher viscosity than AHPCS and may be used in solutions for casting, coating substrates by dip- or spin coating. They can also be applied in templating processes to form ceramics of controlled porosities (SCHMIDT et al., 2017).

Moreover, it was also demonstrated (by Schmidt et al. (2017)) that low boron content AHPCS displays appropriate re-

quirements for facile processing in solution such as impregnation of host carbon foams. Hydroborated AHPCS with low boron content could also be casted and thermally crosslinked at 230 ºC (annealing time of 12 h), leading to infusible solid bodies. After extraction from the mold, the green body was pyrolyzed at 1000 ºC then annealed at 1500 ºC under argon to obtain a dense material.

Using an inorganic matrix with higher boron content, an attractive technique is the fabrication of ceramic dense parts and porous parts through warm pressing, which limits the shrinkage volume of the material. Thus avoiding the loss of oligomers during pyrolysis, which frequently leads to an increase of the ceramic yield (KAUR; RIEDEL; IONESCU, 2014b; GAO, 2014).

Warm pressing is recognized as an effective technique for bulk shaping. This is due to the fact that the polymeric precursor undergoes a crosslinking process which occurs during material compaction. In the appropriate mold, with prensing, through all the controlled pressure exerted on the press, green bodies with controlled porosity are obtained.

A typical scheme, which is used in this work, for forming green bodies is presented in Figure 13. The pressing process depends on the type of precursor used, its rheology, but generally the operation conditions used for this methodology vary between 120 and 320 ºC and the pressure, also determined by the type and mold size, goes from 20 to 710 MPa (usual values also reported by Kaur, Riedel e Ionescu (2014b)).

Figure 13: Warm pressing of a preceramic powder (in yellow).
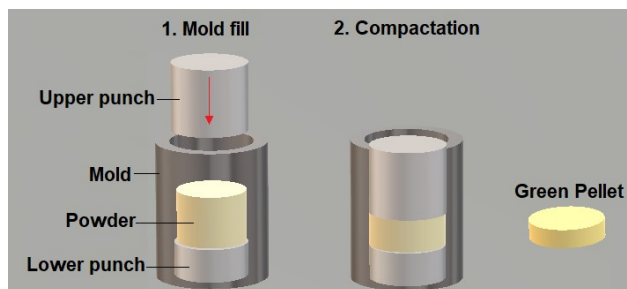
For pressing, when the preceramic precursor is liquid, it is first necessary to perform the pre-crosslinking step, which densifies the material, and then press it. Pre-crosslinking is similar to partial crosslinking, where the precursor is solidified, but reactive groups remain for further crosslinking during shaping (GAO, 2014).

A specific need for processing ceramic materials using preceramic polymers is that, after shaping (casting, pressing, fiber drawing, etc.), the green body needs to be converted into a meltable thermoset component, capable of retaining the shape during ceramization (FIOCCO, 2016; GREIL, 2000). It is also important to mention that the introduction of a catalyst may benefit crosslinking during shaping, thus obtaining already reticulated green bodies before pyrolysis.

2.2.4   Crosslinking of preceramic polymers

As previously discussed, AHPCS possesses an unsaturated functional group (allyl) which was introduced to the precursor moleculein order to increase the ceramic yield, and which promotes crosslinking reaction.

Studies on polycarbosilane's reticulation mechanisms revealed that this process involves dehydrocoupling and hydrosilylation reactions (Figure 14). Hence, liquid SMP-10 thermally cured at moderate temperatures ($T \leqslant 200\ ^oC$) through hydrosilylation, which in absence of oxygen involves reactions of Si–H bonds with Si–CH$_3$ groups leading to Si–CH$_2$–Si linkages (MERA et al., 2015), proving a cure polycarbosilane.

Figure 14: (a) Hydrosilylation reaction and (b) dehydrocoupling reactions that occur during thermal crosslinking of AHPCS.
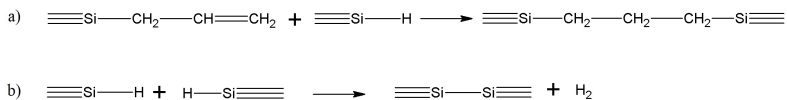
Source: Kaur, Riedel e Ionescu (2014b)

Additional polymer reticulation occurs through dehydro-coupling reactions and involves the elimination of molecular hydrogen from the SiH_n groups in higher temperatures ($T \leqslant 300\ ^oC$), which significantly improved molecular weight and reduced the vaporization of precursor fragments (KAUR, 2016; ZHONG et al., 2017; YU et al., 2010).

However, for liquid SMP-10 precursor to be thermally converted into powder, as required in many processes it is necessary a relatively high temperature (above 250 ^oC) as shown by Kaur, Riedel e Ionescu (2014b) when producing monoliths using uniaxial warm pressing.

Therefore, the use of agents like borane dimethyl sulfide (BDMS) may contribute to obtain powders at lower temperatures, as demonstrated by Schmidt et al. (2017), as boron contributes to the modification of the AHPCS-to-SiC transformation mechanism, especially in the low temperature regime of the thermal decomposition (SCHMIDT et al., 2017).

2.2.5 Polymer Pyrolysis

Pyrolysis of polycarbosilanes at temperatures between 800 ^oC and 1000 ^oC yields amorphous silicon carbide based materials after the liberation of gaseous species containing Si-H, $Si-CH_3$ and $Si-CH_2-Si$ groups (MERA et al., 2015). Additional competitive decomposition lead to the formation of segregated carbon, as well as pending bonds inside the amorphous ceramic and it is also relevant to add that polycarbosilane polymers form small graphite clusters at 1000 ^oC and in general it disappears at 1300 ^oC under conventional furnace heating (MERA et al., 2015; MCNAUGHTON, 2007).

As the annealing temperature exceeds 1000 ^oC, hydrogen is liberated and the amorphous material crystallizes into cubic-SiC (MERA et al., 2015). In Figure 15 a typical structural transformation during thermal decomposition of a polycarbosilane and thermogravimetric (TG) curve showing the weight loss are depicted (GREIL, 1995).

Boron-modified precursors tend to be slightly more resis-

tant to crystallization. Some authors have suggested that its introduction may form a barrier to the nucleation of the crystals. Bordia, Tomar e Henager (2015) exemplified this behavior when boron was added to SMP-10 by including 1 wt% decaborane to the liquid polymer (B-SMP-10), illustrating through XRD of the sample at 1100 ⁰C with and without boron, as shown in Figure 16.

Figure 15: Typical structural transformation during the thermal decomposition of a polycarbosilane according TGA.
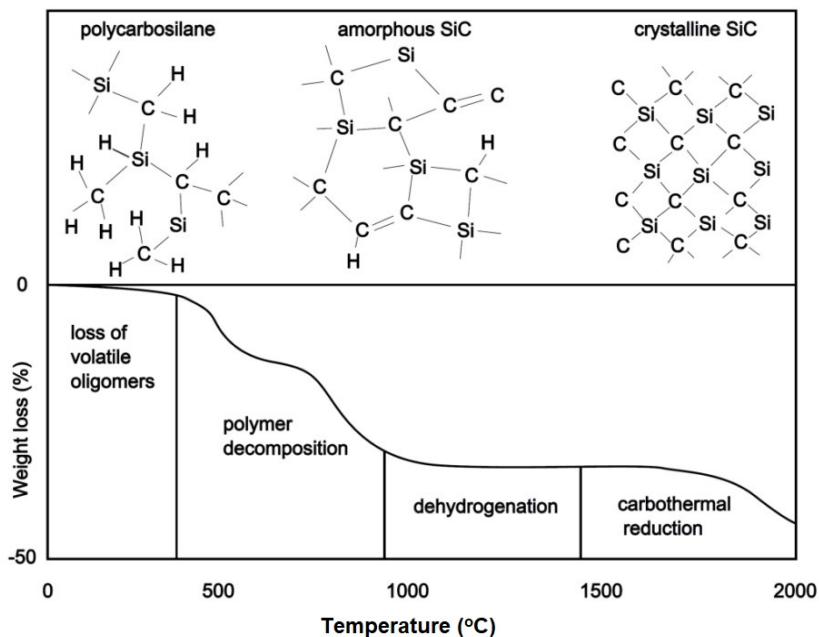
Source: Greil (1995).

However, the results of this and other research groups Schmidt et al. (2017), Kaur, Riedel e Ionescu (2014b) demonstrated that an increase in the boron content in the AHPCS-derived ceramics increases their degree of crystallization at high temperatures. The mechanism that boron affects the sintering

Figure 16: XRD of SMP-10 and B-SMP-10 at 1100 ^{o}C.
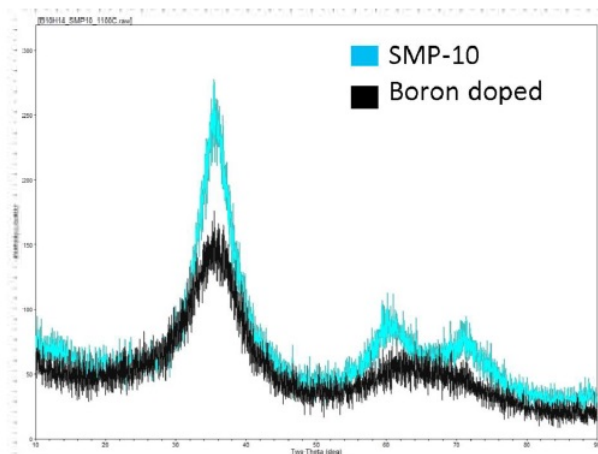
Source: Bordia, Tomar e Henager (2015).

of silicon carbide is complex. It is believed that boron supports
mass diffusion thus increasing sintering (PUERTA et al., 2003).

2.2.5.1 Sintering process of SiC

Naturally, the most common technique for pyrolysis is us-
ing a furnace, where circulating gas continuously removes
from the system the decomposition gases (BLUM; SCHWARTZ;
LAINE, 1989). Some techniques were developed for the sintering
of ceramic materials, such as Field Assisted Sintering Technol-
ogy (FAST), also known as Spark Plasma Sintering (SPS), Direct
Current Sintering (DCS) and Flash Hot Pressing (FHP). These
techniques are used for the consolidation of already pyrolyzed
powders rather than as ceramization methods (COLOMBO et
al., 2010).

Industrial implementation of SPS showed a huge growth
over the last years as a consequence of the possibility of us-
ing high sintering temperatures (up to 2400 ^{o}C), high heating
rates (up to 600 ^{o}C.min^{-1}) and the application of mechanical

pressures of up to ∼100 MPa, which enable ceramic sintering in shorter periods than sintering without pressure or warm pressing (usually 10 to 30 minutes and sometimes even up to a few hours) (MUNIR; ANSELMI-TAMBURINI; OHYANAGI, 2006; ZAPATA-SOLVAS et al., 2015).

Hence, the basis of the process is modified warming pressing, where the electrical current passes directly through the mold (which is pressed to the material), instead of through an external heater, in a pulsating electrical current, named "spark plasma effect". Consequently, fast heating and short process cycles can be reached (KESSEL et al., 2008).

Rahman et al. (2014) used AHPCS as pyrolyzed preceramic in inert atmosphere for the conversion of amorphous SiC (at 1400 ºC). Subsequently, they utilized SPS to compact the SiC powder at temperatures ranging from 1600 to 2100 ºC at an uni-axial pressure of 70 MPa and a dwelling time of 10 min. According to their results, *in situ* crystallization of amorphous SiC in fine grained structure with grain size ranging from 97 to 540 nm were observed and the maximum relative density obtained in this investigation was about 95 % at 2100 ºC sintering temperature (RAHMAN et al., 2014).

Another field-assisted phenomenon, called Flash (Ultra-Rapid) Spark-Plasma Sintering (FSPS), allows for very fast densification (a few seconds long) of ceramic specimens (mostly oxides, and some carbides). With this process, using SiC powder (result of 1-2 seconds of processing), Olevsky, Rolfing e Maximenko (2016) obtained high relative density (99 %), with the evidence of the limited grain growth.

Moreover, other authors, such as Manière, Lee e Olevsky (2017) and Grasso et al. (2016), worked with silicon carbide, as well as Niu et al. (2016) with boron carbide, and obtained high density ceramics using FSPS.

FSPS is not padronized, therefore, research groups monitor the electric field and shrinkage condition during tests, as well as the different geometries of the samples, etc. Hence, there are many sintering works with different types of equipment using SPS furnaces to perform the FSPS experiments.

For instance, Grasso et al. (2016) demonstrated that conventional SPS equipment could be used for flash sintering by replacing the graphite die's with graphite felt, which favors the current flow through the sample (beginning at the external border in contact with felt), facilitating the Joule effect.

Despite not existing a standard experimental apparatus for rapid/flash sintering, it can be said that the basic setup is a high-temperature furnace and a power supply attached in some way to a ceramic sample (DANCER, 2016). Figure 17 shows 3 typical designs of flash sintering apparatus.

Figure 17: Flash sintering apparatus configurations. (a) Vertical tube furnace with dogbone sample; (b) Adapted dilatometer/mechanical loading frame; (c) Flash spark plasma sintering/adapted hot press.
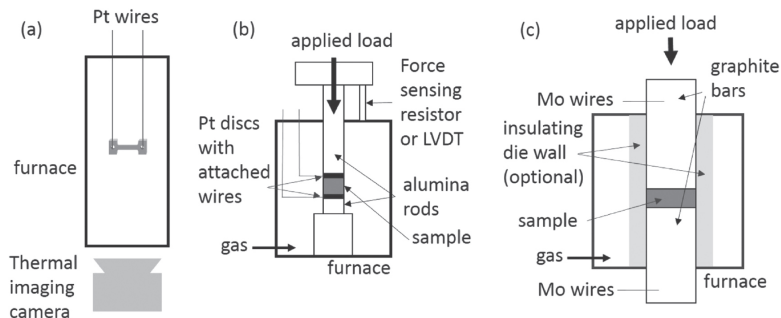
Source: Dancer (2016)

In the first image, a vertical tube furnace with the dogbone-shaped sample suspended horizontally from platinum wires, which also serve as electrodes, can be visualized (COLOGNA; RASHKOVA; RAJ, 2010; DANCER, 2016). On the second image, a pellet-shaped specimen is placed between two electrodes usually made of platinum and supported by alumina push-rods. This is mounted in a furnace, such as a dilatometer chamber or a split-furnace on a mechanical testing frame (DANCER, 2016).

On the last image, it is the most similar example to a SPS or hot pressing apparatus in design. This approach has been

employed in flash spark plasma sintering (FSPS), such as the
one used by Zapata-Solvas et al. (2015), where ceramic powder
is loaded into an insulator-lined die and the electrodes are the
top and bottom graphite plungers (DANCER, 2016).

2.3   Dense pieces using the PDCs route

Several techniques aim at obtaining dense ceramics with
low volume shrinkage and crack-free, eliminating not only unde-
sirable porosity, as well as the remaining impurity of the materials
which hinder the characteristics of the final ceramic.

It is, without doubt, a challenge to produce ceramics that
are fully dense through PDC, controlling the shrinkage and struc-
tural integrity of the products during polymer-to-ceramic trans-
formation.

Gas release during pyrolysis not only leads to the forma-
tion of undesirable/uncontrolled porosity, but also provokes a
substantial breakage of monolithic pieces (BERNARDO et al.,
2014; SHAH; RAJ, 2002; DIRE et al., 2011). Naturally, regard-
ing thinner pieces (such as fibers, microtubes, small monoliths,
among others), this is not the case, as due to short intrinsic
diffusion pathways for generated gases, leading to a lower accu-
mulation of internal pressure (BERNARDO et al., 2014).

It is important to remind that the use of sintering aids (as
boron, for example) and high temperatures are normally used to
enhance densification, due the covalent nature of the Si-C hence,
there is a low diffusion coefficient in SiC, and thus producing
dense ceramics (RIEDEL et al., 1992; SHAH; RAJ, 2002).

An example is described in another work from this re-
search group (SCHMIDT et al., 2017), where AHPCS thermally
crosslinked at 230 ^{o}C (annealing time of 12 h) was used to pro-
duced infusible solid bodies, later pyrolyzed at 1000 ^{o}C and then
annealed at 1500 ^{o}C under argon to obtain a dense object.

However, significant volume shrinkage (> 60 %) occurred
during pyrolysis, which results in defects and cracks. With the
molecular addition of boron (through a hydroboration process),
dense pieces were also obtained by warm pressing, which in turn,

using temperatures lower than 140 ^{o}C and pressing below 74MPa and posterior pyrolysis at 1000 ^{o}C yielded dense monoliths without evidence of high open porosity, cracks, or other defects (SCHMIDT et al., 2017).

The same technique, using uniaxial warm pressing was applied by Kaur, Riedel e Ionescu (2014b), also using AHPCS as the ceramic precursor. In their work, however, there were no additives, hence it was necessary to compact the powder at tempertures as high as 300 ^{o}C. The process also included subsequent pyrolysis and sinterization to prevent the presence of pores, turning it quite expensive.

It is highlighted the necessity of a high degree of crosslinking to increase the ceramic yield and prevent microfracture during pyrolysis. In the work under discussion (KAUR; RIEDEL; IONESCU, 2014b), ceramic monoliths prepared upon pyrolysis of the green bodies at 1100 ^{o}C and subsequently annealing at 1700 ^{o}C were immersed in SMP-10 in argon atmosphere for approximately 1 day (polymer-infiltration-pyrolysis (PIP) technique) to obtain crack-free monoliths, despite of a large volume shrinkage occurring upon pyrolysis.

Figure 18 shows a Scanning Electron Microscopy (SEM) image of the monolith obtained by Kaur, Riedel e Ionescu (2014b).

Figure 18: SEM images of silicon carbide monolith (4 PIP cycles) (b) after annealing at 1050 ºC.
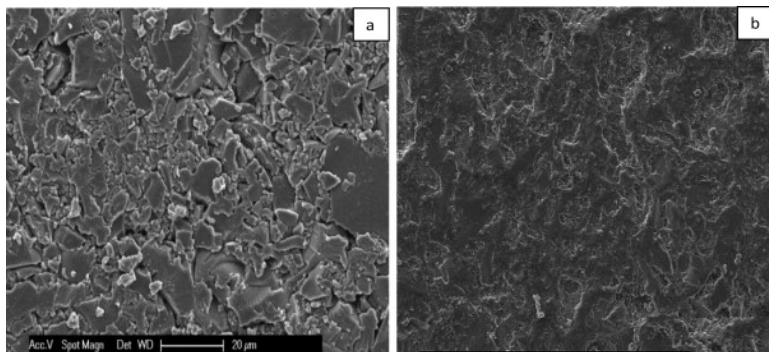
Source: Kaur, Riedel e Ionescu (2014b).

As seen in several works, methods for advanced dense ceramics production which involve a pressing mechanism for the shaping stage are quite common, with techniques such as: hot pressing, hot isostatic pressing, uniaxial warm pressing, etc.

Other works besides the ones already mentioned use such techniques, as, for example, Haug et al. (1999), which investigated the densification using precursors of the systems Si–C–N and Si–B–C–N.

Another method that has been researched is adding various fillers (actives or reactives such as a pure, fine-grained metal), so that near non-shrinkage can be achieved, and the gas released can be markedly reduced, thus avoiding cracks.

Inert or passive fillers are ceramic powders that do not react with ceramic residuals from the preceramic polymer, the decomposition gases or the heating atmosphere. Meanwhile, charge active fillers are metallic or intermetallic powders that react during pyrolysis with these elements (GREIL, 1995).

It is important to have in mind that, for most techniques, just performing green bodies pyrolysis the obtained samples will not be absolutely dense, but with very low porosity values (5-15 %) and an homogeneous distribution of very fine crystals

that generally leads to mechanically efficient materials, like dense materials. It is clear that dense zones are generally surrounded by a number of submicron pores, which could be ascribed to the gas evolution upon ceramic transformation (BERNARDO et al., 2014).

2.4   Porosity design methods based on PDCs

While several strategies for the production of dense objects are conducted with the goal of reducing porosity, mainly generated by gases during the conversion of the ceramic precursor into the final material, for porous ceramics this concept is explored intensely for the opposite purpose: increasing the presence of pores.

Production of porous ceramic from preceramic polymers brings several advantages due to the relative simplicity to process these materials. In addition to this route providing other positive aspects with a greater control over the porosity and final material composition. Moreover, another advantage are the unique polymeric properties, such as plasticity, CO_2 solubility and solubility of ceramic precursors into organic solvents (VAKIFAHMETOGLU; ZEYDANLI; COLOMBO, 2016; KIM et al., 2010).

There is a wide array of strategies for producing porous materials. Despite being heavily studied, these ceramics are constantly being innovated due to its unique resulting properties: low density (unlike dense ceramics), high permeability, chemical stability, thermal shock resistance, oxidation and corrosion resistance, among others (VAKIFAHMETOGLU; ZEYDANLI; COLOMBO, 2016; LALE et al., 2018).

Some of the processes that employ porous ceramics are: filtration (solid particles from molten metals, water, hot gas), absorption, membranes (for hydrogen separation from hydrogen-rich mixtures), light structure materials, porous bio-implants, catalyst supports, sensors (such as humidity), etc. (NETTLESHIP, 1996; ADHIKARI; FERNANDO, 2006; ZHU; JIANG; TAN, 2002; CHOU; LEE; LIU, 1999; INUI; OTOWA, 1985;

SALAZAR et al., 2006).

The porosity design in PDCs can be processed by different approaches; most of them being based on templating methods in order to satisfy the associated requirements of porosity, such as pore size distribution (PSD), specific surface area (SSA), interconnectivity degree, among other characteristics (LALE et al., 2018; CHAE et al., 2009).

Regarding the pore size (illustrated in Figure 19), this work will follow the terminology defined by the International Union of Pure and Applied Chemistry (IUPAC), shown below:

- Microporosity: pore size < 2 nm

- Mesoporosity: pore size between 2 and 50 nm

- Macroporosity: pore size > 50 nm

Figure 19: Scheme showing intersecting pore types.
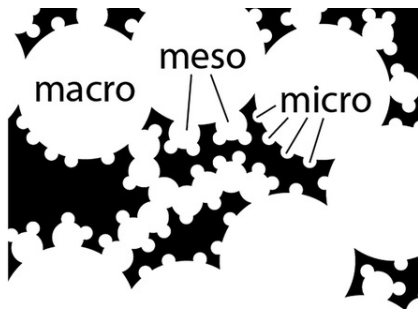
Source: Eisenberg et al. (2016).

This research group, through the article published by Lale et al. (2018), considered the following approaches to tune the porosity of PDC at different length scales, as depicted in Figure 20.

Figure 20: Processing strategies for fabrication of PDC at different length scales.
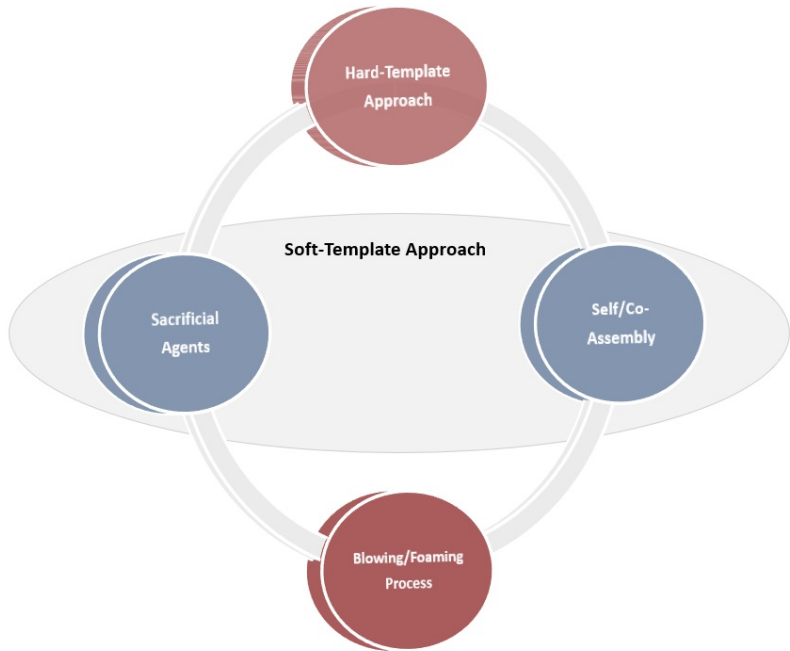
2.4.1   Processing strategies to design porous PDC - The Template Approach

In the following sections the most common methodologies for producing porous ceramics will be discussed. Clearly, several other template-free direct deposition of materials methods, such as three-dimensional (3D) printing, extrusion and spinning processes, are used for processing porous ceramics through the PDC method, but will not be object of this study.

The template approach, as a design strategy, was thoroughly investigated and consists of employing a preceramic precursor impregnated into a porous structure (template) or mixed with templates. It is followed by pyrolysis and substrate (tem-

plate) removal to obtain a porous ceramic with cell morphology similar to that of the original template (replica) (VAKIFAHME-TOGLU; ZEYDANLI; COLOMBO, 2016; LALE et al., 2018).

   This technique is usually divided into two approaches: soft-template and hard-template (also known as nanocasting).

   Section 2.4.1.1 will describe the hard-template method, followed on Section 2.4.1.2 by the soft-casting method, which will be used for producing porous materials by the PDC route in this work.

2.4.1.1   Hard-Template methodology

   The hard template technique or so called nanocasting by PDC route is probably the most common method employed in the fabrication of porous ceramics through replication of rigid material (continuous solid template).

   It is based on filling or coating of a rigid template with pre-ceramic polymer solution or melt and followed by pyrolysis and substrate removal (mold), thus obtaining a porous ceramic with cellular morphology similar to the original model (LALE et al., 2018; BERNARD; MIELE, 2014a; YANG; ZHANG; SCHNEPP, 2015).

   Ceramic fabricated through this method can take a range of forms including hollow materials from coating a template, or inverse materials from infilling of voids within a template (YANG; ZHANG; SCHNEPP, 2015), as it is shown in Figure 21.

   Several templates have been used on the production of both macroporous and mesoporous ceramics through PDC. However, silica and carbon deserve special attention for these applications.

   Sung et al. (2002) produced macroporous SiC with a highly ordered pore (Figure 22) for the first time by infiltrating the polymeric precursors (polymethylsilane/polycarbosilane) into a colloidal silica crystalline arrays as template. Subsequently, the template was etched off using Hydrofluoric Acid (HF) after pyrolysis in argon atmosphere. In this case, pyrolysis was performed at a low heating rate below 600 ^{o}C, as a faster gaseous evaporation under fast ceramization would be harmful to the homogeneous

Figure 21: Nanocasting steps. Infilling of a hollow (A1) or particulate (B1) template or coating (C) of a template followed by removal of the template to leave inverse (A2) or hollow (B2), (C2) replicas.
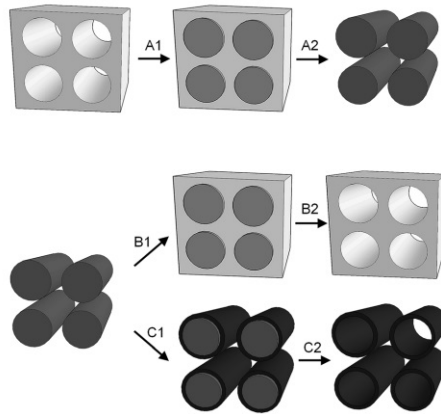
Source: Yang, Zhang e Schnepp (2015).

pore order.

Figure 22: SEM images of surface of macroporous SiC from PMS (a) and PCS (b).
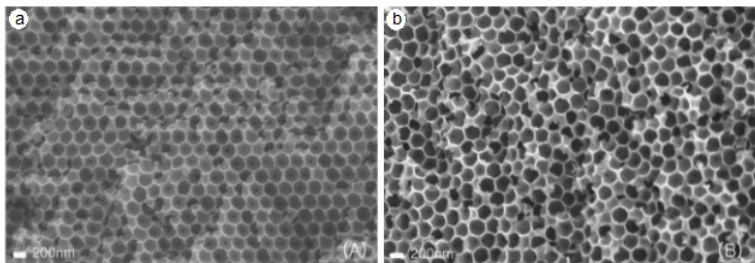
Source: Sung et al. (2002).

Using the same strategy, similar to that of the produc-

tion of macroporous SiC, Park, Sung e Kim (2004) first reported the elaboration of mesoporous SiC using a preceramic polymer (AHPCS) in a randomly packed silica colloidal sphere template with a diameter of $\sim$30 nm. This structure was removed by aqueous HF after pyrolysis in argon atmosphere at 1000 - 1400 ^{o}C. The ceramic exhibited a significantly high surface area of 612.7 m^2.g^{-1}, with a bimodal pore size distribution. In Figure 23 different silica template sizes can be seen on SEM images.

Figure 23: SEM images of mesoporous SiC obtained by pyrolysis at 1000 ^{o}C of the infiltrated templates; (A) from a 70 – 100 nm silica sol, (B) from a 40 – 50 nm silica sol and (C) from a 20 – 30 nm silica sol.
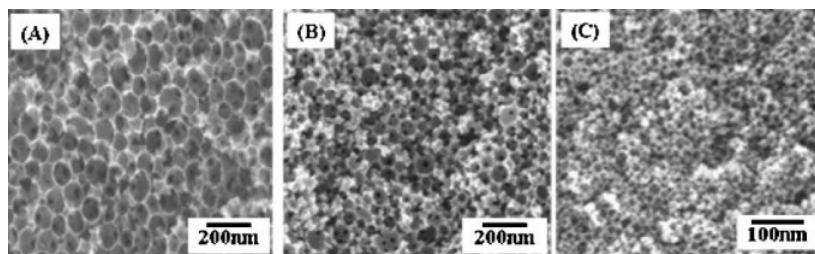
Source: Park, Sung e Kim (2004).

A wide array of ordered mesoporous carbon such as CMK-3 have been formed from the use of ordered mesoporous silica templates. Highly ordered mesoporous SiC materials were also prepared using trimethylsilyated SBA-15 and mesocellular siliceous foam as sacrificial hard templates (YOON; HONG; KIM, 2010).

Despite the hard-template methodology not being part of the process of porous ceramic production developed in this work, it is still a very relevant technique which opens up several future possibilities based on the work developed in this research. Also, regarding future works with known templates, in spite of silica being very common, it should be noted that the porous SiC products prepared from silica templates had severe oxygen contamination as a result of oxygen diffusion at the interface dur-

ing the pyrolysis of the infiltrated preceramic polymers (YOON; HONG; KIM, 2010).

2.4.1.2 Soft-Template methodology

The soft template methodology is also an efficient tool for the introduction of porosity in ceramics. It is based on the molecular modification of the precursors by a structure-directing agents (SDA) or by the addition of sacrificial materials.

Compared to hard-template methods, soft-templating can provide an alternative practical way to control the porosity structure and to avoid the hazardous chemicals employed (such as HF or NaOH) for the removal of hard templates.

Moreover, the preceramic polymer rheology, the need for total impregnation and oxidation of the final ceramic are some of the processing difficulties that need to be controlled with hard-templating techniques. Under this context, many authors have been attempting soft-template approaches. In the following section some of the relevant soft-template techniques for this work will be discussed: self-/co-assembly of preceramic polymers with structure-directing agents and the use of sacrificial polymeric micro/nanospheres.

2.4.1.2.1 Self/co-assembly of preceramic polymers

In principle, self/co-assembly is a process in which components, either separate or linked, spontaneously form ordered aggregates.

The addition of modelling agents in preceramic precursors, such as structure-directing agents (amphiphilic molecules, which are either cationic, anionic or non-ionic surfactants as block copolymers), have been the main route for the formation of non oxide nanostructured ceramics (WHITESIDES; GRZYBOWSKI, 2002; LALE et al., 2018).

Despite hard-template being commonly used to obtain porous ceramics at a wide length scale, the soft-template method

is quite innovative and can be very efficient for ordered meso-
porous yields.

Mesoporous structures is one of the topics of this work,
therefore, introducing the self-assembly technique in conjunction
with preceramic polymers is fundamental for the understand-
ing of the methodologies for obtaining some ceramic structures.
With this technique, morphology and domain size, characteristics
of the final ceramic, can be adapted. This is done by controlling
the interaction between the molecular weight of the SDA, more
precisely block copolymers (BCPs), as well as the relative block
lengths and selective solvent interactions (MALENFANT et al.,
2007), as it will be better detailed in Section 2.4.1.2.2. Moreover,
when discussing the PDC route, there is a prerequisite for "com-
patibility" between structure directing agent and the preceramic
polymer.

The majority of mesoporous materials are of oxide type
formed by a self-assembly process using the sol-gel route (MERA
et al., 2015). However, other works have been developed, break-
ing paradigms on the use of techniques for the production of
oxygen-free ceramics.

Ordered mesoporous non-oxide ceramics have been syn-
thesized via two synthesis pathways (as depicted on Figure 24)
(LALE et al., 2018; SHI; WAN; ZHAO, 2011):

1. Using a single organic-b-inorganic copolymer in which the
   preceramic polymer (or the molecular precursor) is cova-
   lently connected to the organic block copolymer (=self-
   assembly) and the inorganic segment serves as a ceramic
   precursor and the organic block as a mesopore template;

2. The SDA and the preceramic polymer are used separately
   (=cooperative self-assembly or co-assembly). The two poly-
   mers are mixed together to form a mesostructured nanocom-
   posite via micro-phase separation, in which the preceramic
   polymer only presents in one phase domain of the SDA
   block copolymer.

Figure 24: The two synthesis pathways for fabrication of ordered mesoporous non-oxide ceramic materials.
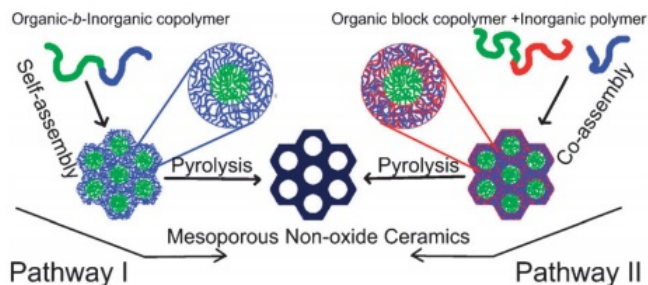
Source: Shi, Wan e Zhao (2011).

Notably, self-assembly based strategy of organic block copolymers followed by removal of one block segment is a powerful method, as described by Mera et al. (2015). Nonetheless, for PDC, co-assembly is very applicable and interesting, providing through an organic system greater accessibility utilizing, for example, a block copolymer for direct incorporation of preceramic polymers or inorganic particles. However, it is important to consider that only one of the segments in block copolymer should be intersoluble and the other block should be insoluble with the pre-ceramic polymer (SHI; WAN; ZHAO, 2011).

The second route, co-assembly, was chosen in this work, for the production of ordered mesostructures, through the usage of a block copolymer and a ceramic precursor, which will be converted *in situ* into an ordered mesoporous non-oxide ceramic.

Utilizing the same route (2), Kamperman et al. (2004) reported the first works on synthesis of mesoporous ceramic materials.

In the first work, amphiphilic poly(isoprene-block-ethylene oxide) diblock copolymer (PI-b-PEO) was used as a structure-directing agent for a polysilazane preceramic polymer commercially known as Ceraset -[poly(ureamethylvinyl)silazane]- its main chain contains –[–Si–N–]– units with alkyl side groups (SHI; WAN;

ZHAO, 2011; GARCIA et al., 2003). Films were formed after casting (50 ^{o}C for 3 h) annealed in a vaccum furnace for 24 h at 50 ^{o}C and subsequntely ramped up to 1250 ^{o}C for 1 h in order to crosslink the silazane.

Nonetheless, on the following year, the same group (Kamperman et al. (2004)), presented the preparation of ceramic materials stable up to 1500 ^{o}C based on a related approach using poly(isoprene-block-dimethylamino-ethyl-methacrylate)   (PIb-PDMAEMA) as structure-directing agent for Ceraset.

In it, a solution of 5 wt % of block copolymer in tetrahydrofuran (THF) was mixed with a radical initiator and the silazane precursor and stirred for 1 h. This solution was poured into a Petri dish and a film cast by solvent evaporation on a hot plate at 50 ^{o}C for 3 h. The film was then annealed in a vacuum furnace for 24 h at 50 ^{o}C and subsequently ramped up to 120 ^{o}C for 1 h to crosslink the silazane. Afterwards, thermal treatment was conducted under nitrogen up to temperatures as high as 1500 ^{o}C (1 ^{o}C.min^{-1} ramp). The output were nanocomposites with hexagonal morphology, shown in Figure 25.

Figure 25: Bright-field TEM images of the as-made composite (a) and ceramic calcined to 1500 ºC (b), demonstrating that the hexagonal structure is preserved during heat treatment.
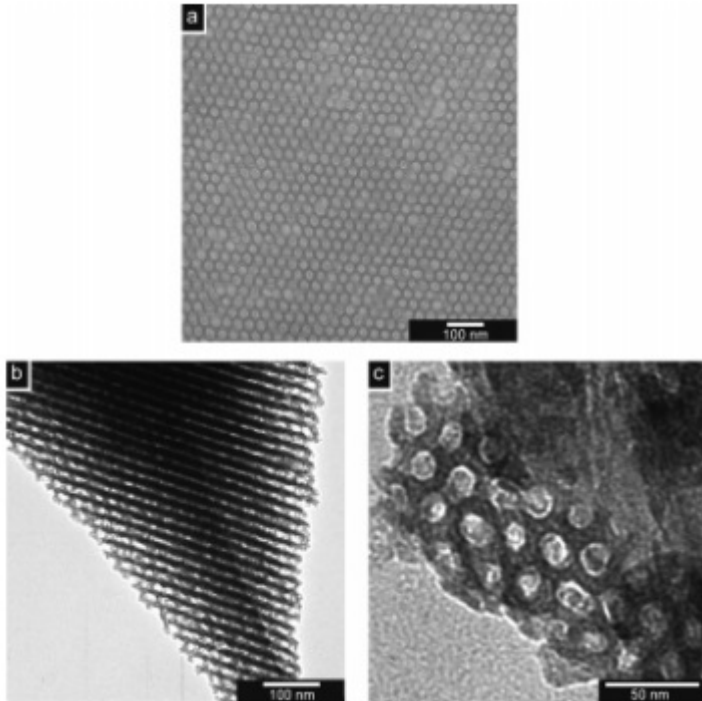
Source: Kamperman et al. (2004).

2.4.1.2.2 Block copolymers (BCPs)

Block Copolymers are defined as polymers that exhibit amphiphilic behaviour, containing two or more chains (homopolymers) with different molecular composition linked at one end. The two different domains of block copolymers are covalently linked in general with a nanometric size scale (GU; GUNKEL; RUSSELL, 2013; BUONOMENNA; YAVE; GOLEMME, 2012).

BCPs are appealing due to their capacity to "self-assemble" in very thermodynamically stable domains, controlling the shape

and size of the domain and resulting a material with controlled pore size in nanometric scale.

The use of block copolymers as SDA in porous non-oxide ceramics allows for the construction of high temperature nanostructure materials, as seen in the first paper of (KAMPERMAN et al., 2004), through easier methods, with less steps when compared, for example, with infiltration processes via templating (nanocasting).

Several resulting morphologies of the co-assembly process using BCPs have already been studied. This is dependent on the molecular weight of the constituent polymeric species and their composition (fa and fb), polydispersity of the copolymer as well as the solvent type and interaction between segments (DARLING, 2007; SMART et al., 2008; MATSEN; BATES, 1996).

Regarding A–B diblock copolymer, the system of interest in this study, composed of a linear chain of type A monomers bound on one end to a linear chain of type B monomers, there is a thermodynamic incompatibility between the A and B blocks which drives a collection of A–B diblock molecules to self-organize via microphase separation.

The most common morphologies for this type of BCP are: bodycentered cubic A spheres in a B matrix, hexagonally packed A cylinders in a B matrix, bicontinuous gyroid, and lamellar (DARLING, 2007; MATSEN; BATES, 1996), which are shown in Figure 26.

An important observation is the fact that the chains self-organize themselves so that contact between the immiscible blocks is minimized, with the structure determined primarily by the relative lengths of the two polymer blocks (fa) (DARLING, 2007).

Figure 26: Schematics of thermodynamically stable diblock A-B copolymer phases, such as the PS-b-PMMA.
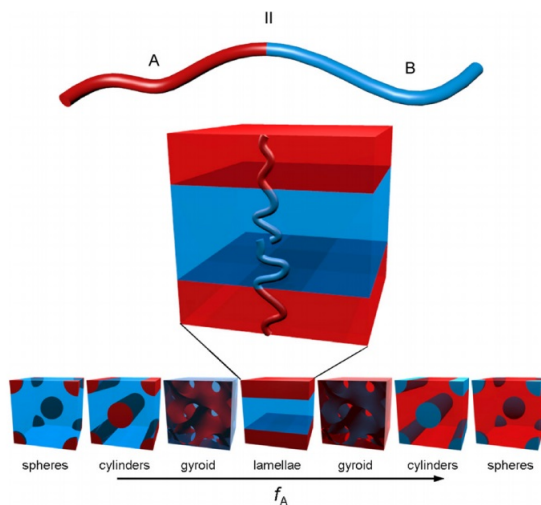
Source: Darling (2007).

A very interesting work demonstrated the behavior of BCPs when mixed with the inorganic precursor for the fabrication of nanocomposites (KAMPERMAN et al., 2008). PI-b-PDMAEMA (poly(isoprene-block-(dimethylamino)ethyl methacrylate)) and semicrystalline poly(isoprene-block-ethylene oxide) (PI-b-PEO) block copolymers were used as structure-directing agents for poly(urea-methylvinyl)silazane (PUMVS).

Mesostructured hybrids were produced by a one-pot synthesis approach, in which the ceramic precursor was expected to swell the hydrophilic block. In it, 5 wt% block copolymer solution in THF or Toluene were mixed with the ceramic precursor and the radical initiator dicumyl peroxide (1 wt%), wand stirred for 1 h. This was followed by EISA strategy and then annealing for 24 h under vacuum at 50 ^{o}C. This approach resulted in a film thickness of about 500 μm. The temperature was then increased up to 130 ^{o}C for 3 h to cross-link the PUMVS.

They observed a change in the morphology by using a block

copolymer as a SDA for PDC precursors (KAMPERMAN et al., 2008), which can be seen in Figure 27 (determined by a combination of SAXS and TEM). In it, a morphology map based on the weight fraction of each component (PI, PDMAEMA, and PUMVS) can be observed. Lamellar (L), hexagonally packed cylinder (C), and body-centered cubic packed spherical (S) hybrid morphologies were found. This demonstrates that by systematically increasing the PUMVS/block copolymer ratio multiple morphologies can be obtained from the same block copolymer.

Figure 27: Morphology diagram mapping the morphologies for various weight fractions of the PI-b-PDMAEMA/PUMVS system. Compositions showing the same hybrid morphology are color-coded, and white domains suggest regions with well-defined hybrid morphologies: cylindrical (C) blue, lamellar (L) orange, cylindrical (C) red, and spherical (S) green. Dark lines connect compositions derived from a specific block copolymer by adding increasing amounts of PDC precursor.
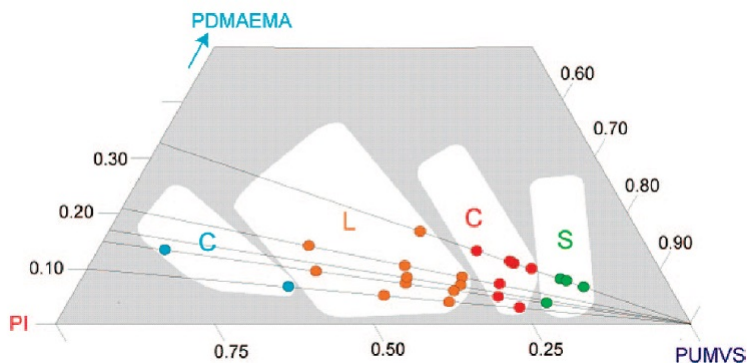
Source: Kamperman et al. (2008).

Another important factor that has been reported in the literature, is the change in morphology according to the system temperatures and the use of different solvents also affecting the output shapes (KAMPERMAN et al., 2008).

In the work by Wan et al. (2005) Polybutadieneblock-poly(ethyleneoxide) (PB-b-PEO) serving as the template for an available polysilazane (PSZ) and dicumyl peroxide initiator were dissolved in a 1:1 mixture of tetrahydrofuran and chloroform. Several solutions with a mass fraction of PSZ ranging from 0.17 to 0.89 were prepared. After evaporation of the solvents, these mixtures were annealed at 100 ᵒC for 12 h.

Through TEM images (shown in Figure 28), it was observed that there is a significant difference when using a pure block copolymer and a series of compositions containing differing amounts of PSZ (WAN et al., 2005). The morphology of pure block copolymer is hexagonally packed cylindrical in which PEO cylinders are surrounded by a PB matrix. By incorporating PSZ there is an increase in the size of the PEO/PSZ domain and transforms the cylindrical structure to a lamellar morphology.

These changes can be explained by the fact that uniformly dissolved homopolymer into a minority phase increases the effective volume fraction of that phase and changes the curvature of the interface, thereby shifting the morphology from cylindrical toward a more symmetric lamellar structure (WAN et al., 2005).

Figure 28: TEM bright field images of pure PB-b-PEO and PB-b-PEO/PSZ mixtures self-assembled at 100 ᵒC for 12 h (ϕ is the composition of polysilazane in wt%).
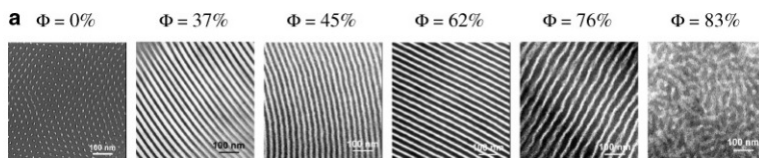
Source: Wan et al. (2005).

Regarding temperature dependent morphology changes, there are cases of annealing these self-assembled mixtures induces an order-to-order phase transition from lamellar to cylindrical as, for example, in the work by Wan et al. (2005), where this effect

was observed and can be seen in Figure 29.

Figure 29: TEM images of PB-b-PEO/PSZ mixtures with 37 wt% and 62 wt% of PSZ after annealing at 200 ^{o}C for 4 h. The image shows cylindrical and inverse cylindrical morphologies, respectively. The dark phase corresponds to the silicon-containing phase (PEO plus PSZ), while the bright phase is the PB phase.
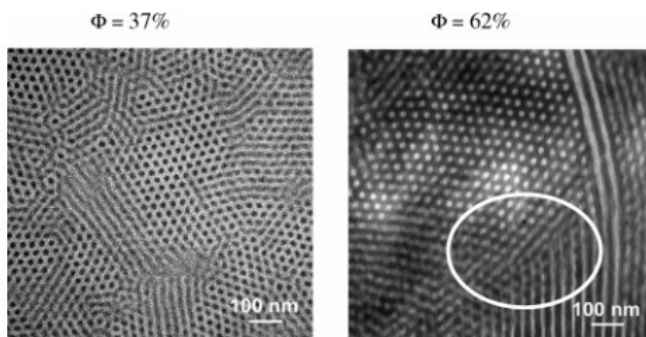
Source: Wan et al. (2005).

2.4.1.3   Sacrificial polymeric agents

Highly porous non oxide ceramics may be obtained using a solid sacrificial phase, which functions as a placeholder during the shaping, in preceramic polymer matrix (LALE et al., 2018; VAKIFAHMETOGLU; ZEYDANLI; COLOMBO, 2016).

The sacrificial phase may be nanoparticles of salts or of synthetic/natural organics, very commonly being Polystyrene (PS) and Poly(methyl methacrylate) (PMMA) organic polymers. It is subsequently extracted/decomposed to generate pores within the microstructure, which is examplified in Figure 30.

The main advantage of using sacrificial models is the precise control over porosity. Therefore, by controlling the fabrication parameters of the sacrificial agents (SA) it is possible, through quantity, shape and size of these particles, obtain an interlocked and open porosity in the final ceramic.

Figure 30: Schematic representation of the use of sacrificial agents in preceramic polymer matrix.
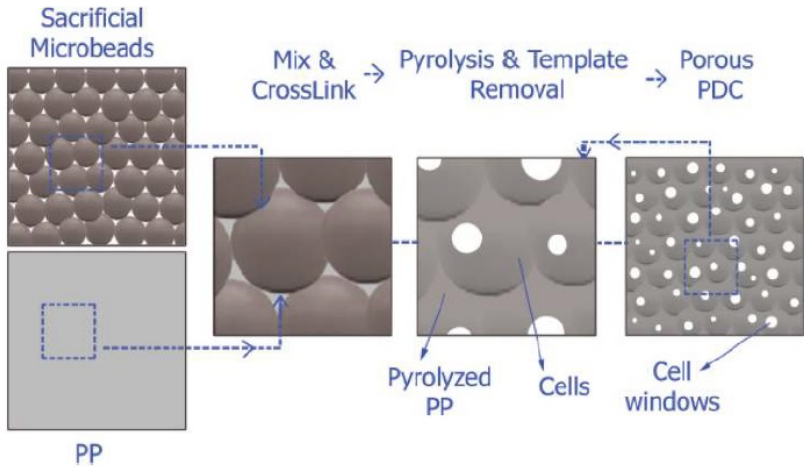
Source: Vakifahmetoglu, Zeydanli e Colombo (2016).

To produce a cellular structure with truly high porosity (greater than 60 vol%), a large porogenic volume needs to mixed with the ceramic phase. This generally leads to generating a large quantity of gas during sintering and, therefore, the process needs to be carefully controlled to avoid the formation of cracks on the ceramic body (COLOMBO, 2006).

The conventional process to fabricate cellular ceramics, object of the study in this work, through the usage of sacrificial agents, goes through the following steps:

1. Mix the preceramic polymer with SA;

2. Warm or cold pressing accompanied by reticulation (by heating or initiators);

3. Elimination of pore forming agents (calcination at moderate temperatures $\sim$400 ^{o}C);

4. Pyrolysis at adequate pressure and temperature.

A flowchart showing the stages and effects of each of these stages on the final ceramic structure is presented in Figure 31.

Figure 31: An overview of the process employing sacrificial templates and the effects of each step on subsequent processing stages and the characteristics of the final component.
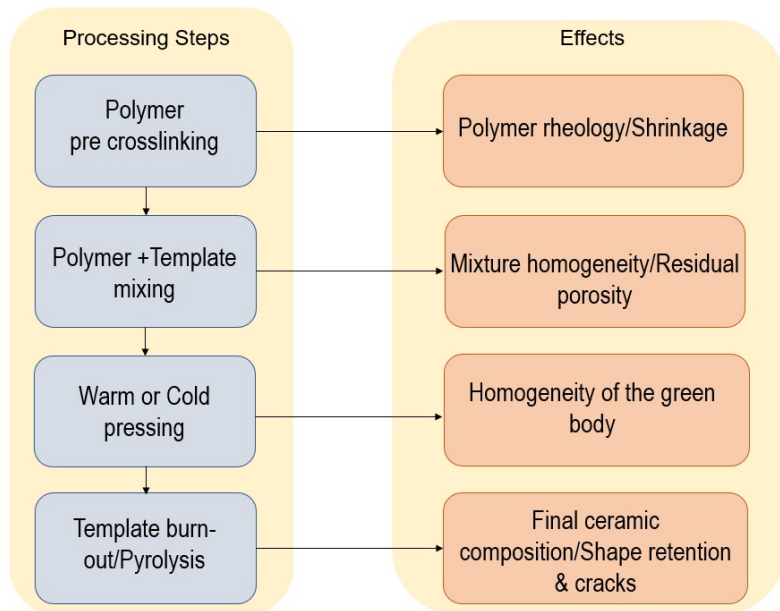
Source: Adapted from Vakifahmetoglu et al. (2009).

Hence, some parameters should be taken into account with the use of organic polymers as sacrificial agents. Among them is the polymer's capacity to retain shape and morphological integrity to avoid a collapse during pyrolysis. The green body cannot be excessively crosslinked, thus preventing cracks during the organic polymer's burn-out. For warm pressing, in addition to the of the precursor's crosslinking degree, the press retention time, temperature and pressure are other very important parameters and depend on the polymeric composition (inorganic/organic) (VAKIFAHMETOGLU et al., 2009).

Many recent studies have utilized organic polymer as SA. One of the most interesting ones used PMMA as sacrificial microbeads in addition to liquid polysilazane (VAKIFAHME-TOGLU et al., 2009). PSZ was first partially crosslinked (300 ^{o}C, dwelling time 8 h). The pre-crosslinked polymer was ground in a planetary ball mill followed by sieving. The pre-crosslinked precursor powder was dry mixed with PMMA microbeads. The powders were homogenized by planetary ball-milling and the mixture was then warm pressed in air for 2 h at 165 ^{o}C by applying a pressure of 13 MPa. The green bodies were subsequently pyrolyzed in Argon. Samples were heated to 450 ^{o}C with a rate of 0.5 ^{o}C.min^{-1}, held for 3 h in order to guarantee the complete decomposition of the sacrificial beads, and then pyrolyzed at 1100 ^{o}C (heating rate of 2 ^{o}C.min^{-1}) for 2 h. Through this procedure the authors obtained the structure shown in Figure 32.

Figure 32: SEM micrographs of the fracture surface of pyrolyzed sample (ratio PMMA:PSZ = 80:20).
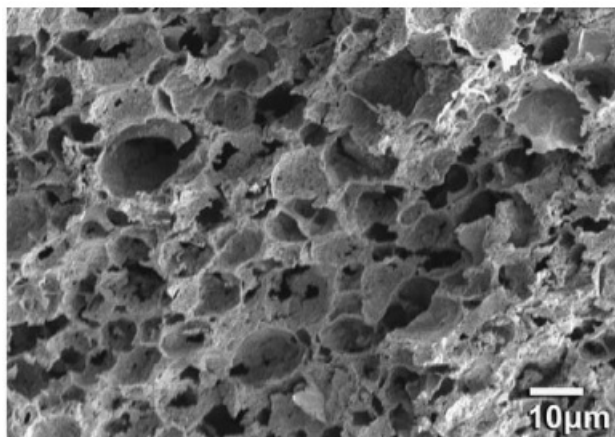
Source: Vakifahmetoglu et al. (2009)

The authors of this work noticed, through SEM micrographs, a large amount of pores, mostly interconnected, with

pores ranging from about 5 μm to 15 μm in size. Also, the cell size and shape were not precisely similar to those of the PMMA templating beads, probably a consequence of significant volumetric shrinkage occurring during the ceramization step (70 vol%). The amount of the total porosity increased with the increased amount of sacrificial templates, while closed porosity showed the opposite trend.

2.4.2   Final remarks on the literature review

This chapter sought to provide the reader a literature review on dense and porous pieces obtained by PDC route. In describing potential applications it had the goal of giving a context to the manufacture of these materials, in particular, the use thereof in filtration processes under more severe conditions of temperature and pressure, for example.

Thus, following this potential, the state of the art in the synthesis of Si-(B)-C, starting from preceramic polymer and boron, was summarized by the PDC route. The PDC route, in turn, was evidenced in this thesis due to its advantages, in particular, its ability to fabricate structures by means of easy-to-reach techniques (as in this case specifically, warm pressing), with the possibility of controlling chemical composition and crystalline phases.

Also, it presented alternatives for the material's densification, that not only by pyrolysis in furnace with inert atmosphere, but using very interesting techniques, such as rapid/flash sintering.

The methodology for obtaining dense and porous structures, which will come in the next chapter of this work, is based on the processes mentioned in this bibliographic review. Particularly, the porous parts will use as a basis co-assembly techniques and the use of sacrificial agents herein.

Thus, given the importance of contextualizing the reader to the next chapters, the materials and methods employed in this thesis are sequenced.

3 Experimental Procedure

The methodology for producing PDCs in this work will be divided in 4 large stages:

- On the first stage are explained the procedures for the synthesis of boron-modified polycarbosilane, using AHPCS as preceramic polymer and two different amounts of boron (BDMS), which results in the samples labelled as PCS_B30 and PCS_B60.

- The second stage encompasses the methodology for the production of Si-(B)-C dense ceramics from boron-modified polycarbosilane through two different approaches: warm pressing and rapid sintering.

- The third stage is the strategy for production of porous Si-(B)-C ceramics via warm pressing. It includes the methodology for the synthesis of the sacrificial agent, poly(methyl methacrylate) (PMMA), for controlled porosity production.

- On the fourth and final stage, methodology of alternative strategies to the use of boron are explained. These which applied versatile additives: dicumyl peroxide and silver benzoate.

3.1 General comments of commercial available materials

Commercially available Allylhydridopolycarbosilane AHPCS (SMP-10) (chemical structure in Figure 33) was acquired from Starfire System®. AHPCS is a relatively viscous, light yellow liquid, which does not require a solvent to be processed. Some of it main characteristics, given by the supplier, are presented in Table 2.

Table 2: Properties of AHPCS (SMP-10)

SiC Properties	
Density	0.998 g/cm^3
Viscosity	40 to 100 cps at 25 ^{o}C
Flash Point	89 ^{o}C
Appearance	clear, amber liquid
Compatible Solvents	hexanes, tetrahydrofurane, toluene, insoluble in water
Odour	None
DOT/IATA Regulation	Non-Hazardous
Storage	Vacuum container or inert environment; Refrigerated

Figure 33: Chemical structure of AHPCS preceramic precursor (SMP-10).
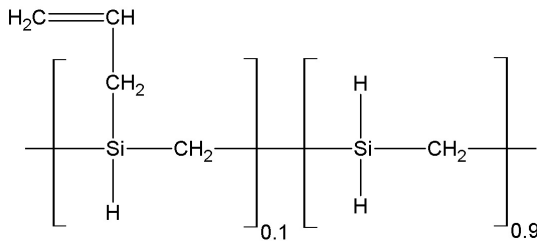
In the first stage of this work, for the modification of AH-PCS with boron, in a process called hydroboration, was used borane dimethylsulfide (BDMS) (2 M solution in toluene) obtained from Sigma–Aldrich without any further purification. BDMS's structure is found on Figure 34. Toluene (99.85 %, Extra Dry over Molecular Sieve, AcroSeal®obtained from Acros Organics) was also employed during hydroboration as a solvent due to its compatibility with the ceramic precursor and already being present in the boron compound.

For the third stage, synthesis of PMMA in two particle sizes, named in this work PAg25 (25 μm) and PAg350 (350 nm), the following reagents (Table 3) were utilized:

PAg25 and PAg350 were functionalized with silver (Ag). Hence, for the synthesis of Ag nanoparticles the following agents

Figure 34: Chemical structure of Borane dimethyl sulfide complex (BDMS).

$$H_3C \diagdown S \diagup CH_3$$
$$| $$
$$BH_3$$
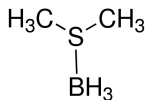
Table 3: Reagents used for the synthesis of PAg25 and PAg350.

Compound	PMMA	Manufacturer
Methyl methacrylate (MMA)	PAg25 and PAg350	Vetec Química Fina Ltda
Poly(vinyl acetate) 78.000 88% (PVA)	PAg25	Vetec Química Fina Ltda
Ethylene glycol dimethacrylate (EGDMA)	PAg25	Vetec Química Fina Ltda
Glyceryl Monostearate	PAg25	Vetec Química Fina Ltda
AIBA (2,2'-Azobis(2-methylpropionamide)dihydrochloride)	PAg350	Sigma-Aldrich
AIBN (Azobisisobutyronitrile)	PAg25 and PAg350	Sigma-Aldrich

were employed: sodium borohydride ($NaBH_4$, Sigma Aldrich) and silver nitrate ($AgNO_3$, Cinética).

Still on this third stage, for the creation of a mesoporous layer through dip-coating technique, block copolymers based on styrene and butadiene (SBS) of various molecular weights (Mw) (Table 4), donated by Kraton Polymers and Sigma SBS donated by Sigma Aldrich, were tested.

Table 4: Block copolymers based on styrene and butadiene (SBS) tested for the formulation of coatings for the porous structures (functionalization)

SBS	Mw (g.mol^{-1}, from Manufacturer)
A	125000
B	120000
C	170000
D	150000

For the last stage, where other ceramic materials synthesis strategies were applied, dicumyl peroxide (Akzo Nobel) and silver benzoate (Sigma-Aldrich) were used as reagents.

3.2   Synthesis of Boron modified AHPCS

In this work, since it deals with non-oxide ceramics, all syntheses envolving AHPCS were carried out in a purified argon atmosphere by means of standard Schlenk manipulations and vacuum/argon-line techniques.

Boron modified AHPCS synthesis was initiated by the assembly of glassware, which were previously heated in the oven at 80 ^{o}C to remove the humidity. For this stage, the following items of glassware were used: a three-necked round-bottomed flask equipped with a dropping funnel connected to a bubbler for gas escape (as shown in Figure 35) and a Teflon-coated magnetic stir bar.

Figure 35: Glassware and scheme for AHPCS hydroboration reaction.
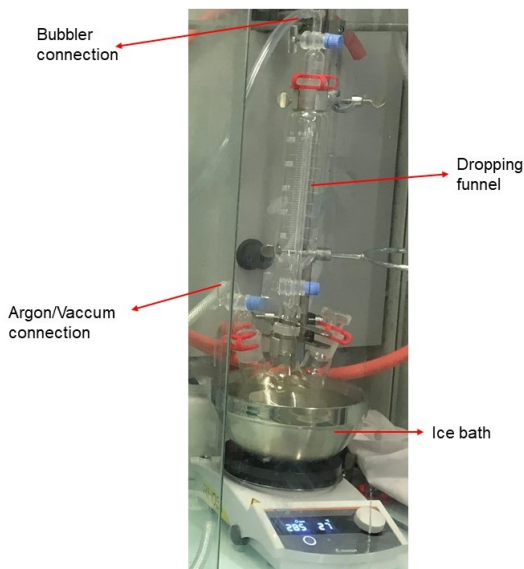
This system was maintained for 30 minutes at vacuum atmosphere. After this time, argon was purged in the system so that the reagents could be added while argon was flowing.

Hydroboration was performed with two different amounts

of boron content, denoted as PCS_BX, where X is the Si:B molar ratio. Thus, PCS_B30 (with higher boron content) and PCS_B60 (with less boron content) were obtained.

For PSC_B30 synthesis, firstly, it was added to the three-necked round-bottomed flask, 70 mL of toluene and 30 mL more of the same solvent on the dropping funnel. This was followed by adding 12 mL of AHPCS (11.98 g, 248.03 mmol) to the round-bottomed flask under vigorous stirring. Lastly, 4.1 mL BDMS (8.3 mmol) was introduced in the dropping funnel alongside the toluene (which had already been added).

The round-bottomed flask containing AHPCS and toluene was cooled down in an ice bath until 0 ^{o}C was reached. Then the toluene and BDMS mixture in the dropping funnel was dropwise added to the AHPCS solution under stirring.

In Figure 36 it is possible to observe the reagents added to the reaction.

Figure 36: Scheme for AHPCS hydroboration reaction.
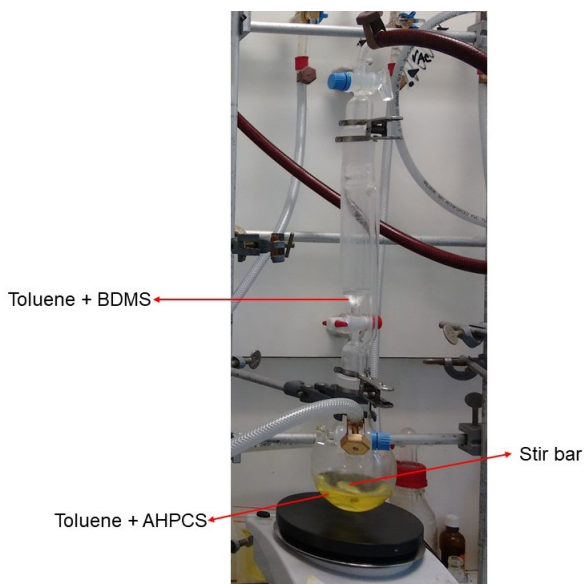
After the dripping is finalized, the system was kept inert.

The temperature was increased naturally up to room temperature (RT) and the mixture was stirred for three days.

All the same procedures were applied for the production of PCS_B60, albeit, with a different boron quantity, through 2.1 mL of BDMS.

The computations to determine the reagent quantity utilized took into account the molecular structure of the compounds.

Figure 37 presents a scheme of the hydroboration reaction. Thus, for complete hydroboration, it is expected that 0.1 mole of allyl groups from AHPCS will react with BDMS's B-H bond.

Figure 37: Hydroboration reaction mechanism.
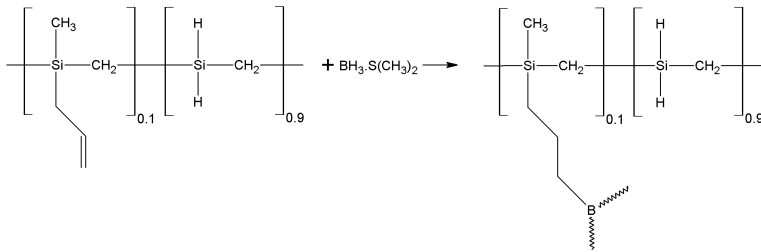
As it can be seen from Figure 37, there are three links on BDMS's molecular structure. Therefore, the number of mols of BDMS added to AHPCS is equal to $0.1\eta/3$, for η mols of AHPCS. The computations made to determine the volume of BDMS (v_{BDMS}) added to the reaction to obtain PCS_B30 follow on the equations below, beginning with Equation 3.1:

$$\eta_{AHPCS} \times 0.1 = \eta_{BDMS} \times 3 \tag{3.1}$$

Where, η represents the number of mols from the reagents AHPCS and BDMS.

$$\eta_{AHPCS} = \frac{m_{AHPCS}}{M_{AHPCS}} \tag{3.2}$$

Here, m_{AHPCS} is the mass of AHPCS in grams and M_{AHPCS}

its molecular weight.

$$\eta_{BDMS} = v_{BDMS} \times c_{BDMS} \qquad (3.3)$$

Where, $M_{AHPCS} = 48.1$ g.mol^{-1} and the molar concentration of BDMS is: $c_{BDMS} = 2$ mol.L^{-1}.

$$6 \times v_{BDMS} = 0.1 \times 0.25 \qquad (3.4)$$

Thus, $v_{BDMS} = 4.1$ mL

Hence, 4.1 mL of BDMS were used for complete hydroboration (PSC_B30).

For the PCS_B60 compound, a hydroboration with half the number of moles was considered. Therefore, 0.05 mole of allyl groups from AHPCS reacted with the B-H bond from BDMS ($\eta_{AHPCS} \times 0.05 = \eta_{BDMS} \times 3$), which results in approximately 2.1 mL of BDMS added to the hydroboration in this sample (using the same volume of toluene = 100 mL).

Once hydroboration was completed, to proceed with the following steps of warm pressing and flash sintering, the hydroborated AHPCS needed first to be solidified. Thus, the solvent was removed from the reactions, as illustrated in Figure 38. This procedure follows the following steps:

1. A bridge was used to extract the solvent. In one of the sided of the bridge a long Schlenck was connected to capture the solvent removed from the solution. While on the other extremity a volumetric balloon was connected. This system: long Schlenck, extraction bridge and volumetric balloon, was kept for 30 minutes under vacuum.

2. After this, argon was purged and the small volumetric balloon was removed under constant argon flow.

3. The dropping funnel was disconnected from the bottom flask under a strong argon flow.

4. The flask with the reaction was connected to the bridge on the location where the small balloon was previously placed.

These steps require a strong argon flow and extra care to avoid contamination of the reaction or the system with oxygen.

Finally, a dwear with liquid nitrogen was assembled to the long Schlenk so that toluene could be collected, being kept frozen until the end of the extraction.

Figure 38: Scheme for toluene (solvent) removal from hydroboration synthesis.

In this toluene removal operation, though pressure difference using vacuum, stirring remained vigorous and the temperature was gradually increased until 100 ^{o}C, where it was kept for 5h.

PCS_B30 after solvent extraction, shown in Figure 39, was a fine dust, with certain clustering. This powder was used, via warm pressing, for the obtainment of dense and porous structures. Beforehand, it was characterized by FTIR, NMR, XRD Elemental Analysis and TGA.

Also, both fine solids PCS_B30 and PCS_B60 were pyrolyzed in different conditions, to characterize these samples in regards with the thermal treatment and the process for rapid synthesis, as it will be shown in the following sections.

Figure 39: a. líquid PCS_B and b. solid (powder) PCS_B after solvent removal.
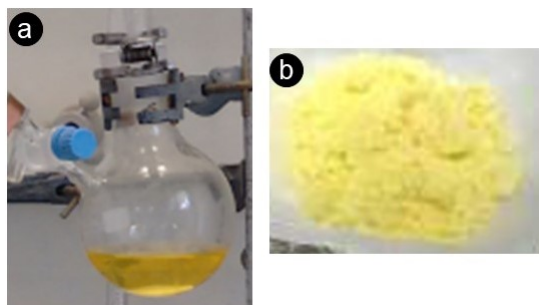
3.2.1 High temperature treatment for PCS_BX powder samples

PCS_B30 and PCS_B60 after the removal of the solvent, as shown in the last section, were kept in a glovebox for up to a week.

Thus, some of the pyrolysis conducted were done in argon atmosphere until 1000 ^{o}C with heating ramp of 5 ^{o}C. min^{-1} and dwelling time of 2 h in graphite crucible. Si-(B)-C ceramic powders were then obtained and followed for analysis of FTIR, XRD and Raman.

Thermal treatment with higher temperatures (annealing), up to 1800 ^{o}C, were also made for both samples (PCS_B30 e PCS_B60) in a vertical furnace (described in Section 3.5) in argon environment with a heating ramp of 5 ^{o}C. min^{-1} and dwelling time of 2 h in alumina crucible.

In addition to the thermal treatment in argon, sample PCS_B30 underwent a pre thermal treatment in ammonia (NH$_3$) (Ammonolysis), to dope the sample with nitrogen while removing carbon at 450 ^{o}C and subsequently pyrolysis under argon up to 800 ^{o}C. These doped samples were posteriorly used in the synthesis of monoliths (disks) via Rapid Hot Pressing (RHP), as it will be seen in Section 3.2.2.2.

AHPCS was also pre treated in ammonia to evaluate the changes with and without boron, comparing it with the result from PCS_B30.

These samples that underwent pre treatment in ammonia and pyrolysis in argon were examined with FTIR, XRD and HRTEM.

The flowchart in Figure 40 provides an overview of the thermal treatments that AHPCS, PCS_B30 and PCS_B60 were submitted through.

Figure 40: Pyrolysis performed with AHPCS, PCS_B30 and PCS_B60 fine solids.

AHPCS

1) Various temperatures up to 1800 °C under Ar (5 °C.min^{-1} for 2h)

2) At 450 °C under NH$_3$ then pyrolysis under Ar between 800 and 1500 °C (5 °C.min^{-1} for 1h)

PCS_B30

3) Various temperatures up to 1800 °C under Ar (5 °C.min^{-1} for 2h)

4) NH$_3$ until 450 °C then Ar between 800 and 1500 °C (5 °C.min^{-1} for 1h)

5) Ar up to 800 °C (5 °C. min^{-1} for 2h)

PCS_B60

6) Various temperatures up to 1800 °C under Ar (5 °C.min^{-1} for 2h)

7) Ar up to 800 °C (5 °C.min^{-1} for 2h)

*** Rapid Sintering: treatments 4 (800 °C), 5 and 7.*

3.2.2   Production of 3D dense disks

3.2.2.1   Warm pressing of boron-modified AHPCS (PCS_B30 powder)

For the warm pressing stage, after the synthesis and removal of the solvent, PCS_B30 was ball milled at 200 rpm for 1 h 30 minutes until it became a finer dust and thus obtain a more homogeneous ceramic. It is important to remember that PCS_B30 was inside the glovebox and the filling of planetary mill (for the ball milling process) was also done inside the glove-

box. Consequently, the samples were never in contact with atmospheric air.

Following ball milling, PCS_B30 was deposited in a specific mold for warm pressing. Three molds of different diameters were used for this purpose: 13 mm, 25.6 mm and 28.5 mm. The aim was to verify the behaviour of the sample (green body) with different sizes, which represents different mass (g), temperature and applied load (tons) of PCS_B30 and how it interferes on the final resulting ceramic.

In Figure 41 are shown the photos of : a) part of the 25.6 mm diameter mold and b) 28.5 mm mold in press machine. In both images, in yellow is the PCS_B30 powder.

Figure 41: Molds with a) 25.6 mm and b) 28.5 mm diameter, used in the warm pressing process of the PCS_B30 sample to produce dense Si-(B)-C 3D pieces.
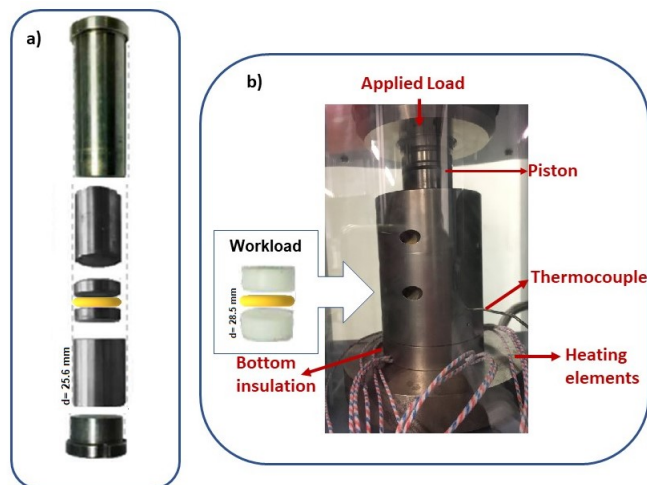
The utilized pressing conditions (temperature, time, force (applied load), sample quantity and pyrolysis condition) for PCS_B30 sample using a 13 mm mold were based on previous works from this research group (SCHMIDT et al., 2017). Now, with the 25.6 mm mold some alternatives were experimented. The established characteristics are shown in Table 5.

Table 5: Warm pressing conditions for dense pieces using the 13 mm and 25.6 mm diameter molds.

Mold (diameter)	13 mm	25.6 mm
PCS_B30 (g)	0.25	1.5 e 2
Temperature (°C)	120	120
Dwell Time (min)	30	30 e 60
Tons	1	4 e 5

For the largest mold, ⌀ (diameter) 28.5 mm, some parameter tests were conducted, with temperature varying from 80 to 110 ^{o}C, force between 4 and 8 T.g (tons x gravity) and dwell time from 30 min to 1 h.

The computation involving the utilized pressing force were based on the fundamental pressure principle ($P = F/A$), with pressure set to 74 MPa for all experiments.

All dense pieces obtained through warm pressing were produced in a heating rate of 10 ^{o}C.min^{-1}. After the end of the pressing, the heating was switched off and the mold naturally cooled down to be put back into the glovebox.

The green bodies were then removed from the mold inside the glovebox and pyrolyzed. Each green body stayed for at most 48h inside the glovebox before being taken to the furnace for pyrolysis, thus avoiding the effects of volumetric expansion.

The optimal temperature of pyrolysis for all dense pieces was found after a few tests. It is defined as follows: heating rate of 1 ^{o}C.min^{-1} up to 1000 ^{o}C dwell time of 2 h.

The dense sample 3D pieces obtained via warm pressing were evaluated according to their Hardness and Young's Modulus through indentation tests. They were also analysed by SEM and computed their thermal diffusivity.

3.2.2.2   Rapid hot pressing (sintering) of boron-modified AHPCS

Rapid sintering procedures were conducted in partnership with the group from professor Zoltan Lences, from Institute of

Inorganic Chemistry, Slovak Academy of Sciences.

Firstly, the powders from PCS_B30 and PCS_B60 samples were ball milled and then pyrolyzed to form an amorphous ceramic.

PCS_B30 samples were pyrolyzed through two methods (to form amorphous ceramics) for rapid sintering. The first in argon atmosphere up to 800 ^{o}C with 5 ^{o}C.min^{-1} heating rate and 2 h dwell time. The second sample PCS_B30 underwent thermal treatment in a furnace with ammonia controlled atmosphere until 200 ^{o}C (5 ^{o}C.min^{-1}) for 1 h, followed by pyrolysis in argon atmosphere up to 800 ^{o}C.

The aim at pyrolysing PCS_B30 in ammonia was to achieve a partial nitridation during crosslinking due to a relative dissolution of nitrogen in SiC. A small part of boron could act as a sintering additive while the remaining boron would bond to nitrogen from this partial nitridation in ammonia to forma B-N bonds. With this, it would be possible to evaluate the samples in relation to the ones solely treated in argon, since some authors consider that polymer-derived Si(B)CN ceramics are great candidates for application of high temperature electroceramics due to their excellently and controllable electrical as well as dielectric properties (CHEN, 2012; LIEW et al., 2002).

In relation to the PCS_B60 sample, this was only pyrolyzed in argon atmosphere with temperatures up to 800 ^{o}C to form amorphous ceramic and subsequently be rapid hot pressed.

After the pyrolysis stage to obtain these amorphous powder, the samples underwent the RHP process. The powder was placed in a graphite die lined with graphite foil. Each sample was rapid hot pressed from room temperature to 1750 ^{o}C at a heating rate of 100 ^{o}C.min^{-1} in argon. Progressive load up to 50 MPa was applied to the sample from 800 ^{o}C to 1000 ^{o}C with a dwell time of 15 min.

The electric current was shut off and the furnaces were cooled down to room temperature at a rate of 15 ^{o}C.min^{-1} (1750 until 1000 ^{o}C) and 20 ^{o}C.min^{-1} (1000 ^{o}C until reaching room temperature). It should be pointed out that in the rapid hot pressing the current supply is continuous.

Yet, another alternative method was applied. The samples (PCS_B30 in argon and NH_3 and PCS_B60) were ball milled in a vibrational agate mill for 2 h in a dry state and followed to the RHP, following the same procedure previously described, however, going up to 1800 ^oC temperature.

The conditions used during flash/rapid sintering of the samples are exhibited in Table 6.

Table 6: Rapid sintering methodology for PCS_B30 e PCS_B60 samples.

Sample	Samples Names	Sintering regime
PCS_B30 (800 ^oC, Ar)	**P1**	**1750 ^oC** (100 ^oC/min) - 50 MPa (800-1000 ^oC), holding time 15 min
PCS_B60 (800 ^oC, Ar)	**P2**	**1750 ^oC** (100 ^oC/min) - 50 MPa (800-1000 ^oC), holding time 15 min
PCS_B30 (200 ^oC, NH_3 / 800 ^oC, Ar)	**P3**	**1750 ^oC** (100 ^oC/min) - 50 MPa (800-1000 ^oC), holding time 15 min
PCS_B30 (800 ^oC, Ar)	**P4**	powder milled for 2 h in a dry state; **1800 ^oC** (100 ^oC/min)- 50 MPa (800-1000 ^oC), holding time 15 min
PCS_B60 (800 ^oC, Ar)	**P5**	powder milled for 2 h in a dry state; **1800 ^oC** (100 ^oC/min)- 50 MPa (800-1000 ^oC), holding time 15 min
PCS_B30 (200 ^oC, NH_3 / 800 ^oC, Ar)	**P6**	powder milled for 2 h in a dry state; **1800 ^oC** (100 ^oC/min)- 50 MPa (800-1000 ^oC), holding time 15 min
PCS_B30 (450 ^oC, NH_3 / 800 ^oC, Ar)	**P7**	powder milled for 2 h in a dry state; **1800 ^oC** (100 ^oC/min)- 50 MPa (800-1000 ^oC), holding time 15 min

Density, eletrical resistivity, eletrical conductivity and thermal diffusivity from the samples obtained through RHP were measured.

3.3   The design of macroporous Si-(B)-C ceramics

3.3.1   Synthesis of silver-functionalized PMMA spheres

Two different approaches were applied in this work to obtain sacrificial PMMA particles of different sizes. For the first one, monodispersed poly(methyl methacrylate) (PMMA) nanospheres of 350 nm (PAg350) where produced accompanied of polyelectrolyte brushes (PEBs, $[=NH_2] + \cdot Cl-$) using a modified emulsifier-free emulsion polymerization technique. After this, silver nanoparticles were stabilized on the surface of PAg350, as it will be discussed on Section 3.3.1.1.

On the second method, PMMA microspheres of 25 μm average particle size were produced by suspension polymerization in the presence of dual dispersion agents and functionalized with silver (PAg25). This method will be explained in more detail in Section 3.3.1.2.

3.3.1.1   PMMA/silver nanospheres by emulsifier-free emulsion polymerization

The method to obtain silver-functionalized monodispersed PMMA nanospheres (with 350 nm average particles size) was divided in two stages. Firstly, the nanospheres were produced accompanied by polyelectrolyte brushes, known as PEBs ([=NH$_2$] + ·Cl-). After this, on the second stage, the surface of these spheres with PEBs were functionalized.

Synthesis was based on the article by Wei et al. (2013), where dendritic Platinum (Pt) nanocrytals stabilized on the surface of PMMA microspheres were produced by the gas bubbling-assisted membrane reduction (GBMR) method.

In this work, the aim of inserting PEBs on the surface of PMMA spheres was so that it would interact with silver through electrostatic affinity and posterior reduction with (NaBH$_4$) leading to metallic Ag particles.

The intention to functionalize the PMMAs particles (for both sizes produced) in this work was so that later, in a continuation of this research, be possible to evaluate the microbiological characteristics of the filtrates using the obtained porous ceramic. Silver nanoparticles (NPs) are used for a wide range of commercial reasons to restrict microbial growth (SWEET; SINGLETON, 2011). Therefore, it is interesting to evaluate this material focused on antimicrobial uses, but it is necessary to study its effectiveness, the mechanisms of toxicity, and effects on the environment in future works.

This system is a technique derived from conventional emulsion polymerization in which polymerization is carried out in the absence of emulsifiers. Another important property for this type of latex generated through this technique is its low polydisper-

sity and small size compared with one obtained by conventional emulsion polymerization.

Therefore, emulsifier-free polymerization was applied for the synthesis of PAg350 with water-oil biphase double initiators. The PEBs ([=NH$_2$] + ·Cl-) came from the initiator 2,2'-Azobis(2-methylpropionamide)dihydrochloride (AIBA). All water in the forthcoming synthetic steps was distilled.

Firstly, a three-necked 500 mL round-bottomed flask with a Teflon stirrer was used. The flask was coupled to a condenser and a thermometer. Then, a mixture of acetone (50 mL) and water (150 mL) was added to it, which was heated to 70 ^{o}C using an oil bath.

After reaching this temperature, 80 mL of monomer methyl methacrylate (MMA) were added, followed by the addition, also at 70 ^{o}C, of a mixture of: 150 mL water, 0.18 g azobisisobutyronitrile (AIBN, oil phase initiator) and 0.31 g of AIBA (water phase initiator), previously set up in a becker. Nitrogen was bubbled to deaerate the mixture.

This system was kept under constant stirring (300 rpm.min^{-1}) at 70 ^{o}C temperature for 2 h. Finally, PMMA microspheres with PEBs were resulted from this process.

The number of PEBs was determined by adding the amount of AIBA in the preparation of nanospheres solution. In Figure 42 are found the chemical equations for the synthesis of PMMA microspheres accompanied with PEBs.

Figure 42: The reaction equations for the synthesis of PMMA nanospheres accompanied with PEBs ($[=NH_2] + \cdot Cl-$). Reaction (1) is the AIBA decomposition. Reaction (2) is the MMA polymerization under the action of the initiators.
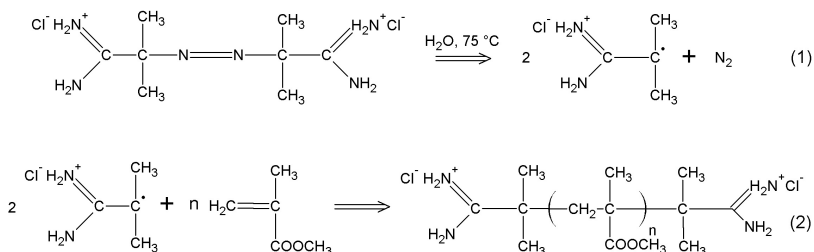
Source: Wei et al. (2013).

After the surface modification of the particles with PEBs, functionalization of PMMA sphere surface with silver was initiated. 250 mL of previously produced PMMA with PEBs latex (solid content ~10 wt%) were added to a three-necked 500 mL round-bottomed flask, coupled with a dropping funnel and under stirring (300 rpm). A solution of 0.01 M of $AgNO_3$ (0.976 g) and water (60 mL) was added to the latex. Approximately 15 minutes after the addition of this solution, stirring was halted and a pipette connected to the pipe to flow argon from the Schlenk line (N_2 aerator as shown in Figure 43), was placed in this round-bottomed flask and a relatively strong flow of nitrogen was bubbled through it.

The nitrogen was responsible for mixing and gently stir the solution, avoiding heavy particle collision and enabling the homogeneous addition of a reducing sodium borohydride ($NaBH_4$) solution. This reducing solution of $NaBH_4$ (0.02 M, 0.138 g $NaBH_4$ and 180 g of H_2O) was then added through to the dropping funnel and slowly dripped into the latex under nitrogen flow, all this at room temperature. The synthesis process was stopped after complete consumption of the $NaBH_4$ solution.

At the end of the reaction, milky coloured latex was transformed into milky yellow, the characteristic color of silver that

was formed on PMMA's particle surface, as it can be seen in Figure 43. This output was then distributed in containers and placed in the oven at 80 ^oC for 3 days or until the complete evaporation of water and obtainment of the nanospheres. Despite forming a structure of blocks, these spheres are not clustered, and can be easily transformed into fine powder after light maceration with pestle in agate mortar.

Figure 43: Apparatus for silver functionalized PMMA 350 nm synthesis.
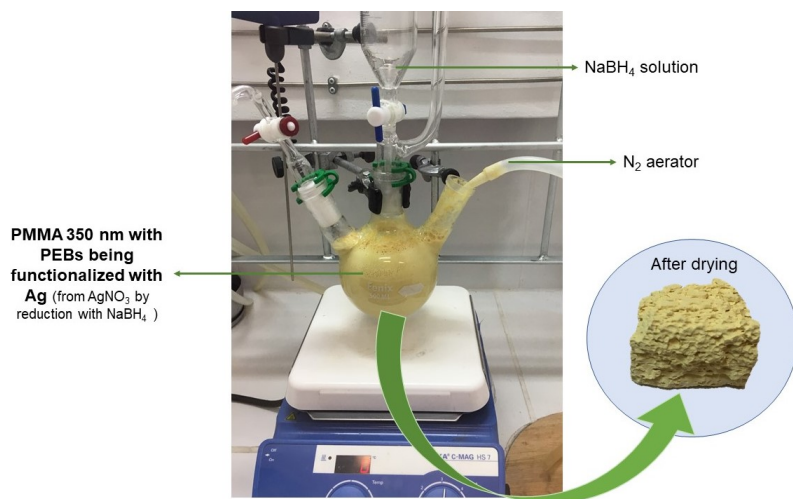
Computation on the quantity of silver included in the reaction were made in relation to the quantity of PEBs added, not exceeding 0.1 % of the mass in silver.

The nanoparticles (PAg350) were evaluated through SEM, TEM and particle size distribution to provide data on their size and silver composition.

3.3.1.2   PMMA/silver microspheres by W/O/W emulsion polymerization

PMMA microspheres were prepared by W/O/W (water-in-oil-in-water) emulsion polymerization in the presence of dual

dispersion agents.

W/O/W emulsion means a double emulsion in which oil (O) droplets enclosing water (W) droplets are dispersing in water (W).

Firstly, a solution of silver was prepared to be used in emulsion polymerization. For such purpose, a 1 mM $AgNO_3$ (250 mL of H_2O and 0.042 g of $AgNO_3$) solution and a 2 mM $NaBH_4$ (250 mL H_2O and 0.019 g $NaBH_4$) solution were prepared. In a 250 mL Erlenmeyer, 75 mL $NaBH_4$ solution was added and placed in ice bath for 10 minutes.

After this period, under constant stirring, 25 mL $AgNO_3$ solution was slowly poured (taking around 4 minutes). To this solution, 5 drops of PVA solution (0.3 wt%) was added to the Erlenmeyer to stabilize the silver nanoparticles for posterior use.

The polymerization reaction followed through by adding 50 mL of the silver solution into a becker and mixing with the oil phase composed of 10 g (10.63 mL) of MMA and 0.3 g of glyceryl stearate (GMS). This silver mixture with the oil phase was placed on an ultrasonic bath for 20 minutes.

Because a small amount of water was introduced into the monomer (MMA) phase during the addition of silver nanoparticles, water-in-oil emulsion was formed in the presence of GMS. In Figure 44 it may be visualized the formation of water/silver "nuclei" in the continuous phase (MMA and GMS).

Figure 44: Formation of water/silver "nuclei" in the continuous phase (MMA and GMS).

EGDMA (10 mL) (crosslink agent), solvent toluene (3 mL) and AIBN initiator (0.2 g) were added to the initial solution with silver, this mixture was then homogenized for 5 minutes at 6,000 rpm with Ultraturrax at room temperature resulting in a fine oil-in-water (O/W) emulsion. A PVA solution (3 g of PVA and 230 mL of water) was solubilized in ultrasonic bath and added to this mixture. It was then taken to Ultraturrax once more for one minute. Due to the synergistic effects of oil-soluble surfactant GMS and water soluble dispersing agent PVA, a W/O/W (water-in-oil-in-water) suspension was formed, and silver nanoparticles were dispersed in the monomer phase.

A chart with the stages described here is presented in Figure 45.

Figure 45: Steps for the synthesis of PMMA microspheres.
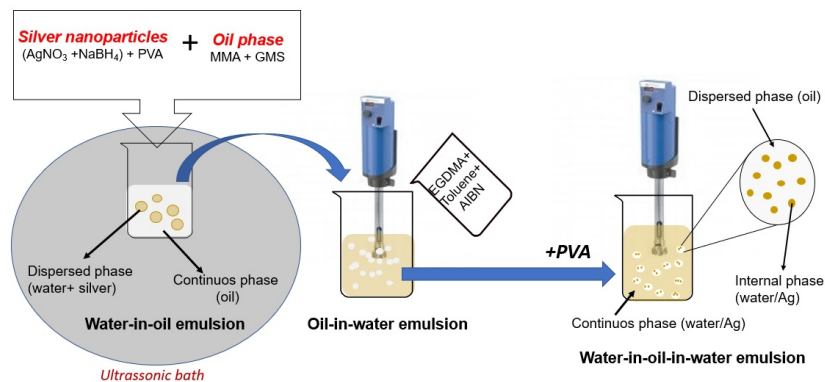
The W/O/W emulsion prepared was transferred into a 1 L doublewalled glass reactor equipped with a mechanical stirrer, a reflux condenser, thermocouple, and a nitrogen gas inlet. The reaction was maintained for 2 h at 80 ^{o}C with mechanical stirring of 300 rpm.

The weight of silver was ignored because the ratio of silver nanoparticles in the PMMA microsphere is less than 0.1 wt%.

The Ag containing micro-capsules produced were repeat-

edly washed in water and dried in oven for 3 days at 80 ^{o}C.

The microspheres were evaluated regarding their size, through TEM and particle size distribution, and also has their thermal diffusivity measured.

3.3.2 Warm pressing of porous Si-(B)-C ceramics

The warm pressing methodology for the production of Si-(B)-C ceramic porous 3D pieces, with or without silver functionalization, was performed with the same equipment (press) that the dense pieces. However, the focus was on using 28.5 and 25.6 mm diameter mold, for the porous tablets (foams).

Three types of foams were produced using the different PMMAs:

1. Commercial 25 μm PMMA (P25).

2. Silver added PMMA microesphere (PAg25), synthesized according to the method described in Section 3.3.1.2.

3. PMMA nanospheres (PAg350), following the production method presented in Section 3.3.1.1.

Based on previous works of this research group, 25.6 mm $\varnothing$ pieces was established as the value of 2 g of total sample (PCS_B30 + PMMA) for automatic pressing with heating slope of 10 ^{o}C.min^{-1} up to 120 ^{o}C maintained then for 30 min, using 5 tons powder compression for green body formation.

For the confection of green bodies, the percentage of pre-ceramic precursor (PCS_B30) was kept constant, being 20 wt% (added after ball milling as in the dense piece production) and 80 wt% of PMMA, when using only P25 or PAg25.

For the production of green bodies with PAg350, 2 g of sample were also used, where 20 wt% were PCS_B30 and 80 wt% of PMMA. However the wt% of PMMA were divided between P25 (80 wt%) and PAg350 (20 wt%).

For the production of foams with 28.5 mm $\varnothing$ mold the same percentage was used: 20 wt% of PCS_B30 and 80 wt% of P25. Two procedures were performed, where 3.2 g of P25 and

0.8 g of PCS_B30 were used. The heating slope used was 10 $^oC.min^{-1}$ up to 80 ^oC in the first procedure and up to 100 ^oC in the second. In both procedures the heating and pressing were maintained for 30 min, using 5 tons powder compression for green body formation.

After pressing, the mold was taken to the glovebox for green body removal from the mold. Thus, the green body remained for at most 48h in the glovebox before pyrolysis.

Pyrolysis was performed with heating rate of 0.5 $^oC.min^{-1}$ up to 450 ^oC, dwell time of 2 h and then 1000 ^oC. These parameters are shown in Figure 46.

Figure 46: Pyrolysis conditions for all warm-pressed pieces of this work (including porous pieces).
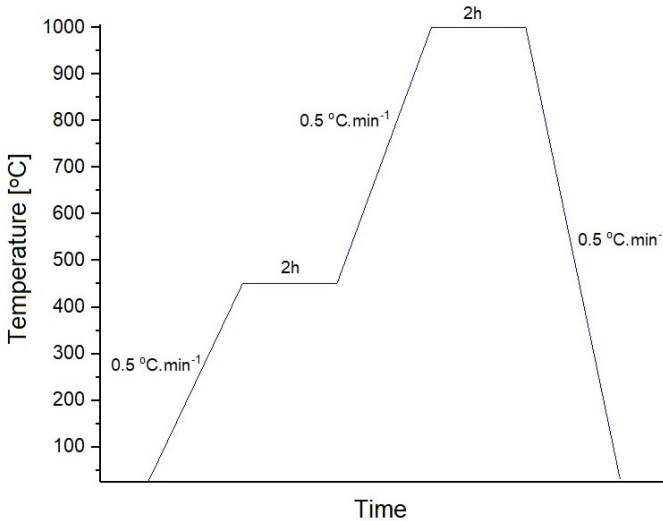
The extremely slow heating rate from room temperature to 450 ^oC is chosen to avoid undesirable cracks due to pyrolysis-gassing and differential shrinkage. Figure 47 shows the decomposition of PMMA spheres (like a space holder), that happens in temperature over 420 ^oC. PMMA particles have been removed completely and the porous structure was formed in Si-(B)-C amorphous foams.

Figure 47: Formation mechanism of Si-(B)-C porous structure using PMMA as sacrificial agent.
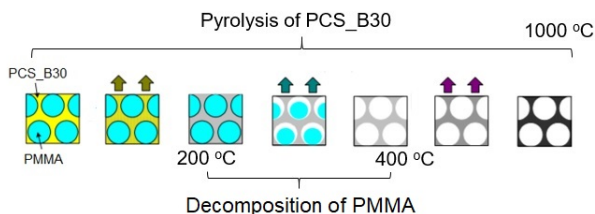
The obtained foams were evaluated via SEM, TEM and also had their thermal diffusivity estimated.

3.3.3 Functionalization of foams (coatings with Kraton)

Block copolymers based on styrene and butadiene (SBS), with basic structure, as seen on Figure 48, were donated by Kraton Polymers and used after dried in oven at 30 ºC during 48 h.

Figure 48: SBS (Styrene-Butadiene-Styrene) block copolymer.
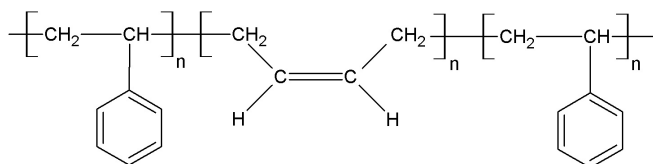
Four types of SBS were experimented, with different molar masses (Mw) and styrene content, being 29.5 % of styrene in SBS A, 30 % for B and C and 31 % for SBS D.

Before the functionalization of the green bodies obtained with the mixture of PMMA and PCS_B30, with the mesoporous layer, films were produced with the block copolymers to enable separate analysis of each of these in solvent. Therefore, they were separately dissolved in solvent toluene.

The solvent and the SBS were mixed together to form a precipitation-free solution with 10 wt% total polymer content. After stirring overnight, the solution was cast in a Teflon mold for solvent evaporation for 24 h at room temperature. After then, the polymer film was peeled from the PTFE (Poly(tetrafluoroethene)) mold, this operation produces the so-called "as-assembled" materials that later were analyzed by Atomic Force Microscopy (AFM).

To finalize the analysis of behavior of structure using swelling agents as well the SBS comportment concerning the micellar transformation, solutions were done using the block copolymers mixed with the borane-modified polycarbosilane precursor (PCS_B30) in solvent (liquid).

Different SBS concentrations were used keeping constant the quantity of PCS_B30 as 0.2 g. The ratios between the ceramic precursor and the SBS (PCS_B30:SBS) were: 0.33, 0.5, 0.66, 1, 1.33 and 1.5. Then these solutions were dripped (with a syringe) into the PTFE molds and kept for 24 h drying in glovebox. Figure 49 shows the procedure to prepare PCS_B30 + SBS films.

Figure 49: PCS_B30 solution with SBS in toluene on PTFE mold before (a) and after (b) the solvent evaporation.
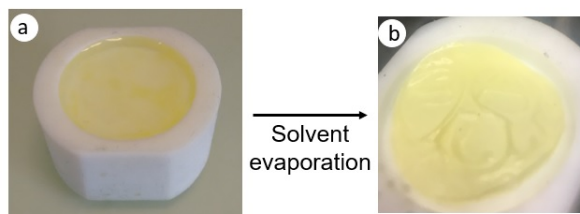
After then the PTFE mold with the sample (like a rubber after solvent evaporation) was ramped to 150 ^oC at 1 ^oC. min^{-1} under argon for 2 h in order to crosslink the structure. After that, the films were peeled from the mold to be pyrolyzed at a rate of 60 ^oC.h^{-1} up to 800 ^oC in argon. The thickness of the prepared specimen was about 0.5 mm. All the operations cited

here were done in a glove box with moisture and oxygen control. These films were evaluated by BET technique in order to obtain results for specific surface area (SSA).

For the functionalization of the foams with the mesoporous layer, the porous green bodies (foams using P25) were covered by dip coating with PCS_B30:SBS solution which presented the best results in previous tests regarding morphological changes (analysed through AFM and BET).

Foams coated with PCS_B30:SBS solution were then directly pyrolyzed at a rate of 60 ^{o}C.h^{-1} up to 800 ^{o}C. The dwell time was 2 h. In order to examine the micro/nanostructures SEM was performed in functionalized porous structures created.

3.3.4 Other methodologies using different additives

Two other methods were applied to evaluate the behavior of AHPCS precursor in terms of its ceramic yield, as well as the possibility of shaping via warm pressing with mixtures of different agents. Such agents may help obtaining the solid precursors during the crosslinking stage, thus making it viable warm pressing and posterior ceramization without a large shrinking effect.

Firstly, dicumyl peroxide (DCP) (linear formula $[C_6H_5C(CH_3)_2]_2O_2$ and 270.37 g.mol^{-1} molecular weight), well-known as a crosslinking agent, was employed as an alternative. Tests with DCP were performed using AHPCS (2 g) and DCP (2 wt%, 0.04 g), without adding solvent. Synthesis was initiated with a Schlenk flask which was kept in vacuum atmosphere for 30 minutes and followed by argon purging, adding AHPCS and DCP reagents while Ar was flowing.

Subsequently, thermolysis at 110 ^{o}C of this mixture was done under constant magnetic stirring at 300 rpm. Thermolysis in vacuum atmosphere was done until solidification (which took around 40 minutes).

This sample was then transferred to the glovebox and mass loss test (TGA) was done. Warm pressing was performed, where this material was deposited in a 25.6 mm diameter mold and pressed at 110 ^{o}C for 30 minutes and 5 tons compression load.

In the other method, DCP (1 wt% in relation to AHPCS) was also used as the crosslinking agent in a silver benzoate solution (silvere's benzoate linear formula: $C_6H_5CO_2Ag$ and molecular weight of 228.98 g.mol^{-1}), utilized as silver precursor (1 wt% in relation with AHPCS) in mixture with AHPCS and toluene (3 mL).

Silver benzoate, DCP and AHPCS were added to a Schlenk flask inside the glovebox. Posteriorly, the flask was removed from the glovebox and maintained under argon atmosphere, where toluene was added. This mixture was sonified for 20 minutes. After sonification, the flask was kept in a vacuum and heated to 110 ^{o}C for 1 h under constant stirring. This turned a solid as shown in Figure 50 This solid was grinded in agate mortar and mixed to 25 μm commercial PMMA (P25), with 20:80 proportion being 80 wt% of P25.

Figure 50: Solidified mixture of silver benzoate, DCP and AHPCS after thermolysis at 110 ^{o}C for 1 h in vacuum atmosphere.
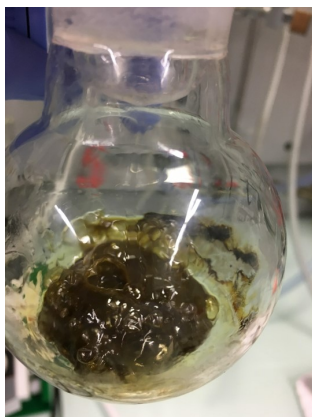
This powder (of DCP+silver benzoate+AHPCS solid and P25) was pressed utilizing a 25.6 mm diameter mold, under the same conditions described for foam production: 10 ^{o}C.min^{-1} heating slope, up to 120 ^{o}C, kept for 30 min using 5 tons for powder compression and green body formation.

For this method ceramic yield was evaluated (TGA analy-

sis) and SEM microscopy was performed.

3.4 Material characterization methods

In this section all techniques used in this work to characterize materials will be described.

3.4.1 Fourier-transform infrared spectroscopy

Through Fourier-transform infrared spectroscopy (FTIR) bonds and functional groups of the compounds were identified. The equipment used was a Nicolet 6700 Thermofisher Spectrometer with OMNIC software for acquisition and treatment of the spectres. For reagents, mixtures and ceramics studies, the spectral band used was from 400 cm^{-1} to 4000 cm^{-1}. The liquid products were analysed using commercial KBr (potassium bromide) cells (Sigma Aldrich) while the powders had added 2 % mass of KBr and were pressed with 5 t for tablet formation.

3.4.2 Raman spectroscopy

Raman spectroscopy provides complementary information to the ones obtained through FTIR; it enables the analysis of quasi-amorphous and crystallines systems. This technique is not destructive and does not require any sample preparation. It involved submitting the sample to a laser excitation and analyse its backscatter signal. This analysis allows to understand structural properties of the material. It is adequate for the structural study of carbons, even for heavily disorganized structures. The G band, commonly observed at 1580 cm^{-1}, is characteristic of graphitic structures and correspond to carbon atoms vibration. D mode, linked with unordered carbon, is found at approximately 1350 cm^{-1} and is the outcome of structural imperfections on the hexagonal structure of the graphene plane.

The device used for Raman analysis was a T64000 Horiba Jolin Yvon, with an argon-krypton laser, $\lambda = 647.1$ nm. The samples were analysed in powder form by being deposited in a

glass blade. The analysis window scans from 200 cm^{-1} until 3000 cm^{-1}. Labspec 5 software was used for the acquisition and analysis of the spectra. In the spectra, the observed band positions were compared to the similar analysis found on the literature.

3.4.3   Nuclear magnetic resonance spectroscopy

On the NMR analysis the bonds and functional groups of the elements contained in the analysed materials were determined with respect to ^{1}H nuclei. The characterized elements were dissolved in deuterated chloroform. Brüker Avance 300 spectrometer and TOPSPIN 2.6 software were used for acquisition and analysis of the acquired spectra.

Solid state samples were analysed via solid state NMR on the Condensed Matter Chemistry Lab in Paris (LCMCP) by Prof. C. Gervais using a Brücker Avance AV 300 MHz. The environments of boron (^{11}B), silicon (^{29}Si) and carbon (^{13}C) nuclei were analysed using a Bruker probe of 4 or 7 mm with frequency of 5 or 10 kHz. The RMN spectra (^{11}B) were registered in Bruker AVANCE 300, 500 or 700 spectrometers using a Bruker prove of 4 mm and 12 kHz frequency. The spectra were simulated using DMFIT8 program.

3.4.4   Thermogravimetric analysis (TGA)

Thermogravimetric analysis (TGA) was performed to determine the loss mass in relation to temperature changes. For this analysis, approximately 30 mg of powdered samples were placed inside a alumina crucible and inserted on a Netzsch STA, 409/449F3, equipment. During this process, the sample undergoes a heating of up to 1400 ^{o}C with a heating rate of 10 or 5 ^{o}C. min $^{-1}$ in argon atmosphere.

3.4.5   X-ray diffraction analysis (XRD)

A key analysis method for advanced ceramics, X-ray diffraction analysis (XRD) allows the characterization of the crystalline

structure of materials, it may also be used to quantify the size of the crystallites (Lc) from carbon materials. DRX is another non-destructive analysis technique, well-established as a mean to measure with good reproducibility structural characteristics of materials.

The equipment used for XRD analysis was a Bruker D8 Advance Serie II, Bruker D8 Advance Da Vinci, while EVA software aided on the analysis of the measured diffractograms. Acrylic disks with varied diameters and depths were used as support for the powder sample during the analysis. The scan ranged from 5 ^{o} and 90 ^{o} in 2 θ, with a 0.05 ^{o} step and 1 second acquisition time for each stage.

3.4.6 Microscopic analysis (TEM, SEM, AFM)

For microscopic structural evaluations, the structures of samples were observed with a transmission electron microscope (TEM) using a Jeol 2010 device, and the microstructures were evaluated with a scanning electron microscope (SEM) Jeol IT 300 LV. For some of the samples it was necessary to coat them with a conductive layer, such as gold or carbon, to improve image quality. SAED (Selected Area Electron Diffraction) was performed using the TEM illumination and it was recorded from an area of interest by placing an aperture in the imaging plane of the image forming objective lens.

The structures of SBS films were determined by Atomic Force Microscopy (AFM) using a Nanoscope III, quadrex controller. This way, a tip connected to a cantilever scanned the surface of thin films with SBS, through a piezoelectric ceramic that is responsible to move it. A laser beams over the cantilever is reflected to a set of photo detectors. The obtained electric signal is feed-backed to the computer while maintaining a constant deflection on the cantilever (contact mode) or the amplitude oscillation (intermittent or no contact mode). The corrections on the z heigh are recorded alongside the x and y locations of the sample, thus generating a topographic image of the studied object.

3.4.7   Density analysis by Gas Displacement Pycnometry and Archimedes' Principle

Gas pycnometry is a techinique to mesure the apparent volume and density. This technique is non-destructive as it uses the gas displacement method to measure volume, in this particular case was used Helium as displacement medium. AccuPyc II 1340 Pycnometer was the device used to measure the density of the researched powders.

The foam's density was measured by the Archimedes' principle. The foams were dipped in beaker with distilled water without touching the bottom or sides of the beaker. Calculations proceeded by recording the difference in mass before and after sample dipping (m_l) into the beaker, as in the following equation (3.5).

$$\rho_s = \rho_l \frac{m_s}{m_l} \tag{3.5}$$

In this equation ρ_s is the foam's density, m_s foam's mass prior the dipping into the beaker and ρ_l the density of water.

3.4.8   Instrumented nanoindentation

The instrumented nanoindentation analysis was done in partnership with the Universidade do Estado de Santa Catarina (UDESC) with the help of Professor Abel André Cândido Recco from Materials Engineering department.

To determine the hardness and modulus of elasticity of substrates, a CTR-UMT-02 indenter was equipped with a Berkovich diamond tip. Load of 40.0 mN was used on the samples. The depth of penetration was recorded and, from the loading and unloading curve, the modulus of elasticity and the hardness were determined using the method of Oliver e Pharr (1992).

3.4.9   Adsorption-desorption of gases - BET

The surface area per volume of the mesoporous ceramic produced in this work was measured by the area occupied by

a certain amount of adsorbed gas molecules on the surface of the material. This process is carried out by the adsorption and desorption of nitrogen gas on the surface and analyzed by the BET technique using Micromeritics ASAP-2020 equipment.

3.4.10 Thermal diffusivity

Thermal diffusivity was measured by the laser flash method (Model TC-7000, ULVAC, Yokohama, Japan), this analysis was performed by professor Zoltan Lences, PhD, do Institute of Inorganic Chemistry, Slovak Academy of Sciences.

The laser flash method involves heating one side of the sample with a laser pulse of short duration and measuring the temperature rise on the rear surface with an infrared detector. The thermal diffusivity is determined from the time required to reach half the maximum temperature of the resulting temperature rise curve for the rear surface (PARKER et al., 1961). Thermal diffusivity (a) was calculated according to the Equation 3.6.

$$a = k \frac{\rho}{C_p} \tag{3.6}$$

where a is thermal diffusivity, K the thermal conductivity, ρ bulk density and C_p the specific heat.

The thermal diffusivity is a thermophysical property measured under transient thermal transfer regime, which expresses the speed to which heat is transferred into the materials. Considering that thermal conductivity and diffusivity are intimately linked, as displayed on Equation 3.6, it is clear that material properties will affect both these variables.

3.4.11 Electrical conductivity

Electrical conductivity was measured by four point probe method at room temperature (RT). Four-point probe characterization is a standard method for studying the electrical properties of solids. A four probe measurement enables to drive current from two terminals and read potential through the sample.

By calculating the material's specific resistance ρ, as shown in Equation 3.7, it is possible to determine the conductivity of the sample.

$$R = \rho \frac{l}{A} \tag{3.7}$$

where R is the conductor's electrical resistance, l its length, A its transverse area and ρ the specific resistance or resistivity of the material.

Conductivity (σ), in turn, is the inverse of the resistivity:

$$\sigma = \frac{1}{\rho} \tag{3.8}$$

3.4.12   Granulometric distribution

Granulometric distribution analysis of PMMA samples were conducted with a Cilas 1190 laser particle size analyser. This research instrument incorporates three lasers which measure range between 0.04 and 2500 microns. The measure can be done in both liquid and dry mode; in this work, they were dispersed in distilled water and sodium lauryl sulfate (SLS) for this analysis.

3.5   Equipments used

A few equipments used in this research are not commonly employed. Therefore, they are revisited in this section.

Materials for Si-(B)-C synthesis are sensitive to both air and humidity and, therefore, must be manipulated in inert atmosphere. Hence, a chemical hood coupled with a standard Schlenk and vacuum/argon-line were constantly used throughout this project. This set up is shown in Figure 51. Argon with 99.9995 % purity, was purified as an inert gas passing through successive columns of phosphorus pentoxide and Sicapent$^{\text{TM}}$ (Sigma Aldrich) before connecting to the line.

A glovebox (Jacomex GP Campus) was used to preserve an inert atmosphere. After the synthesis, the materials were manipulated and stored in this equipment, filled with argon (as shown

Figure 51: Schlenk manipulations and vacuum/argon-line

in Figure 52). Hence, humidity and molecular oxygen levels were restricted to very low levels. This equipment is possesses two vacuum chambers, allowing materials to enter a neutral atmosphere without contamination. It has a closed loop gas circulation system with regenerative purifying loads, maintaining $H_2O < 1$ ppm and $O_2 < 1$ ppm.

Figure 52: Glovebox used in this research.

For uni-axial pressing, Atlas Auto Modelo Specac press was used in conjunction with heating molds (which were 13, 25.6 and 28.5 mm in diameter). These are shown in Figure 53.

Figure 53: a) Equipment used for warm pressing processes. b) Mold holder for heating (for 13 and 25.6 mm diameters molds).
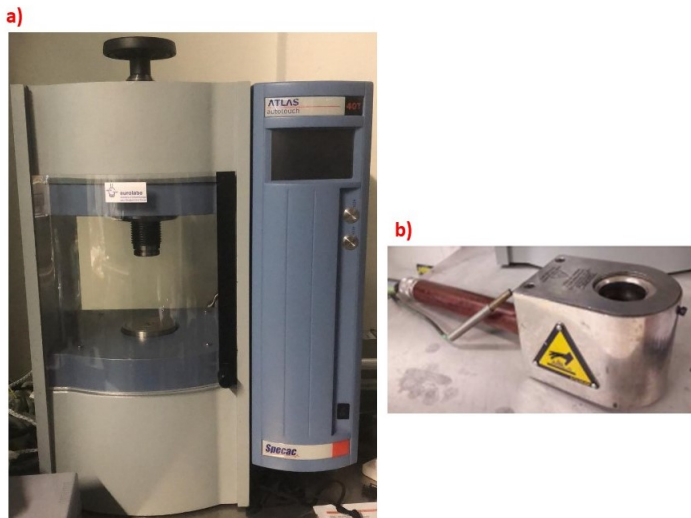
Some furnaces were used for thermal treatment of the materials according to the required pyrolysis temperature. For treatments up to 1000 ^{o} C, a Carbolite horizontal device, depicted in Figure 54, with alumina tube was used. In particular, this furnace was used for pyrolysis in argon atmosphere.

Higher temperature treatment (from 1100 ^{o}C to 1800 ^{o}C) were performed in a vertical furnace, shown in Figure 55. Treatments using these device were also done in argon atmosphere (99.9995 % purity) with the samples initially placed in a graphite box.

Figure 54: Furnace for preceramic precursor, dense and porous pieces pyrolysis using argon as atmosphere up to 1100 ^{o}C.

Figure 55: Vertical furnace for high temperature pyrolysis (between 1100 ^{o}C and 1800 ^{o}C).
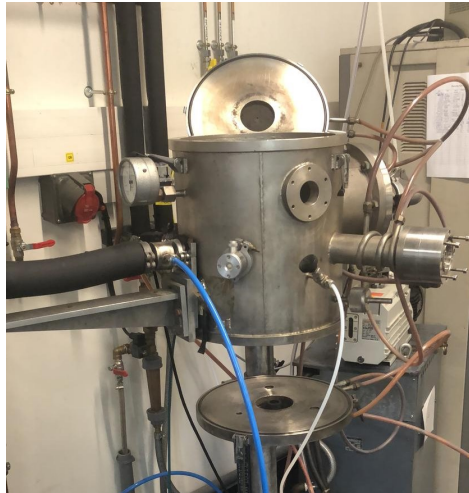
4 Results and Discussion

This chapter will be divided in 5 different sections:

- The first section, starting with (4.1), encompasses the characterization of AHPCS (SMP-10) as a preceramic polymer showing results regarding its structure and behavior during polymer-to-ceramic transformation.

- Section 4.2 is dedicated to the presentation of data showing the modified structure of the single source precursor, the effect of boron on the crosslinking, ceramic yield, and the evolution at different temperatures, using Ar and NH_3 as the thermal treatment gas.

- The third section 4.3 discusses the results of feasibility of the polymer-processing route for preparing dense and crack-free pieces (disks). It will, therefore, expose results of the usage of the following techniques: warm-pressing and rapid sintering, for production of these ceramic pieces with a range of sizes.

- Section 4.4, is dedicated to results on the design of macroporous Si-(B)-C ceramics, with the study for the fabrication of porous SiC-based ceramic pieces (foams) via PDC route using PMMA as sacrificial agent and co-assembly technique using BCPs to coat the foams. SBS as block copolymer and its structural arrangement will be discussed, as well as the functionalization of the PMMA polymeric particles with silver.

- The final section (4.5), additional results of experiments which were not the main objective of this thesis are presented. They are related to the application of additives to AHPCS, such as dicumyl peroxide and silver benzoate. Therefore, analysis of ceramic yield and production appli-

cability of ceramic structures with these will be shown in this section.

4.1 AHPCS as preceramic precursor for SiC

Here the characteristics of AHPCS ceramic precursor are presented through the stages of crosslinking and ceramic conversion. The main goal is to demonstrate the behavior of the pure precursor for subsequently, on the following sections, evaluate the modification process with other reagents explored in this work. In addition to this, the potential of SiC and its important characteristics and wide applications, in special for high temperature and harsh environment settings will be ratified.

4.1.1 AHPCS characterization

AHPCS, as shown in the previous chapters, possesses allyl (10 %mol) group molecular structural, which collaborates for two different mechanisms during the crosslinking process: hydrosilylation and dehydrocoupling process.

At room temperature, AHPCS is liquid, which exempts the use of solvents for some types of mixtures, allowing for the direct production of the ceramic (SiC) from the pure precursor.

Structure investigation of liquid AHPCS is presented in Figure 56 by means of FTIR. Its ^{1}H NMR spectroscopy is shown in Figure 57.

Hence, it may be see a large number of peaks between 740 - 1040 cm^{-1} on the infrared spectrum. These are attributed to the stretching and deformation vibrations of: Si$-$CH$_3$ rocking (around 742 cm^{-1}), Si$-$C stretching (833 cm^{-1}), Si$-$H bonds (928 cm^{-1}). There is also the presence of CH$_2$ bending in Si$-$CH$_2$$-$Si at 1037 cm^{-1}. This last band, as well as the ones at 1351 cm^{-1} and at ca. 2910 cm^{-1} (C$-$H stretching in Si$-$CH$-$), are present in all samples and indicate the backbone of AHPCS (Si$-$CH$_2$$-$Si). Moreover, the Si$-$H grouping are also visible in strong band at ca. 2117 cm^{-1}. For the allyl groups the bands at 1629 cm^{-1} (C=C stretch in $-$CH=CH$_2$) and 3076 cm^{-1} (C$-$H
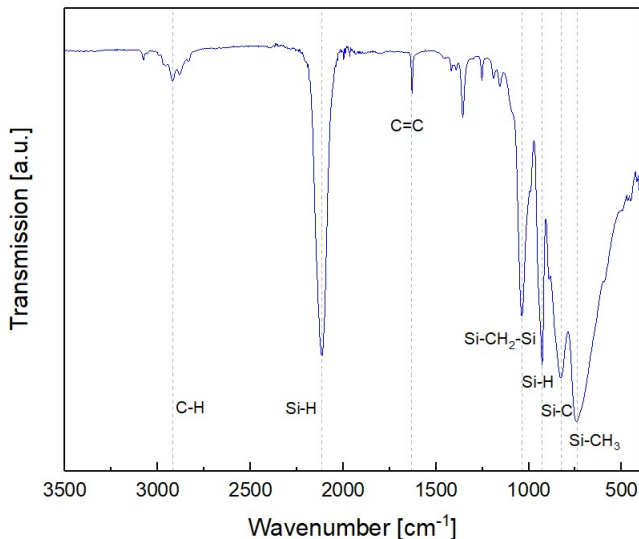
Figure 56: FTIR analysis for preceramic precursor AHPCS (SMP-10).

stretch in $-CH=CH_2$) are attributed to this group. The absorption band at 1251 cm^{-1} corresponds to the $Si-CH_3$ rocking (bending).

In agreement with the IR spectrum for the liquid polymer, the RMN ^{1}H spectrum also demonstrates the presence of the same groups, where signals ranging from 3.4 to 4.10 ppm are consistent with the proton absorption of SiH_2 and SiH groups: 3.40 - 3.9 ppm for the $-SiH_3C\equiv$ grouping and 3.90 - 4.10 ppm relative to SiH and $-SiH_2CH_2$ groups. The $Si-CH_2-CH=CH_2$ bond appears at ca. (1.50 - 1.9 ppm), also the relative signals of the two multiples $-Si-CH_2-CH=CH_2$ (5.77 - 5.9 ppm) and $-Si-CH_2-CH=CH_2$ (4.90 – 5 ppm), indicating the presence of allyl groups to the side chain of the polymer. The groups of signals around 0 ppm are assigned to the $Si-CH_3$ and $Si-CH_2$ functionalities.

It is important to highlight that the research group led by the co-advisor of this thesis (Samuel Bernard), while investigat-
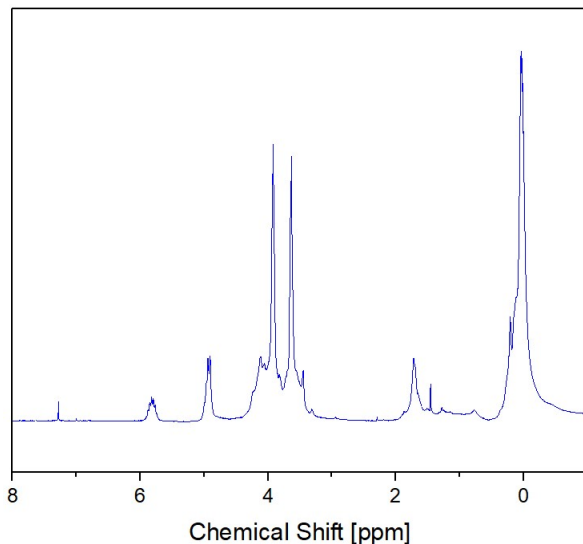
Figure 57: ^{1}H NMR analysis for preceramic precursor AHPCS (SMP-10).

ing elemental analysis of AHPCS, noticed a higher percentage of carbon than notified by the supplier (Starfire system®). It was also observed the presence of oxygen, in low quantities. These differences, in relation to the theoretical composition suggest the presence of $O-CH_2$ or $O-CH_2-CH_3$ bonds at the end of the polymeric chain (SCHMIDT et al., 2017).

Elemental analysis for the chemical species present in the AHPCS were performed in Pascher Laboratory in Germany and the results are introduced in Table 7.

As a reference, the formula for AHPCS's molecular structure $[(Si(CH_2CHCH_2)HCH_2)_{0.1}(SiH_2CH_2)_{0.9}]_n$, based on $Si_{1.0}$, was used.

All these results were in agreement with observations made from other recent articles studying SMP-10 ceramic precursor for advanced ceramics production (SCHMIDT et al., 2017; YU et al., 2010; LIJUAN et al., ; HONG et al., 2014; YU et al., 2014; MUHE et al., 2009).

Table 7: Pre-ceramic polymer AHPCS elemental analysis.

Composition	**Si** (wt%)	**C** (wt%)	**H** (wt%)	**O** (wt%)	Empirical Formula
Theorical	59.05	31.89	9.06	0	$Si_1C_{1.3}H_{4.4}$
Analysis experimental	54.77	34.97	8.31	1.95	$Si_1C_{1.5}H_{4.2}O_{0.1}$

4.1.1.1   Polymer to ceramic transformation of AHPCS

One of the most important analysis to assess the applicability of a preceramic polymer is looking at the ceramic yield through thermogravimetric analysis (TGA). As AHPCS is the basis precursor utilized in all the chemical reactions in this work, it is of key importance to understand its behavior before evaluating it in its following applications.

Hence, through TGA analysis it was observed a ceramic yield of approximately 70 wt% when heated up to 1400 ^{o}C. This result can be visualized in the graphic in Figure 58.
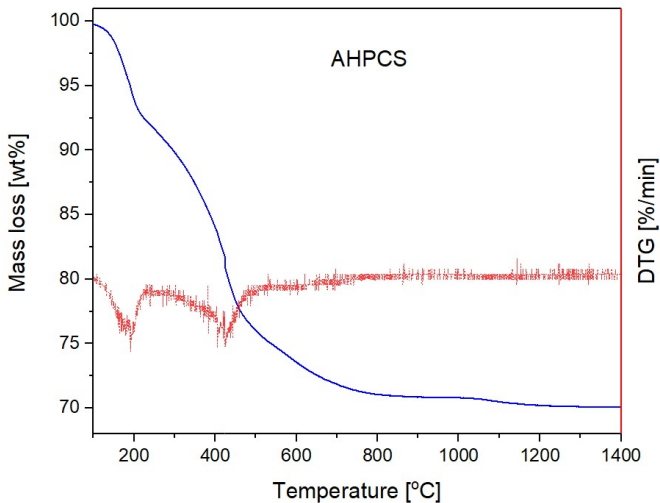
Figure 58: AHPCS thermogravimetric analysis up to 1400 ^{o}C under argon atmosphere: in blue weight loss curve and in red weight loss derivative.

This outcome is in agreement with the expected valued and similar to what has been observed by other authors (ACTON, 2012; KAUR, 2016).

Moreover, observing this graphic in more detail, it can be seen that weight loss occurs in two main stages. The first, accounting for around 7 wt% of weight loss, happens slightly below 200 ^{o}C. This may be attributed to oligomers of low molecular weight, but mainly to hydrogen (m/z = 2). Therefore, during this stage occurs polymer reticulation through allyl groups and Si−H through hydrosilylation (without weight loss).

The second weight loss stage (around 13 wt%) occurs between 300 and 650 ^{o}C due to dehydrocoupling, which represents the conversion of the preceramic polymer into an inorganic materials, liberating H_2, SiH_4 (m/z = 32), and CH_3SiH_3 (m/z = 46).

No significant weight loss happens at temperatures above 800 ^{o}C. This is due to the conclusion of the transformation process of polymer into ceramic, which generally ends at 800 ^{o}C. Similar results were observed by Kaur, Riedel e Ionescu (2014a) when preparing dense monoliths from AHPCS.

In practice, in tests with pure AHPCS, it was noted that the temperature for the formation of viscous gel, or crosslinking initiation (the temperature that the tridimensional polymer net begins to form, greatly increasing the viscosity) is around ∼200 ^{o}C and only above such temperatures, ∼230 ^{o}C, AHPCS becomes solid.

This crosslinking reaction initiation may be observed through infrared analysis for different temperature, this is shown in Figure 59. It is possible to observe the disappearance of the allyl groupings (1629 cm^{-1}, C=C stretch in −CH=CH$_2$ and 3076 cm^{-1}, C−H stretch in −CH=CH$_2$) of the polymer at 200 ^{o}C, indicating the crosslinking reaction at this temperature. Associated to the temperature rise and the disappearance of the allyl group is the reduction of band intensity for Si−H bonds (ca. 2117 cm^{-1}), suggesting that the hydrosilylation stage is the first reaction that initiates reticulation. The temperature rise (450, 700 and 800 ^{o}C) is linked with significant reduction in the bands at-

tributed to Si−H, C−H and CH$_2$ unities. The bands attributed to these groups and unities disappear to product the basic SiC net.
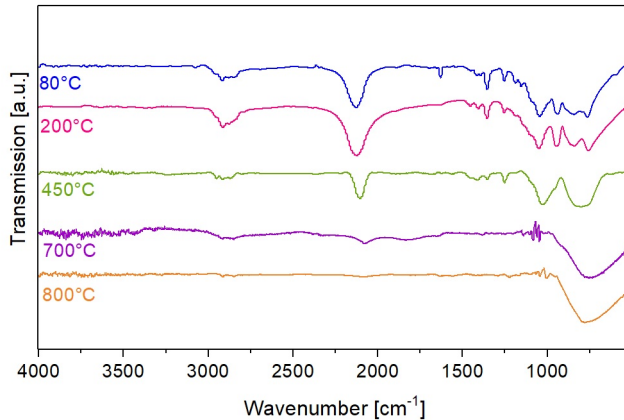
Figure 59: FTIR analysis for preceramic precursor AHPCS with temperature increasing.

Yet, regarding the transformation of polymer into ceramic, it may be observed through the diffractogram (XRD) in Figure 60, despite annealing at elevated temperatures (1500 ^{o}C), AHPCS is still not completely crystalline and the formation of β-SiC prevails, even with small α-SiC amounts.

At 1500 ^{o}C, the characteristic peaks of the β-SiC phases are distinct and attributed to the plane (111) at $2\theta = 35.67$ ^{o}, (220) at $2\theta = 60$ ^{o} and (311) at $2\theta = 71,8$ ^{o}. Moreover, it may be observed the formation of shoulder on the peak, representing the polytipe 2H- SiC (plane (100)) appearing at $2\theta = 33.6$ ^{o} for 1500 ^{o}C, which becomes clearer on the peak for 1800 ^{o}C.

It is also discreetly present at 1500 ^{o}C the representative deformation of β-SiC (222) plane, which is confirmed at 1800 ^{o}C through the presence of the $2\theta = 75.5$ ^{o} peak. A similar case to the $2\theta = 41.2$ ^{o} position representing the plane (200) of β-SiC. Moreover, at 1800 ^{o}C appears the 26.67 ^{o} peak which is linked with (002) plane from graphite.
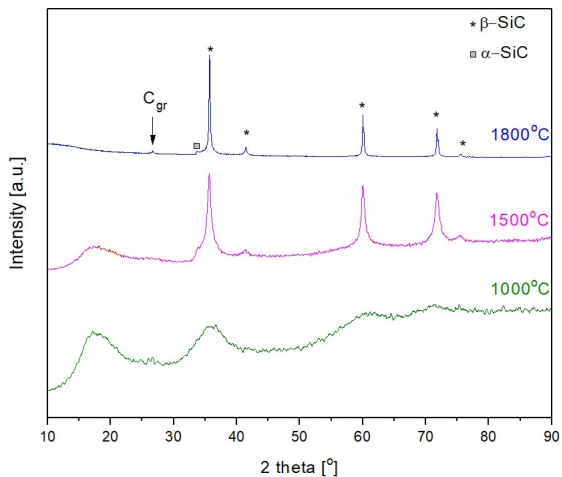
Figure 60: AHCPS's X-ray diffraction at 1000, 1500 e 1800 ^{o}C temperatures in argon.
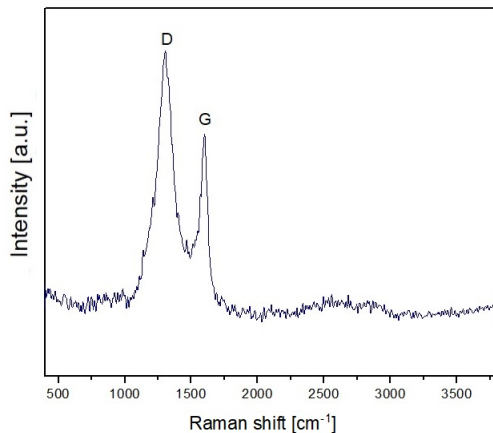
Figure 61: Raman Spectra for AHPCS at 1000 ^{o}C.

In the Raman spectrum of the ceramic precursor at 1000 ^{o}C, it is confirmed the free carbon in the bands at approximately 1305 (D) and 1600 (G) cm^{-1}, which are characteristic of sp^2 carbon.

Nonetheless, it is not present SiC's representative band between 800 and 1000 cm^{-1}, which highlights the amorphous phase of SiC at this temperature.

4.1.2 Summary

This first characterization stage of the AHPCS polymer verified that it possesses a significant weight loss during pyrolysis (around 30 %), however, its use is still interesting for many direct applications, as after pyrolysis it becomes an amorphous ceramic at high temperatures. However, as it can be seen through Raman analysis, there is a presence of free carbon sp^2, which may comprise its resistance to oxidation and ceramic corrosion (given that in this work the pyrolysis temperature for the shaped polymers will be 1000 ^{o}C).

Thus, to form a superior quality ceramic and increase the processability of the polymer, a chemical modification fo the AHPCS was performed. Boron containing SiC single-source-precursor is a very interesting alternative, due to the greater homogeneity of the resulting ceramics from the molecular addition of boron through the reaction with BDMS.

The aim of inserting reactive groups was of reducing the crosslinking temperature, hence turning the polymer processing into ceramic more viable, with lower and faster heating. Furthermore, the validation of the shaping possibilities, with more structure green bodies formation, faster and without losing SiC ceramic's stability at higher temperatures is very attractive, as well as the increase of ceramic yield. The obtained results with this molecular modification using boron can be seen in the following sections.

4.2   Boron Modified AHPCS

As previously discussed, groups of allyl- and hybrid-substituents at silicon in AHPCS (SMP-10) contribute in the adjustment of these polymer structure. With the insertion of boron in the allyl grouping it is aimed at producing a single-source-precursor Si-(B)-C through the hydroboration reaction.

Thus, analyses were conducted to verify AHPCS behavior under these hydroboration reactions. These results are of extreme importance, given that they influence the final result regarding the production of dense and porous ceramics.

4.2.1   Chemical characterization of boron modified AHPCS

Two compounds of different molecular boron quantities were studied: PCS_B30 (total hydroboration) and PCS_B60 (half hydroboration). The infrared spectra at room temperature of both of these compounds, in contrast with AHPCS polymer, can be see in Figure 62.

The corresponding AHPCS peaks, which represent allyl groups, are located at 1629 cm^{-1} and 3076 cm^{-1}. Thus, it may be noted a strong reduction of these peaks, or even their disappearance. This indicates, for the PCS_B30 sample, the total hydroboration, showing that the BDMS reaction occurred as expected. Following the same tendency, PCS_B60 does not show a complete hydroboration, thus occurring only a reduction of these peaks instead of completely disappearing.

This same reduction was able to be observed through the allyl groups spectra in hydrogen NMR analysis, as presented in Figure 63.

The peaks relative to the two multiplets 5.77-5.9 ppm $-Si-CH_2-C\mathbf{H}=CH_2$ and $-Si-CH_2-CH=C\mathbf{H}_2$ (4.90–5 ppm) are reduced, indicating hydroboration. However, contrary to what was seen in the FTIR spectra, it still may be observed the existence of allyl groups in the sample with greater boron incorporation (PCS_B30).

Figure 62: FTIR analysis for PCS_B30 and PCS_B60 in comparison with AHPCS.
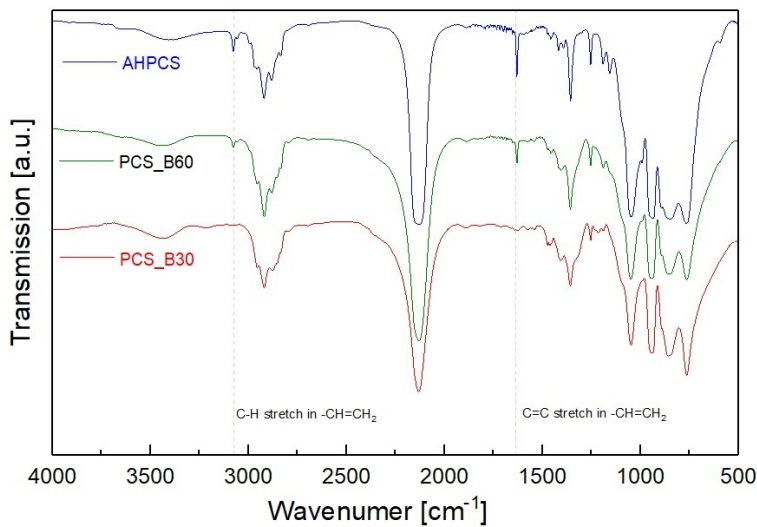
Some signals appear between 1.26 and 1.73 ppm, which designate alkyl chains resultant from the incorporation of boron by hydroboration at the β and/or γ position of the silicon (β location: $CH_3 - CH\mathbf{B} - CH_2Si$; γ location: $CH_2\mathbf{B} - CH_2 - CH_2Si$). The representative signals of the residual solvent (toluene) at approximately 7.26 and 2.36 ppm and BDMS in ca. 7.28 and 2.38 ppm appear at the same zones, making this analysis more complex, despite of a representative increase of these bands in the sample with greater boron quantity (PCS_B30).

To evaluate the boron insertion, elemental analysis of the PCS_B30 sample was performed, as it can be seen in Table 8.

This analysis showed a higher percentage of equivalent boron in PCS_B30 than expected, as the atomic ratio is Si:B = 29.4, a close measure to the one determined based on the quantity of reagents on the performed synthesis (=AHPCS, BDMS). It is also worth pointing out that the oxygen quantity also increased a little, however, it remains insignificant.

Solid-state NMR spectroscopy was performed to better anal-

Figure 63: ^{1}H NMR of PCS_B30 and PCS_B60 in comparison with AHPCS.
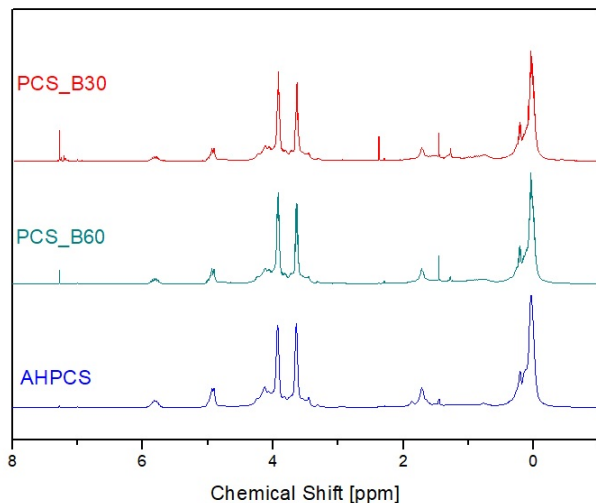
Table 8: PCS_B30 sample elemental analysis.

Composition	Si (wt%)	B (wt%)	C (wt%)	H (wt%)	O (wt%)	Empirical Formula
	52.3	0.7	35.2	8.8	1.9	$Si_{1.0}B_{0.034}C_{1.6}H_{4.7}O_{0.3}$

Referenced to $Si_{1.0}$ and normalized to 100 wt%. Oxygen values < 2 at%. Schmidt et al. (2017)

ysis the structural modifications that occurred with the addition of boron to the samples. Local [11]B, ^{13}C and [29]Si environments were probed, following the methodology described by Schmidt et al. (2017), from this research group. Figure 64 presents the results from this analysis.

The cross polarization technique (CP) was used for ^{13}C and ^{29}Si NMR analyses towards obtaining spectrogram signals with shorter acquisition times. Solid-state ^{11}B MAS NMR recorded at 7 T exhibits a main resonance with a maximum around 5 ppm. This position does not correspond to the chemical displacement

Figure 64: ^{1}H NMR of PCS_B30 and PCS_B60 compared to AHPCS.
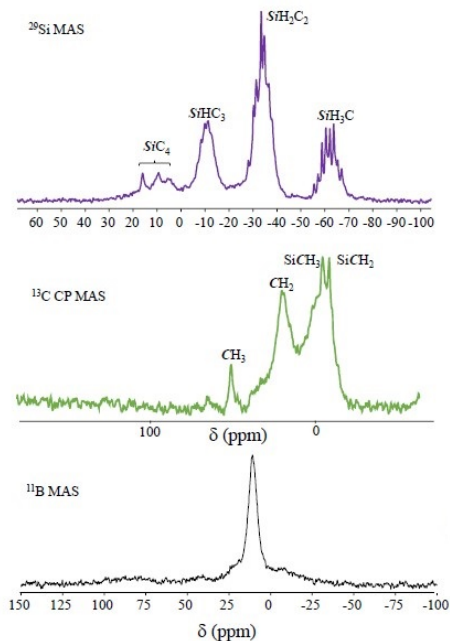
Source:Schmidt et al. (2017)

of the BC_3 environments, it is probably derived from vinyl unities, which are known to appear at ca. 60-80 ppm and boron modified polysilazanes (SCHMIDT et al., 2017; GOTTARDO et al., 2012). In addition to this, the signals related to C_2BH or CBH_2 environments are typically observed between 70 and 80 ppm (SCHMIDT et al., 2017).

The signals observed between 5 and 30 ppm may be attributed to unities of BN_3 from trigonally coordinated boron, which indicate the presence of B-C bonds, which is unlikely as it has already been observed by Schmidt et al. (2017) and Berger et al. (2005). Therefore, as boron may only be linked to H and C atoms in this system (as it can be seen through the structural

formula of PCS_B30), this result may be attributed to tri or tetra-coordinated boron of the BHxCy ($0 < x \leq 4$, $0 \leq y < 4$) type.

However, according to some previous findings from this research group (Schmidt et al. (2017)), in tests were computations of the parameters for optimized geometries of simple models presenting representative boron environments, based on the principle that the boron content is very low and that is unlikely the formation of some environments (as BH_3C and BH_4, for example), it was concluded that the mains signal is due to boron-oxydized environments.

Elemental analysis of the PCS_B30 sample demonstrated the low amounts of oxygen content. Therefore, the presence of BO_3 groups (19 ppm) and BO_4 groups (0 ppm) can be considered viable.

The ^{13}C RMN spectrum was performed with this same sample (PCS_B30). Allyl $-CH_2-CH{=}CH_2$ grouping signals, which were predicted around 135 ($=CH_2$) and 115 ppm ($CH=$) were not observed.

However, it is noted the presence of carbon for $-Si-CH_2-CH(B)-CH_3$ (19 ppm), $-Si-CH_2-CH-(B)-CH_3$ (26 ppm) and $-Si-CH_2-CH_2-CH_2B$ (from 18 to 32 ppm) environments (MAJOULET et al., 2011; GERVAIS et al., 2003; SCHMIDT et al., 2017). The presence of these groups confirm that hydroboration is complete and not region selective.

The main signals from -10 to 3 ppm may be attributed to $Si-CH_3$ and $Si-CH_2$- groups, while the signal at 50 ppm is related to the $-OCH_3$ environment.

^{29}Si RMN spectrum from PCS_B30 indicates the presence of signals at -62 ppm, -34 ppm, -10 ppm and between 2 and -18 ppm, respectively attributed to SiH_3C, SiH_2C_2, $SiHC_3$ and SiC_4 environments.

Combining the results presented in this section, it can be concluded that the modified structure with boron has a very complex form. The presence of unexpected radicals, such as $SiCH_3$ and $-OR$ ($R = -CH_2-$ and $-CH_3$) contribute to this complex yield. Nonetheless, this does not affect the synthesis of modified

AHPCS with boron, as these groups probably do not participate in the reaction.

The main expected reaction is, in fact, between the bonds $B-H$ from BDMS and the allyl groups linked to Si in AHPCS. Thus forming $\equiv Si-C-C-C-B=$ or $\equiv Si-C-C(B=)-C\equiv$ units (SCHMIDT et al., 2017).

4.2.2 Polymer to ceramic transformation of boron modified AHPCS

Ceramic conversion of the hydroborated compounds was studied though TGA in argon atmosphere. Boron incorporation results in an increase of AHPCS crosslinking, turning the hydroborated samples in this study solid at lower temperatures and with direct effect on the ceramic conversion.

This behavior can be observed in Figure 65, where a noticeable reduction in the weight loss of the polymers can be seen with the inclusion of boron.

As expected, PCS_B30 showed an increase of the ceramic conversion, increase of almost 18 wt% over pure liquid AHPCS.

It is very clear the change in behavior of the derived weight loss graph, depicted in Figure 66, where between the temperatures of 100 ^{o}C and 250 ^{o}C there is a less accentuated loss of oligomers for compounds with boron, suggesting that it limits the volatility of the oligomers at low temperatures.

As indicating in this graph, it may also be noted that there is a significant difference in weight loss in the 300–500 ^{o}C range for AHPCS when compared to hydroborated AHPCS, which will have a greater effect on the final ceramic yield of these two compounds.

Hence, as verified in the work by Yu et al. (2010) and originaly in the work by Puerta et al. (2003), for both normal and boron modified AHPCS, the weight loss up to 300 ^{o}C were due to the loss of H_2, CH_4, and CH_3-CH_3. While at the 300 - 500 ^{o}C region, AHPCS modified with boron (9-borabicyclo[3.3.1]nonane, called 9-BBN) exhibited significantly lower weight losses (2 %) than those observed for AHPCS (13 %). This behavior is jus-

Figure 65: TGA graph of the PCS_B30 and PCS_B60 samples in comparison to AHPCS.
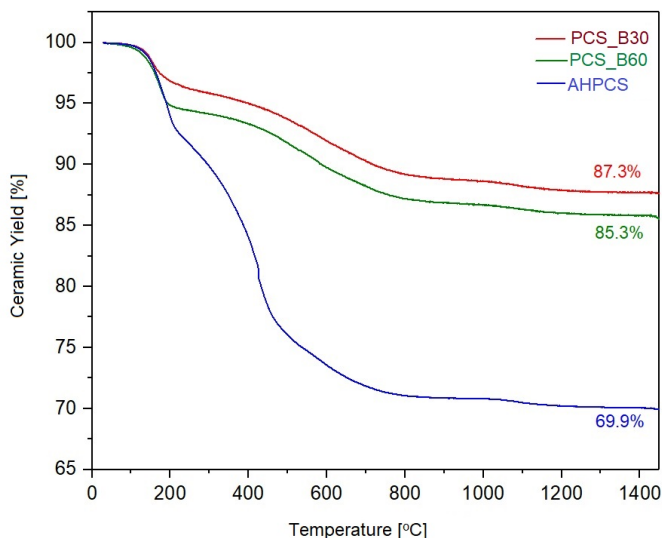
tified by that at the 300–500 ^oC range the evolution of volatile gases (CH_3CH_3, SiH_4 and CH_3SiH_3) were suppressed in 9-BBN-modified AHPCS, whereas the AHPCS showed losses of these three gases. As a result, the introduction of a small amount of boron to the polymer precursor improved the final ceramic yield, which for Puerta et al. (2003) was (for AHPCS-9-BBN-derived ceramics) of 82 - 85 % at 1300 ^oC, higher than that of AHPCS (73 % of ceramic yield), as also observed in this work.

Considering Figure 67, the effects of temperature on the PCS_B30 structure in argon atmosphere may be visualized.

Considering pyrolysis of the PCS_B30 sample (solid, powder), it may be observed a great reduction of the intensity in the Si–H (ca. 2130 cm^{-1} 940 cm^{-1}) absorption bands and its disappearance at 700 ^oC. This is due to the cleavage of the Si–H (Si-H = Si + H) bond. This complete disappearance confirms the complete crosslinking of the polymer.

Furthermore, there is a very considerable reduction of the

Figure 66: Graph of the derived weight loss of PCS_B30 e PCS_B60 compared to AHPCS.
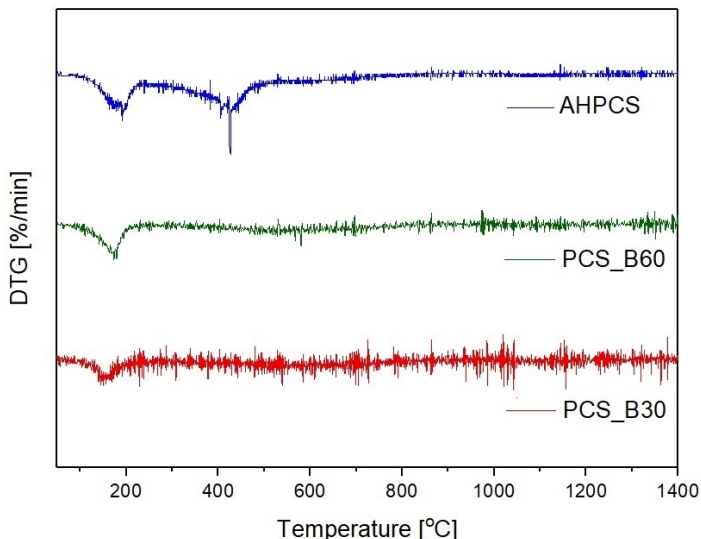
bands between 1352 and 1510 cm^{-1}, which represent aliphatic hydrocarbons. This change indicates hydrosilylation occurring at low temperatures. This reaction, therefore, also leads to the formation of carbosilane chains and polymer reticulation. After the hydrosilylation process is complete, it is expected that the subsequent crosslinking to be based solely on the dehydro-coupling reactions, which also influence on the reduction of the representative band of Si-H ($\equiv$Si$-$H$+\equiv$Si$-$H$\rightarrow\equiv$Si$-$Si$\equiv+$H$_2$) bonds.

It may also be observed the reductions of the Si$-$CH$_2-$Si groups at 852 and 1047 cm^{-1}, as well as the increase of the band attributed to SiCH$_3$ group at 1251 cm^{-1} (700 ^{o}C) . This strong intensity increase clearly shows the Si-H and SiCH$_2$Si bonds and the formation of radicals, such as Si$-$CH$_3$ (Si$-$CH$_2$ radicals generate Si$-$CH$_3$ groups by reacting with H· radicals).

Interestingly, in an article by Yu et al. (2010) doing the modification of polycarbosilane with boron, absorption band of

Figure 67: PCS_B30 sample FTIR in relation to different thermal treatment temperatures in argon atmosphere.
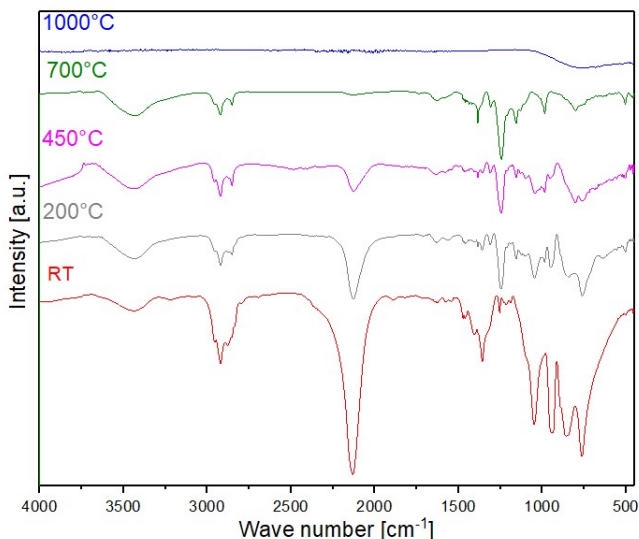
Si−CH$_3$ at 1251 cm^{-1} was significantly reduced with temperature increase. This phenomenon was attributed to the decomposition of organic side groups. This different behavior can be explained by the volume of added boron, as well as the different production route taken in this work.

A band appears in ca 1156 cm^{-1}, which may be attributed to BC$_3$ groups. Also, there is a complex of diffuse bands at approximately 1300 and 1700 cm^{-1}. Amorphous carbon representative band, which may be observed at 1382 cm^{-1} and the bands 1474 and 1627 cm^{-1} may indicate the presence of boron at BCB and CBC unities, however, it is difficult to define them, as discussed also by Schmidt et al. (2017).

At 1000 ^{o}C, signals become more ample, as a consequence of the formation of a amorphous ceramic net. The spectrum only show the representative bands of vibrations of Si-C bonds, typically observed at around 790 cm^{-1}.

4.2.2.1   XRD and Raman analysis in Argon atmosphere - Si-(B)-C

In Figure 68 the diffractogram of the PCS_B30 sample at different temperatures is presented. Through this graph it is possible to observe that at 1000 ^{o}C the sample is amorphous and disordered, increasing the temperature to 1200 ^{o}C causes a sharpening of the peaks, which indicates incomplete crystallization.

Figure 68: Diffractogram of the PCS_B30 sample at different temperatures in argon atmosphere.
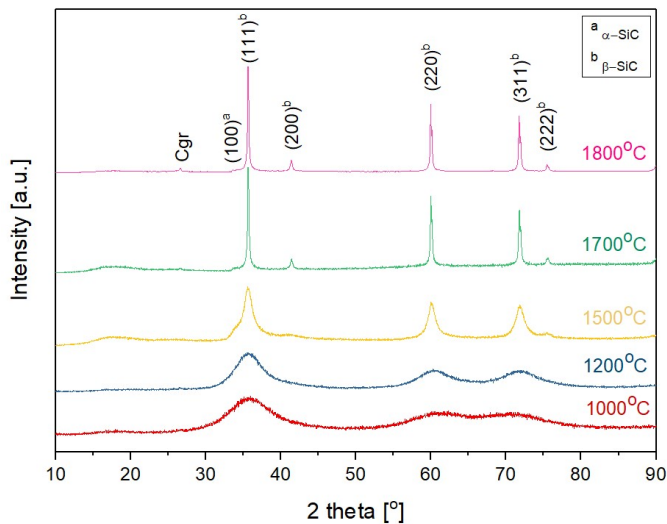
After a heat-treatment to 1500 ^{o}C, all the samples exhibit distinct XRD peaks related to the β-SiC phase. Thus, it is understood that the SiC crystallites size is on a scale of a few nanometers. There is the formation of large Bragg reflections in $2\theta =$ 35.6, 60.5 and 71.18 ^{o} angles, corresponding to (111), (220) and (311) planes, respectively. These peaks, as well as the one with lower intensity, which correspond to the (200) and (222) planes can be indexed to β-SiC. These reflections have their amplitude reduced and the peak becomes narrower as the temperature rises. These changes are characteristics of these samples that denote

that due to the temperature effect there is a significant evolution on the formation of crystalline β-SiC.

At 1700 ^{o}C, β-SiC phase is completely crystallized. The small peak at around 34 ^{o}, is due to stacking faults (type of defect which characterizes the disordering of crystallographic planes) like α-SiC in β-SiC, as previously described by Fang et al. (2008).

Just as AHPCS's diffractogram, in both PCS_B30 and PCS_B60 samples (Figure 69), with temperature increase, an additional reflection related to graphitic carbon in approximately 26.6 ^{o} appears.

The PCS_B60 sample, as demonstrated by the peaks on its diffractogram, has a behavior similar to PCS_B30 as the temperature is increased.

Figure 69: PCS_B60 sample diffractogram at different temperatures in an argon atmosphere.
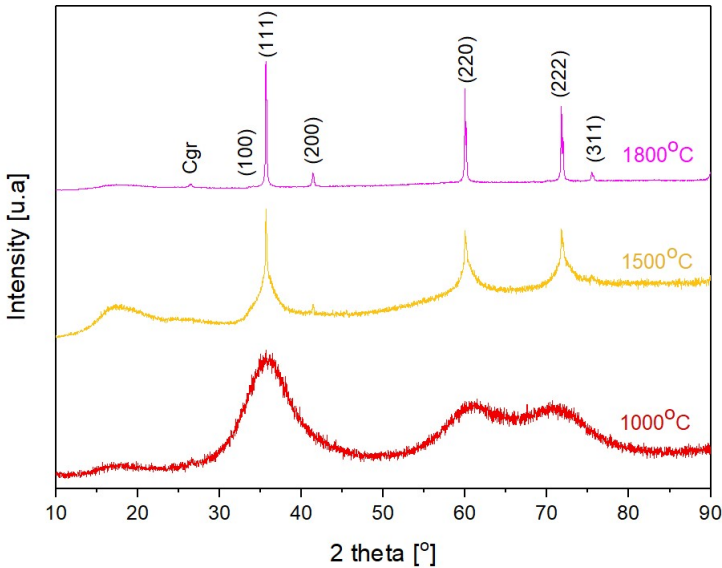
However, for a better understanding of boron's influence in crystallites's size (Dhkl) of the PCS_B30 and PCS_B60 samples at 1500 ^{o}C, was applied Scherre's equation, Equation 4.1, which

shows that the crystallite size is inversely proportional to the peak width (FWHM).

$$Dhkl = \frac{k\lambda}{\beta\cos\theta} \qquad (4.1)$$

Where k is a dimensionless shape factor (considered here being 0.9), λ is the radiation wave length, β the full width at half maximum peak (FWHM, as shown in Figure 70), and θ the diffraction angle.

Figure 70: Full width at half maximum peak (FWHM).
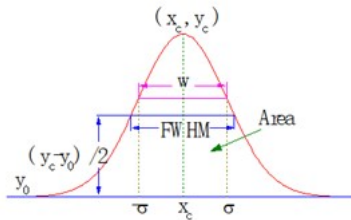
The sofware Origin was used to determine the FWHM value. In the diffractogram in Figure 71 the fitted curves for the PCS_B30 and PCS_B60 samples are shown, respectively, in pink and green colors. The fitting has been done with Gaussian curves and the analysis values are found in Tables 9 and 4.2.2.1.
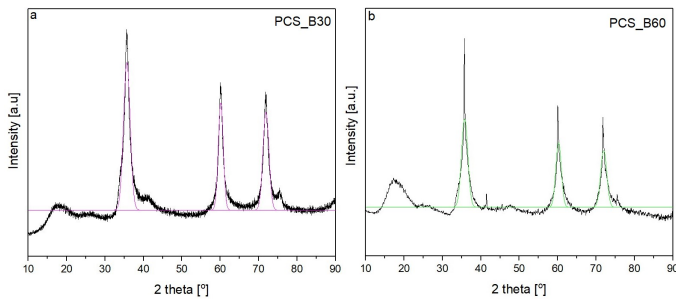
Figure 71: Fitting with Gaussian curves to discovery the crystallite size of a) PCS_B30 and b) PCS_B60 both at 1500 ^{o}C pyrolyzed in an argon atmosphere.

Table 9: Crystallite size analysis result of the PCS_B30 sample at 1500 ^{o}C.

PCS_B30	2θ	FWHM (rad)	Error	Crystallite size (nm)
Peak 1	35.66	0.030	± 0.017	4.86
Peak 2	60.14	0.023	$\pm\ 0.02$	7.05
Peak 3	71.9	0.027	$\pm\ 0.02$	4.86
				Average size= 5.6 nm

The values found for the SiC crystallite average size of the PCS_B30 and PCS_B60 samples were 5.6 and 5.22 nm, respectively. This difference in size, albeit small, shows that there is an increase in size with the addition of boron. This behavior is in accordance to previous experiments (SCHMIDT et al., 2017).

Interestingly, on the diffractogram for the PCS_B60 sample there is a peak at ca. 41.48 ^{o} (200) better shaped than in PCS_B30 at the same temperature.

In Figure 72 are shown the Raman spectra for the PCS_B30 sample. The Raman spectra of the boron-SiC sample shows the presence of a band which relates the stretching of the C-C bond in graphitic materials, and is common to all sp^2 carbon systems, called G band.

Disordered or nanostructured carbon-based materials (which might contain also some amount of sp^3 hybridization) exhibit an additional band which relates to breathing modes of sp^2 carbon atoms within rings (so-called D band) (KAUR, 2016). Hence, these two bands, D and G, confirm the presence of turbostratic carbon (structure intermediate between graphite and amorphous carbon) in the system.

Also, at 1800 ^{o}C it is possible to see two other signals around 2620 and 2920 cm^{-1}, attributed to the bands 2D and D+D' related to the segregated carbon phase in the samples. The presence of the D+D' band in the Raman spectra indicates the presence of defects and disorder in the structure of PCS_B30. Two bands (better visualized in the amplified Figure

72) are centered at 790 and 9605 cm^{-1} and they are assigned to the transversal optic (TO) and longitudinal optic (LO) modes of β-SiC, respectively (WIELIGOR; WANG; ZERDA, 2005).

Figure 72: Raman spectra of the PCS_B30 sample in argon.
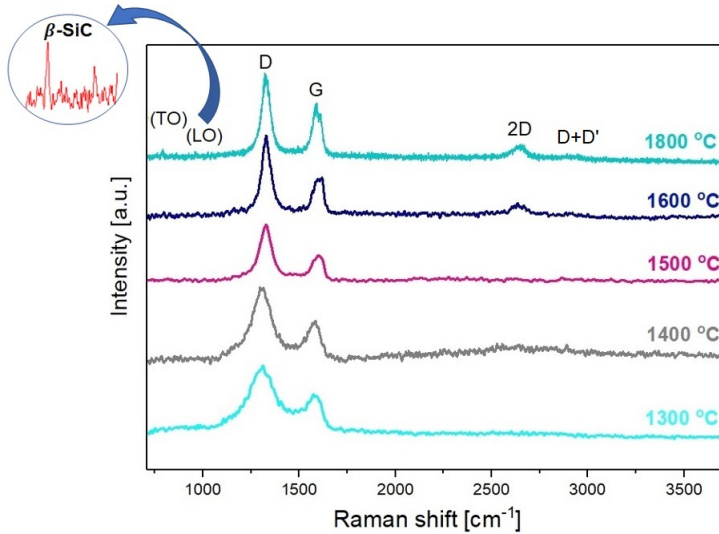
Also, from the Raman spectra, the intensity ratio I$_D$/I$_G$ has been largely used to compare the quantity of defects in graphitic samples (ARAYA et al., 2018). In this work I$_D$/I$_G$ ratios were calculated from the peak integrals of D and G bands for the samples at 1500, 1600 and 1700 ^{o}C. The ratios are calculated after a Lorentzian fitting of the data by the software Origin. This analysis is based on the intensity in this ratio because absolute Raman intensities are hard to measure. In Figure 73 it can bee seen the I$_D$/I$_G$ ratios for PCS_B30 (SiC) in some pyrolysis conditions.

I$_D$/I$_G$ ratios demonstrate that increases in temperature lead to decrease in disorder of the system, which provides the understanding that there is also an increase in sp^3 hybridization (ordered carbon).

Figure 73: I_D/I_G ratios for PCS_B30 samples at 1500, 1600 and 1700 ^oC.
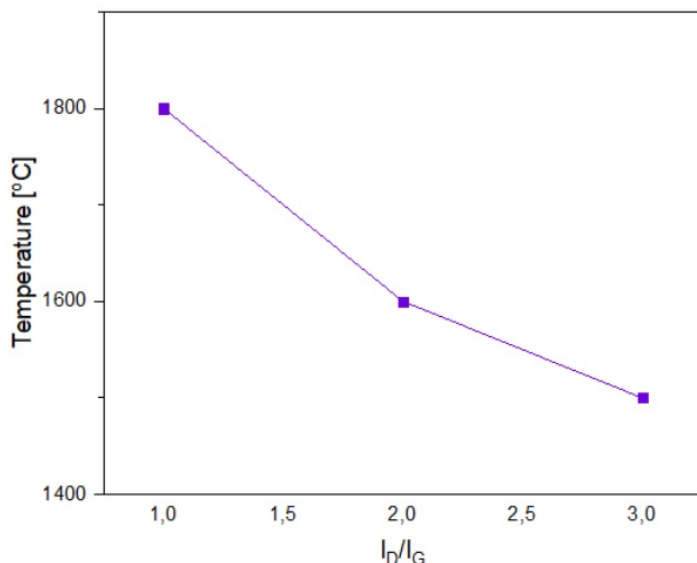
4.2.2.2   Contribution of ammonia as atmosphere in the low temperature regime of the pyrolysis

In order to manipulate the chemistry of the polymer precursor AHPCS and PCSB_30, an ammonia pre-treatment was added in the pyrolysis step of the powder (up to 450 ^oC), followed by pyrolysis up to 800 ^oC in argon atmosphere.

Ammonia gas was introduced into the tube furnace within which the polymer powder PCS_B30 ou AHPCS, resulting in an exchange of nitrogen, boron and carbon between the materials and the atmosphere. The extent of the reaction was controlled by the temperature of the ammonolysis. The range of 400 to 600 ^oC temperature was shown to be the most effective for nitridation and carbon removal as demonstrated in previous studies. Within this temperature range, the thermal decomposition of the polymer catalyzes the decomposition of ammonia (BURNS; CHANDRA, 1989).

Thus, to analyze the influence of intermediate pyrolysis on the behavior of PCS_B30, a comparison between the infrared spectra at 450 ^{o}C in argon and ammonia atmospheres was performed. This comparison is presented in Figure 74.

Figure 74: FTIR of the PCS_B30 sample at 450 ^{o}C in ammonia and in argon.
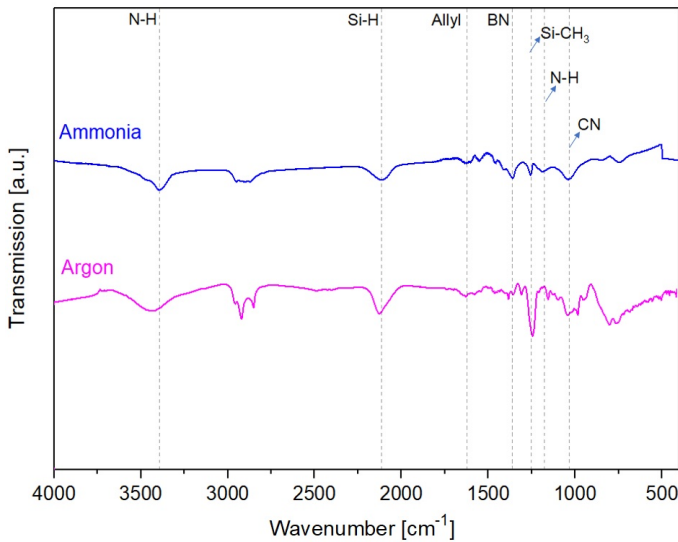
Thereby, on the infrared spectrum graph from the PCS_B30 sample, it is observed the $N-H$ stretches vibration at 3400 cm^{-1} and 1180 cm^{-1}. Wan, Gasch e Mukherjee (2002) described that when ammonia is utilized, specially at temperatures above 400 ^{o}C, this gas may then participate of the cleavage of Si-C bonds from the polymeric precursor and consequently there is a loss of carbon-containing functional groups, e.g., $-CH_3$, which is then replaced by $-NH_2$ through the reaction, following Equation 4.2.

$$\equiv Si-CH_3 + NH_3 \rightarrow \equiv Si-NH_2 + CH_4 \qquad (4.2)$$
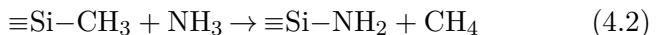
As this reaction occurs, there is a reduction of the Si$-CH_3$ (1255 cm^{-1} stretching) group, which is seen in the spectrum of

this sample in ammonia. Nonetheless, it is particularly interesting that PCS_B30 had a considerable increase of the band corresponding to $Si-CH_3$ when thermally treated in argon atmosphere (450 ^{o}C).

The bands at ca. 2955 and 2912 cm^{-1} are attributed to C-H asymmetric and symmetric stretching, and the band at 1640 cm^{-1} is due to the allyl group (C=C stretching), common in all polymers discussed here at this temperature.

Si-H stretching in ca. 2117 cm^{-1} has its signal reduced due to Equation's 4.3 reaction (WAN; GASCH; MUKHERJEE, 2002).

$$\equiv Si-H + NH_3 \rightarrow \equiv Si-NH_2 + H_2 \qquad (4.3)$$

However, as there are no signals of the $Si-NH_2$ bond in the spectrum, it is believed that there is formation of $Si-NH-Si$ by crosslinking reaction (Equation 4.4), indicated by the band in 1180 cm^{-1} (NH stretch).

$$\equiv Si-NH_2 + CH_3-Si\equiv \rightarrow \equiv Si-NH-Si\equiv + CH_4 \qquad (4.4)$$
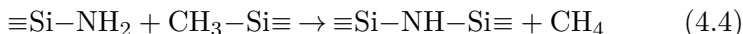
Similar results were obtained by Wan, Gasch e Mukherjee (2002), where ammonia was introduced while pyrolyzing commercially available polyureasilazane, which already contain repeat units in which Si atoms are bonded in an alternating sequence to N atoms.

Finally, despite a band possibly related to the B-N bond at ca 1370 cm^{-1} (sp^2 bonds of hexagonal h-BN phase), as also observed for Sahu et al. (1998), Ansaloni e Sousa (2013) in their works, and another band related to the C-N stretch bond (alkyl), it is not possible to conclusively assert, using only the infrared spectrocospy data, the formation of these bonds.

The use of Ar/NH_3 atmospheres allows the preparation of a range of SiCxNy materials but the detection of the presence of N in materials with values of y < 1 is very difficult (SCARLETE et al., 1995).

It is important to highligh that the PCS_B60 sample did not undergo an intermediate ammonia treatment, as the intention

of this pre-nitridation was of a small part of boron acting as a sintering additive and the remaining boron to form B-N bonds. With a lower boron content, there is no reason to use PCS_B60 in this process. About AHPCS, only for comparison reasons, regarding the influence of boron on the structure, it was also underwent a previous ammonia treatment at 450 ^{o}C.

Thus, the diffractograms and the respective formation of crystals in the AHPCS and PCS_B30 samples, with initial ammonia treatment at 450 ^{o}C and posterior pyrolysis in argon up to 1000 ^{o}C, are shown in Figure 75.

Figure 75: Diffractogram of PCS_B30 and AHPCS samples at 450 ^{o}C in ammonia, with posterior pyrolysis up to 1000 ^{o}C in argon.
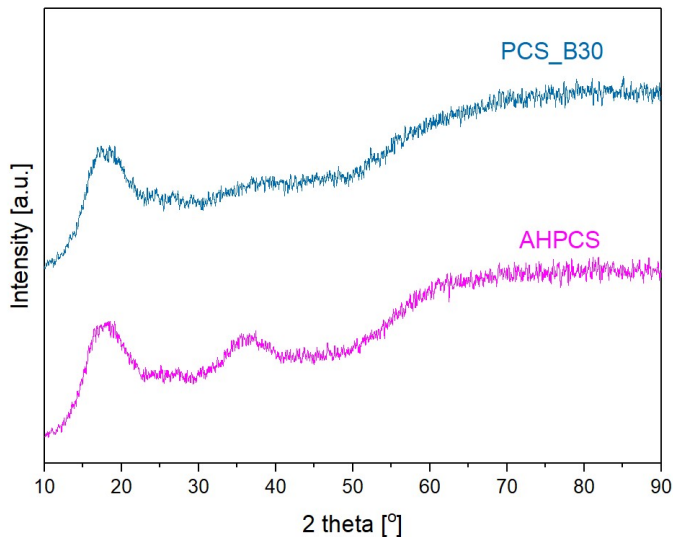
The appearance of a clear stacking fault in PCS_B30 at 1500 ^{o}C (Figure 76) shows that crystallization is happening at faster rates when compared to the same temperature treatment in argon.

Figure 76: Diffractogram of PCS_B30 and AHPCS samples at 450 ^{o}C in ammonia, with posterior pyrolysis up to 1500 ^{o}C in argon.
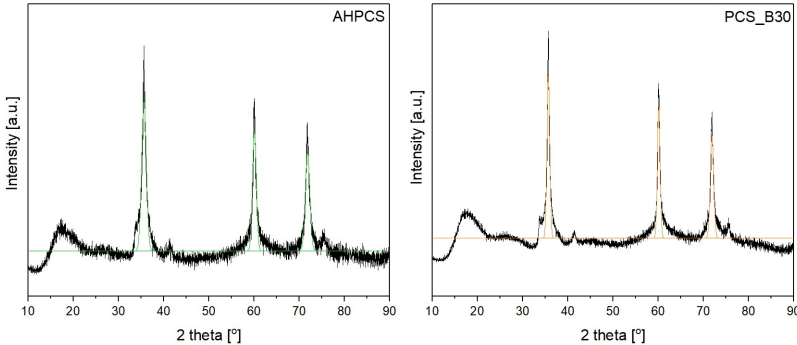
XRD of the sample evidenced larger crystallites for the PCS_B30 sample, of 12.1 nm at 1500 ^{o}C, while for the AHPCS sample, the value found was 8.85 nm.

The density found for these samples were:

- AHPCS pre-treated in ammonia at 450 ^{o}C and posterior pyrolysis at 1800 ^{o}C: 2.57 g.cm^{-3}

- PCS_B30 pre-treated in ammonia at 450 ^{o}C and posterior pyrolysis at 1800 ^{o}C: 2.8345 g.cm^{-3}

These density results were similar to the ones obtained by Puerta et al. (2003) when using argon as the thermal treatment. The authors demonstrated that the density of the derived ceramic increased considerably when small amounts of boron were incorporated into the precursor AHPCS. This way, they obtained 1800 ^{o}C ceramics derived from the AHPCS and 9-BBN-3 with 2.75 g.cm^{-3} density and AHPCS 2.54 g.cm^{-3}. These results are very close to the ones presented here despite the different gases used.

It is hard to establish the specific reason for which boron and ammonia (as thermal treatment gas) combined affect the sintering of silicon carbide (and its densification). There is no record in the literature of data regarding the ammonolysis de

poly(boron)carbosilanes, which makes a more detailed investigation difficult and requiring other experimental analysis to determine the real structure of the formed ceramic.

To evaluate the crystalline net that was formed in the sample pretread in ammonia and after at 1800 ^{o}C in argon, HRTEM analysis (High Resolution Transmission Electron Microscopy) was performed, as can be seen in Figure 77, accompanied by SAED (Selected Area Electron Diffraction) to identify the crystal structures.

Figure 77: HRTEM image of PCS_B30 at 1800 ^{o}C showing the nanowires with numerous stacking faults. In the upper right corner SAED image collected on the nanowire.
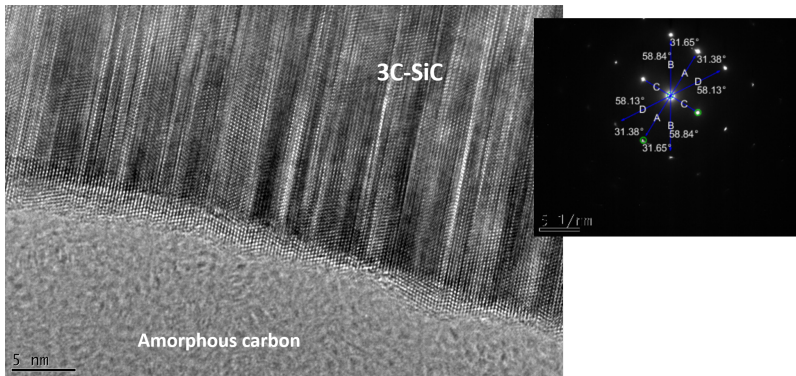
Through the HRTEM image it can be confirmed the formation of 3C or β-SiC structure, which with SAED evidences the planes (220), (311) and (111), regarding d-spacing of 0.148, 0.126 and 0.242 nm, respectively. It may also be observed the presence of an amorphous phase at this same temperature, as well as stacking faults on the limit between the amorphous and crystalline phase, which had already been confirmed by XRD (in the sample pretreated in ammonia and after at 1500 ^{o}C in argon).

4.2.3   Summary

As discussed in Section 4.2.1 on the hydroboration of AH-PCS, it may be concluded that boron reacts non regio-selectively with the allyl group, enabling the beginning of the crosslinking reaction at lower temperatures (approximately 100 ^{o}C). Therefore, it shows that boron in polymer-derived Si-(B)-C materials is not incorporated into the silicon carbide lattice (at least not in significant amounts).

This crosslinking effect enables the acquisition of solids at lower temperatures which may then undergo through the important PDC route, which is shaping, resulting in structures which will be seen and discussed in the next sections.

In addition to this, boron increases the ceramic yield and enables the obtainment of β-SiC at temperatures higher than 1200 ^{o}C.

In the presence of ammonia gas, it was noted the possible formation of infrared bands relative to Si(B)CN ceramics. However, more analysis are required to confirm the effects of the gas on the structured formed with intermediate ammonolysis, as well as on the final structure.

It is known that there is a significant difference, as it will be seen in the following sections, with the result using nitrided material. Therefore, this stage of the process heavily affects the obtained ceramic.

4.3   Design of dense Si-(B)-C ceramics

In this section it is discussed the processability of hydroborated ceramic precursors, which may be understood as the possibility to apply shaping techniques to obtain complex structures, as described on the PDC route. There, results regarding the processing of single source precursors PCS_B30 and PCS_B60 will be described.

Firstly will be analysed the method to fabricate dense amorphous ceramics disks through warm pressing (with pyrolysis temperatures of 1000 ^{o}C in argon atmosphere after the obtainment of green bodies).

Also, the method for production of ceramic bodies at high temperatures (1750 e 1800 ^{o}C) via rapid hot sintering will be discussed.

4.3.1   Dense 3D pieces by warm pressing

The following parameters for dense piece production through warm pressing were studied: temperature, load for powder compaction and holding time for different mold sizes.

After solvent extraction at 100 ^{o}C, PCS_B60 became solid with a gelatinous appearance. This way, during the pressing it did not form a sufficiently solid structure to follow through with the pyrolysis stage. Only with PCS_B30 it was possible to obtain green bodies during pressing which were good enough to undergo pyrolysis.

The reason that PCS_B60 did not manage to become a solid capable of retaining the disk shape is possibly due to the hydroboration stage. It is known that hydroboration with low boron content result in liquid compounds with a higher viscosity than AHPCS and, as the Si:B ratio decreases, the higher the viscosity becomes, thus obtaining solid compounds (SCHMIDT et al., 2017). Therefore the scheme for the steps performed during this stage using PCS_B30 are shown in Figure 78.

Figure 78: Scheme of the steps performed to obtain 3D dense disks. First, by the hydroboration reaction PCS_B30 is obtained in form of agglomerated powder, being posteriorly ball milled. Then it goes to warm pressing stage, obtaining a green body capable of retaining the shape in disk format. The last step, pyrolysis, turns the green body into amorphous ceramic (1000 ^oC).
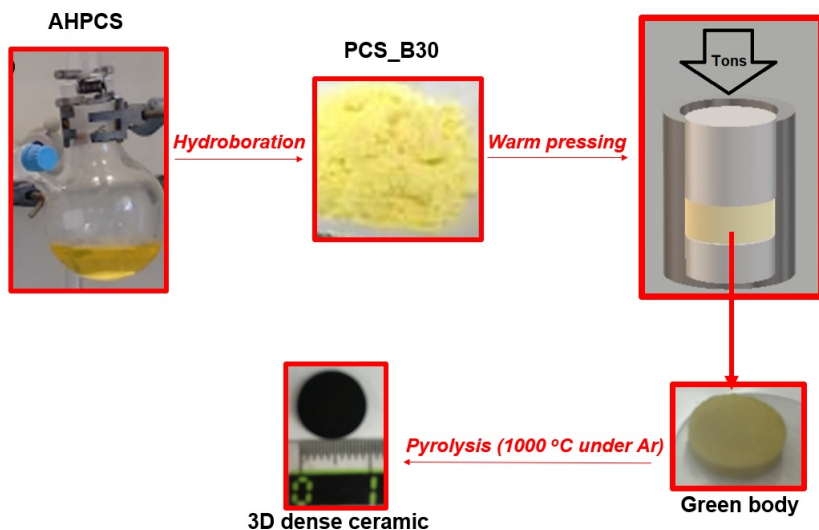
Results from warm pressing experiments were divided according to the diameter size of the used mold (13, 25.6 and 28.5 mm), as it will be shown on the following sections.

4.3.1.1   Dense pieces by 13 mm ⌀ mold

Figure 79a presents the resulting green body after warm pressing with a 13 mm mold, using 0.25 g of PCS_B30, 1 ton, 120 ^oC and 30 min holding time, as pressing parameters. The amorphous ceramic, after pyrolysis at 1000 ^oC can be visualized in Figure 79b.

Figure 79: a) warm pressing of PCS_B30 using $\varnothing$ 13 mm mold and b) 3D dense ceramic after pyrolysis at 1000 ^{o}C.
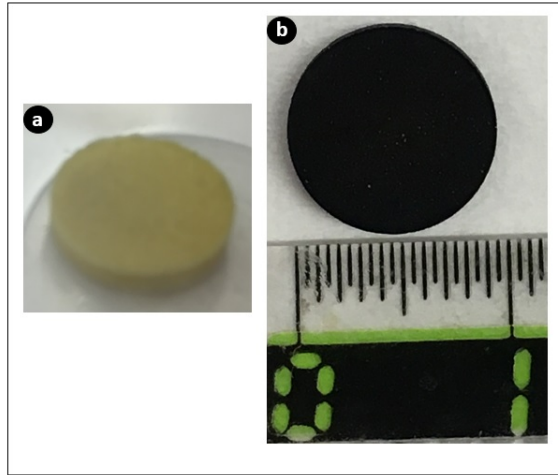
This sample will be denoted as PSB30d$_{13}$, where d refers to it being dense and 13 the mold size.

Warm pressing technique was used aiming at producing dense objects after pyrolysis of the compacted green bodies.

Through pyrolysis, the object loses oligomers and other compounds, this thermal decomposition generates gases that lead to a non-visible in optical microscopy, porosity in dense objects. It is during it that objects gain structure and with this effect end up suffering volume retraction and weight loss.

These factors, porosity, volume retraction and weight loss, may be correlated to the yield of PCS_B30 precursos, which in this and other studies was higher than of other materials (AH-PCS, PCS_B60) due to the addition of boron. Thus, boron increases polymer reticulation and prevents distillation of small polymer fragments favoring material densification.

For the PSB30d$_{13}$ sample, weight loss was of 11 % and volume retraction was approximately of 50 %.

The pressing operation also will influence, with the temperature, duration, pressure and force parameters, the compaction of the green bodies.

In Figure 80 is shown the SEM of the PSB30d$_{13}$ sample. The SEM micrographs support the presence of residual porosity from the monoliths. Despite the presence of some pores, which is common due to gas releases, they were filled by ceramic and thus a dense surface was obtained without cracks.

Figure 80: PSB30d$_{13}$ SEM image.
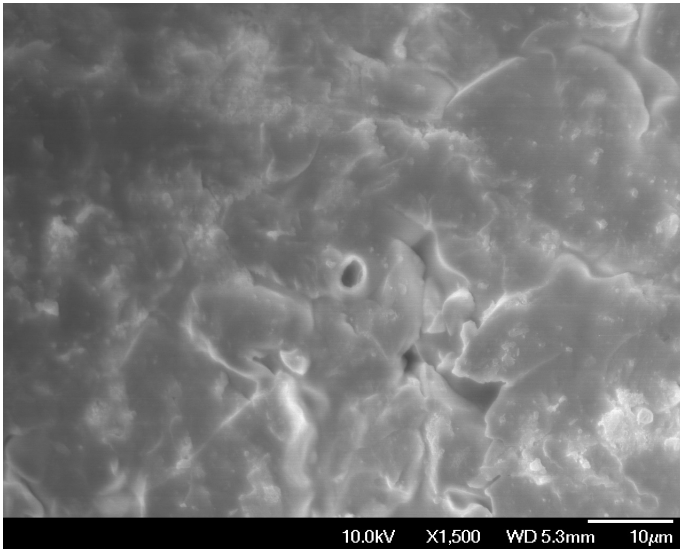
Piece density was measured by the Arquimedes principle and was found to be 2.45 g.cm^{-1}, which is representative the densification the material went through. Kaur, Riedel e Ionescu (2014a), obtained SiC dense monoliths utilizing AHPCS at 1050 ^{o}C with bulk density of 2.67 g.cm^{-3}, performing, however, pre-crosslinking at 250 ^{o}C and warm pressing at a considerably higher temperature (300 ^{o}C) and no characterization of the ceramics was done.

Hardness (H) and Young's modulus (or elastic modulus (E)) analysis by indentation tests of PSB30d$_{13}$ after sanding and polishing were 26.73 GPa and 368.4 GPa, respectively, with a maximum load of 40.12 mN, as it may be observed in the graph on Figure 81. In Figure 82 are shown the load-depth curves of

instrumented indentation test.

Figure 81: Hardness analysis (H) and Young's modulus (E) by indentation tests of PSB30d$_{13}$ after sanding and polishing the ceramic 3D sample.
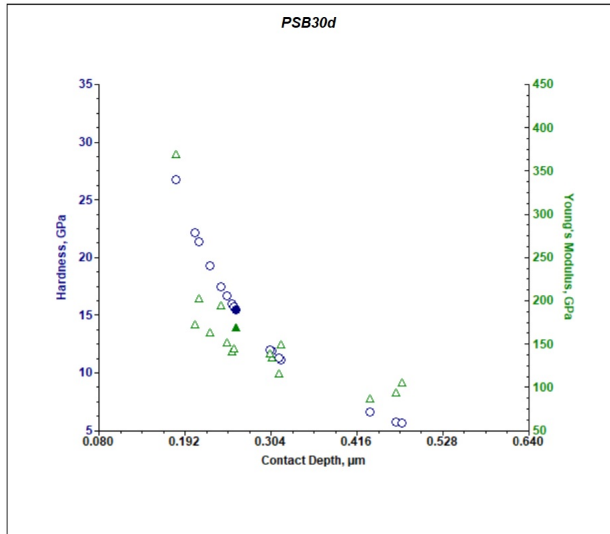
Figure 82: Load-depth curves of instrumented indentation test.
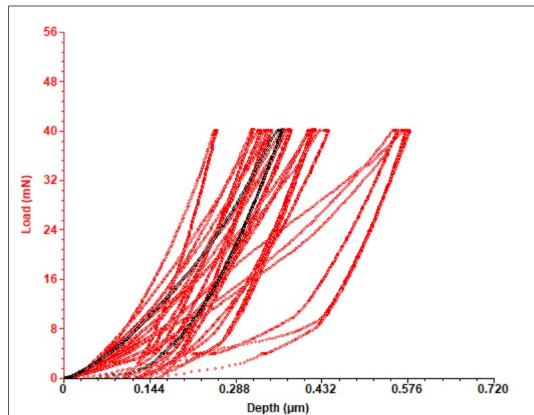
These hardness and elastic modulus values are relatively high, given that for SiC, for example, its hardness is between 21 a 25 GPa (solid state sintered) (ABDERRAZAK; HMIDA, 2011).

Zunjarrao, Rahman e Singh (2013) measured these characteristics from AHPCS derived SiC as a function of processing temperature and they obtained for 900 ^{o}C hardness and Young's modulus of respectively 22 and 183 GPa. Increasing the temperature to 1150 ^{o}C, they obtained 23 (H) and 227 (E) GPa. Even for 1400 ^{o}C, the values reached: 25 (H) and 250 (E) GPa; are inferior to the ones found in this work using boron.

It is important to highlight that since boron linked to allyl grouping may cause a reduction of impurities, such as carbon present at the grain limits, during ceramization. This may, in turn, lead to increased hardness and Young's Modulus.

In Figure 83 is found PSB30d$_{13}$'s image from an optical microscope, after sanding and polishing (a), and the image used to count SiC grains (b). In image (a), dark regions are amorphous carbon and grey areas are the SiC grains.

Figure 83: PSB30d$_{13}$ by optical microscopy (a) after sanding and polishing, dark areas are due to amorphous carbon and grains in gray, SiC. (b) Image used for amorphous carbon analysis by ImageJ software.
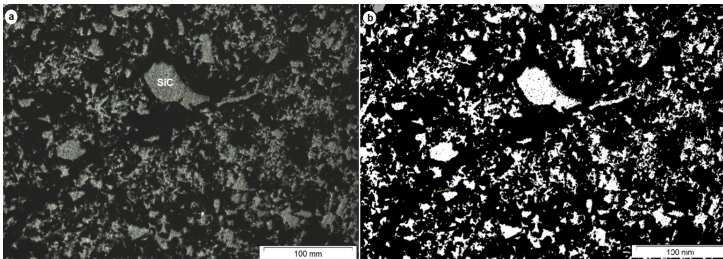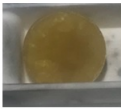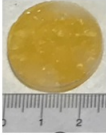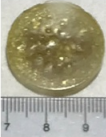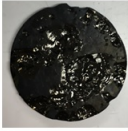
According to ImageJ image analysis software, the percentage of SiC grains, with white appearance in Figure 83 b, is 21% of the whole sample area. Considering that this sample was pyrolysed at 1000 ^{o}C and the structure is still very amorphous,

however with a crystallization induction due to the presence of boron, this value is as expected.

4.3.1.2 Dense pieces by 25.6 mm ⌀mold

When the 25.6 mm diameter mold was used for warm pressing, different parameters where applied to the green bodies, as it is shown in Figure 84, with photos that illustrate the 3D green disks and the amorphous ceramic after pyrolysis at 1000 °C.

Figure 84: Variables and warm pressing results for PCS_B30 sample using the 25.6 mm diameter mold.

PCS_B30 (g)	Temperature (°C)	Hold time (min)	Tons	Green body	After pyrolysis
2	120	30	4		
1.5	120	30	4		
2	120	60	5		

This way, as it may be observed in the table in Figure 84, the configuration that was shown to be viable for the confection of 3D dense disks was using 4 tons for 30 minutes for compaction at a temperature of 120 °C with 2 g of PCS_B30. This ceramic was named as PSBd$_{25}$.

A lower quantity of precursor, 1.5 g, generated a disk with considerable losses after pyrolysis, leading to several structural

defects. This is probably caused by problems during powder compaction in the mold during pressing.

Besides a longer exposition duration at 120 ^oC a green body with a molten appearance, which was also probably influenced by the higher load (5 tons) lead to ceramic deformation after pyrolysis.

For $PSBd_{25}$, the weight loss was of 10.67 % and volume retraction was approximately 50.75 %. These results are similar to the ones obtained for $PSBd_{13}$, therefore representing that the almost twofold increase in diameter and eight times in weight did not lead to greater weight loss or shrinkage.

It is important to highlight that both these ceramic samples ($PSBd_{13}$ and $PSBd_{25}$) utilized the same apparatus for mold heating 120 ^oC. Meanwhile, for the 28.5 mm diameter mold a different equipment was used for this purpose, which influences on the confection of the green bodies, as it will be seen in Section 4.3.1.3.

The thermal diffusivity of $PSBd_{25}$ was measured and it value found to be 0.42 $mm^2.s^{-1}$ at room temperature.

In another work (ANJOS et al., 2006), 3C-SiC fibers thermal diffusivity at 1200 ^oC was measured to be 5.7 $mm^2.s^{-1}$. However, these fibers were densified by chemical vapour deposition of SiC obtained from mixtures of methyltrichlorosilane and hydrogen. In this way, there was a higher densification of the sample than in this work, which led to a higher diffusivity.

This diffusivity indicates that this material can be a good thermal insulator. In other words, it can be specifically designed to reduce the heat flow by limiting heat conduction, convection and radiation. Some authors (Jang e Sakka (2007), Nakano et al. (2004), Lee et al. (2008)) have showed the strong dependence of thermal diffusivity and thermal conductivity on porosity and temperature.
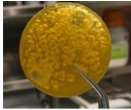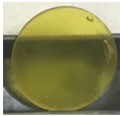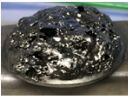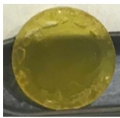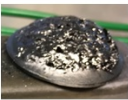
One of the causes is given by the phonon scattering due to a higher volume fraction of pores, which reduces the mean free path of phonons spread throughout the solid and ultimately reduces thermal diffusivity. Phonon refers to the mechanical excitation that propagates through the crystalline network of a solid.

Usually this excitation moves as a wave through the material and the higher the temperature the greater the number of phonons.

4.3.1.3 Warm pressing using 28.5 mm ∅ mold

As it can be seen in the table presented in Figure 85, none of the attempts of obtaining 3D ceramic pieces using PCS_B30 in a 28.5 mm mold was successful.

Figure 85: Variables and results of warm pressing of PCS_B30 samples in a 28.5 mm diameter mold.

PCS_B30 (g)	Temperature (°C)	Hold time (min)	Tons	Green body	After pyrolysis
4	80	30	4		
4	100	30	5		
3	100	30	5		
3	110	30	5		

Other attempts using different temperature settings were also performed, as shown in the Table 11, though without images.

Table 11: Alternate attempts with the 28.5 mm diameter mold.

PCS_B30 (g)	Temperature (^{o}C)	Hold time (min)	tons	After pyrolysis
3	100	30	4	Bubbles
3	100	40	4	Bubbles
2.5	90	40	4	Bubbles
3	90	40	5	Bubbles
2.5	80	40	4	Bubbles
4	80	30	8	Destroyed

Thus, several hypothesis can be given to the failure to obtain structures using this mold:

(i) The quantity of oligomers has greatly increased, which leads to a a higher release of compounds during pyrolysis, forming bubbles and ultimately destroying the pieces.

(ii) During warm pressing, with the obtainment of green bodies, in many of the reported cases, there was the appearance of bubbles. The formation of gas bubbles in the green body which due to the evaporation of low molecular weight oligomers, dissolved gases and/or dissociation of weakly attached end groups (JANAKIRAMAN; ALDINGER, 2009). This occurred at both higher temperatures (120 ^{o}C) and lower temperatures (80 ^{o}C). This leads to the understanding that the mass quantity definitely has an impact and that the mold design may have an effect on the gas exhaustion during pressing.

(iii) Even in the 3D pieces with less quantity of PCS_B30 (2.5 g, similar to the one used on the 25.6 mm mold) and with pressing temperatures of 90 ^{o}C, after pyrolysis, there was the formation of bubbles which damaged the ceramic structure. So possibly, even though the green body is thinner and larger, this was not enough to enable gas exhaustion. This may be due to a lower crosslinking undergoing PCS_B30, which had its pressing temperature lower than the one for precursor solvent extraction. This may also explain why the green body was completely destroyed at 80 ^{o}C pressing, which was the worst outcome of all tests.

(iv) It may be the case that the batch of AHPCS precursor used to produce these pieces of 28.5 mm of diameter, contained a higher oligomer amount than reported by the supplier, leading to a greater weight loss and increasing the difficulty to generate structured ceramics.

(v) Another possible reason is that the relatively higher thermal conductivity of the pressing mold's piston, which is made of metal (note that the 28.5 mm mold is different from the others and possesses another temperature control system). With a rapid heating rate, in contact with the sample (the sample having poor thermal conductivity), may have induced significant thermal gradients across the sample thickness, causing bubbles in the green bodies.

4.3.2 Summary

As seen in the sections on warm pressing for different mold sizes, it was only possible to obtain 3D denses ceramics with 13 and 25.6 mm diameter molds, which did show interesting mechanical properties (mold of 13 mm of diameter).

Clearly, further developments are necessary to successfully produce ceramics using the 28.5 mm diameter mold. A possible path is to perform solvent extraction of PCS_B30 samples at temperatures higher than 100 ^{o}C and for longer, so that volatiles from the structure may be released prior to warm pressing.

Bubble formation happens by many reasons. For which the processability is determined by reticulation temperature, heating rate, ambient pressure and polymer viscosity, among other factors.

Also, the surface to volume ratio of the reticulated green body limits the removal of gaseous subproducts liberated during pyrolysis reactions. This increases the pressure inside it, leading to bloating and/or cracks.

It was important to observe during the experiments the need to guarantee the correct temperature gradient to ensure that throughout the volume transformation of polymer to ce-

ramic from the surface to the nucleus of the sample does not happen, avoiding a large shrinkage. This could also cause cracking or complete disintegration of the pyrolyzed body, as seen on the 28.5 mm diameter disks.

However, despite difficulties found trying to obtain dense pieces by the direct application of a preceramic precursors, results showed that this method is possible and that it does not necessarily need high temperatures and complex apparatus to obtain ceramics with excellent mechanical properties, such as hardness and elastic modulus.

4.3.3 Rapid hot pressing (sintering)

For the hot sintering method, the samples specified in Table 12 were used. Table 13 shows the weights before and after the sintering process.

Table 12: Rapid sintering methodology for PCS_B30 and PCS_B60 samples.

Sample	Samples Names	Sintering regime
PCS_B30 (800 ^{o}C, Ar)	**P1**	**1750** ^{o}**C**(100 ^{o}C/min) - 50 MPa (800-1000 ^{o}C), holding time 15 min
PCS_B60 (800 ^{o}C, Ar)	**P2**	**1750** ^{o}**C** (100 ^{o}C/min) - 50 MPa (800-1000 ^{o}C), holding time 15 min
PCS_B30 (200 ^{o}C, NH$_3$ / 800 ^{o}C, Ar)	**P3**	**1750** ^{o}**C** (100 ^{o}C/min) - 50 MPa (800-1000 ^{o}C), holding time 15 min
PCS_B30 (800 ^{o}C, Ar)	**P4**	powder milled for 2 h in a dry state; **1800** ^{o}**C** (100 ^{o}C/min)- 50 MPa (800-1000 ^{o}C), holding time 15 min
PCS_B60 (800 ^{o}C, Ar)	**P5**	powder milled for 2 h in a dry state; **1800** ^{o}**C** (100 ^{o}C/min)- 50 MPa (800-1000 ^{o}C), holding time 15 min
PCS_B30 (200 ^{o}C, NH$_3$ / 800 ^{o}C, Ar)	**P6**	powder milled for 2 h in a dry state; **1800** ^{o}**C** (100 ^{o}C/min)- 50 MPa (800-1000 ^{o}C), holding time 15 min
PCS_B30 (450 ^{o}C, NH$_3$ / 800 ^{o}C, Ar)	**P7**	powder milled for 2 h in a dry state; **1800** ^{o}**C** (100 ^{o}C/min)- 50 MPa (800-1000 ^{o}C), holding time 15 min

Therefore, according to Table 13 it can be seen that there is weight loss (4.38 wt%) after hot pressing sintering (1750 ^{o}C) which is greater for the PCS_B30 (P3) sample with NH$_3$ pretreatment (200 ^{o}C) and subsequent pyrolysis in Ar (800 ^{o}C). This was followed by the sample with a higher sintering temperature (1800 ^{o}C) (P6), leading to 4.25 wt%.

Table 13: Weight loss percentage Δm after thermal treatment.

Samples	(g) *before sinter.*	(g) *after sinter.*	Δm (%)
P1	3.28	3.2	2.44
P2	3.28	3.22	1.83
P3	3.2	3.06	4.38
P4	3.24	3.19	1.54
P5	3.2	3.12	2.5
P6	3.18	3.045	4.25
P7	3.35	3.3	1.36

These conclusions were already expected, given that pre-treatment in Ammonia will remove a considerable amount of carbon, as seen by the infrared images in Section 4.2.2.2. Hence, the weight loss is also expected to be considerable.

Only for PCS_B30 (800 ^{o}C) (P4), the weight loss was lower than when exposed to temperature increase (from 1750 to 1800 ^{o}C). This is a good indicator of the effectiveness of the sintering process and of hydroboration, given that boron is known to be a sintering agent.

The sample with the lower boron content (heat treatment only in argon atmosphere) had a greater weight loss during sintering at the highest temperature (1800 ^{o}C), this may be an indicator that crosslinking of the structure is really more effective when boron incorporation is high.

Despite the sample (only in argon atmosphere total treatment) with the lowest boron content (P2) having a lower weight loss variation during sinterization at 1750 ^{o}C, compared to the one with total hydroboration (P1), this was not significant enough when compared to the weight values before and after sinterization, with a difference of only 0.02 g.

Regarding the sample densities through this technique, it may be observed in Table 14, and on the graph in Figure 86, that there is high density for PCS_B30 pyrolysed in argon (P1 and

P4), for both rapid sintering temperatures (1750 and 1800 ^{o}C), with values of 2.89 and 2.86 g.cm^{-3}, respectively.

Table 14: Sample density after grinding and polishing.

Sample	Samples names	Measured density after grinding and polishing (g.cm^{-3})
PCS_B30 (800 ^{o}C, Ar) (**1750 ^{o}C** RHP)	**P1**	2.89
PCS_B60 (800 ^{o}C, Ar) (**1750 ^{o}C** RHP)	**P2**	2.59
PCS_B30 (200 ^{o}C, NH$_3$ / 800 ^{o}C, Ar) (**1750 ^{o}C** RHP)	**P3**	2.21
PCS_B30 (800 ^{o}C, Ar) (**1800 ^{o}C** RHP)	**P4**	2.86
PCS_B60 (800 ^{o}C, Ar) (**1800 ^{o}C** RHP)	**P5**	2.47
PCS_B30 (200 ^{o}C, NH$_3$ / 800 ^{o}C, Ar) (**1800 ^{o}C** RHP)	**P6**	2.36
PCS_B30 (450 ^{o}C, NH$_3$ / 800 ^{o}C, Ar) (**1800 ^{o}C** RHP)	**P7**	2.6
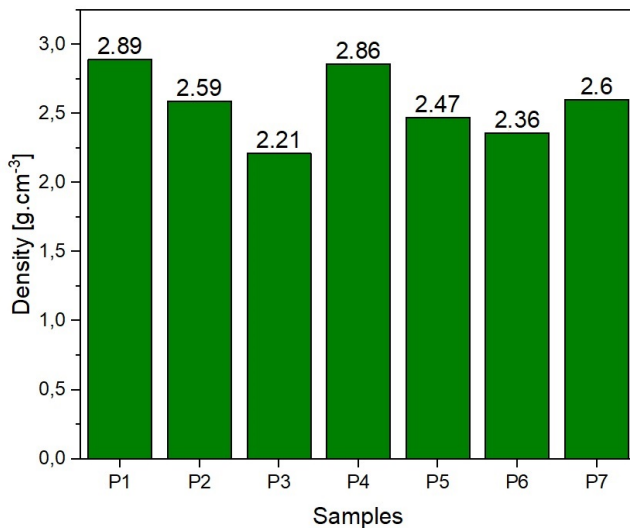
Figure 86: Sample densities after sintering.

These results are in agreement with the ones found by Stobierski e Gubernat (2003), which concluded that the densifica-

tion degree of the materials increases with boron concentration, which is likely due to two competing process: transport mechanism activation and boron dissolution in SiC. The same study also suggests that porosity is eliminated due to boron.

It is interesting to note that for both hydroborated samples in argon heat treatment (P1 and P2), density reduces with sintering temperature rise, this is not unusual, due to the tendency of closed porosity created at higher temperature. A possible explanation is that the samples were ball milled (P4 and P5), this factor (ball milling), probably increased the surface area of these samples. This increase in surface may have contributed for the diffusion in the gas phase or surface diffusion, thus reducing densification at higher temperatures. However, with a very low difference between the results P1 and P4 there is also the chance of being only a very small deviation from the result, since the temperature difference was not so high (50 ^{o}C).

Between the samples treated in ammonia, P7 had a higher densification with sintering at 1800 ^{o}C and previous ball milling. It is hard to evaluate the causes for this behavior, a possible reason is due to the loss of nitrogen and formation of boron bonded Si and C.

It can be seen that two materials (P3 and P6) lost considerable weight in two sintering regimens and possess a lower density. For the last sample, P6, this is probably due to a higher porosity cause by the liberation of compounds during thermal treatment caused by the previous ammonolysis, as previously discussed.

Li et al. (2015) measured the average weight loss ratio of pure BN after sintering at 2150 ^{o}C in argon, and was found to be ~4.61 wt%, a value very similar to the ones of P3 and P6 from the ammonolysis in this work (4.38 and 4.25 wt%). The theoretical density of sintered SiC-BN can therefore be well approximated by the rule of mixtures (MOGSTAD, 2016).

An important fact is that the sample with previous thermal treatment in ammonia at 450 ^{o}C (P7) had a smaller weight loss, as seen in Table 12 and had a higher densification than the P5 sample (PCS_B60) at 1800 ^{o}C sintering regimen. This demonstrated that the incorporation of nitrogen through ammonia gas

was effective, and samples with initial treatment at 200 ^{o}C were not effectively doped to the level of functionalizing the structure to improve the material. This means that probably there is boron acting as sintering agent and less Si-B or B-N in sample P7.

Also, this sample (P7) may have had a greater densification due to containing a larger quantity of boron content than sample P5 (PCS_B60). However, P7 densification was lower than P1, given the loss of nitrogenated radicals at high temperatures.

4.3.3.1   Thermal and electrical properties of RHP ceramics

Electrical conductivity and thermal diffusivity of the materials discussed on the previous section are shown in Table 15 and also presented in Figure 87.

Table 15: Electrical conductivity and thermal diffusivity of RHP ceramics.

Sample		Electrical conductivity (S.m $^{-1}$)	Thermal diffusivity at 20 ^{o}C (mm ^{2}.s $^{-1}$)
PCS_B30 (800 ^{o}C, Ar) (**1750°C** RHP)	**P1**	1076.08	23.1
PCS_B60 (800 ^{o}C, Ar) (**1750°C** RHP)	**P2**	337.61	20.2
PCS_B30 (200 ^{o}C, NH$_3$ / 800 ^{o}C, Ar) (**1750°C** RHP)	**P3**	387.28	5.96
PCS_B30 (800 ^{o}C, Ar) (**1800°C** RHP)	**P4**	3096.25	17.5
PCS_B60 (800 ^{o}C, Ar) (**1800°C** RHP)	**P5**	580.38	10.6
PCS_B30 (200 ^{o}C, NH$_3$ / 800 ^{o}C, Ar) (**1800°C** RHP)	**P6**	391.85	3.55
PCS_B30 (450 ^{o}C, NH$_3$ / 800 ^{o}C, Ar) (**1800°C** RHP)	**P7**	194.65	3.12

Therefore, it is seen that the electrical conductivity of the PCS_B30 in argon (P1 and P4) samples were considerably higher than the other ones ($1.07.10^3$ and $3.90.10^3$ S.m^{-1}, respectively). Moreover, P4 sample at a higher sintering temperature increased in almost three times its conductivity.

The increase in the electrical conductivity of these specimens can be attributed to the densification and to the improvement in the connectivity of the grains, which can be due to boron and more specifically to the B-C linkage.

Figure 87: Eletrical conductivity of the samples post sintering.
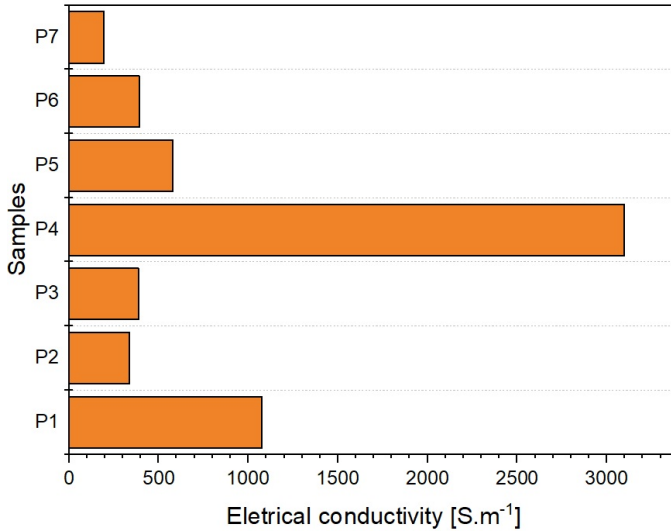
Reminding that silicon carbide is one of the most used semiconductors in electronic, specially in MEM that combine mechanical and electrical function in devices at very small scales (FRAGA et al., 2014; SPEARING, 2000; KUSUNOSE; SEKINO, 2014).

Electrical conductivity of silicon carbide depends on its structural polytype (IRMSCHER, 2002). However, SiC-based ceramics can be tailored to display very diverse electrical conductivity values within a range from 10^{-9} to 10^5 S.m^{-1}, depending on the type of doping, often resulting from sintering additives (ROMAN-MANSO et al., 2015).

Kusunose e Sekino (2014) described that for sintered SiC (temperatures of 1750 and 1850 ^{o}C), the location of the liquid phase and of the smaller pores disappear, and the grain boundary phase is less present at higher temperatures, thus, increasing the contact between the SiC grain and ultimately improving conductivity. Boron, as discussed in this work, has an effect in sintering and through it could increase conductivity.

For the remaining samples, with much lower electric con-

ductivity, probably there is a conformation of unordered crystals, where the grain boundary hinders SiC conductivy and augments the resistivity.

For the samples that underwent ammonolysis, N-atoms prefer to substitute C sites in SiC, creating a donor level near the conduction band of SiC and thus increasing the electrical conductivity of SiC. However, the nitride additives like BN where cations that could decrease the electrical conductivity by compensating for the N-derived donors (MALIK et al., 2018).

Thermal diffusivity of each of these samples was also measured and the results are presented in Table 15. There it may be observed that the greatest diffusivity was of argon pyrolysed PCS_B30 at 1750 ^{o}C (P1), followed by PCS_B60 sample with the same pyrolysis temperature (P2). The diffusivity values decreased for ammonia pre-treated samples, as well as with sintering temperature of 1800 ^{o}C.

These diffusivity levels decrease as the temperature increases (maximum at 500 ^{o}C, as shown in Figure 88 (for the samples with only argon treatment). In Figure 89 it is possible to see the same behavior for samples with ammonia pre-treatment and argon post-treatment.

Thermal diffusivity is strongly dependent on the density, thus, these results are comprehensible given the density variation. When comparing these values to steel, for example, which has a thermal diffusivity of 22.8 mm^2/s and quickly responds to thermal variations of the environment, it can be seen that samples P1 and P2 have a similar magnitude and will be expected to behave similarly to thermal changes.

The thermal diffusivity will also be affected by the degree of porosity (RUH; BENTSEN; HASSELMAN, 1984), as it will be seen in the results from 3D pieces using PMMA as sacrificial agent.

Figure 88: Thermal diffusivity as a function of temperature for samples obtained through pyrolysis under argon.
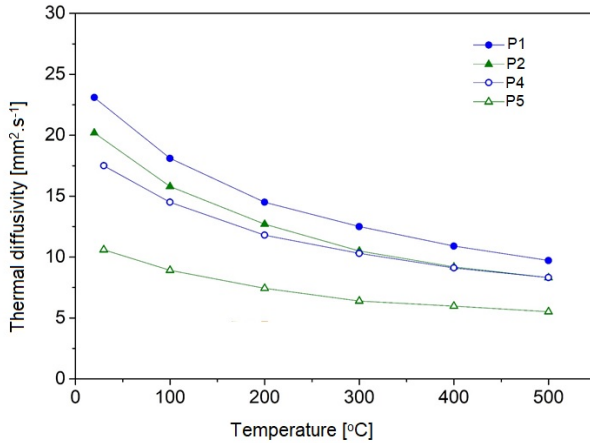
Figure 89: Thermal diffusivity as a function of temperature of the samples obtained through pre-treatment in ammonia and pyrolysis under argon.
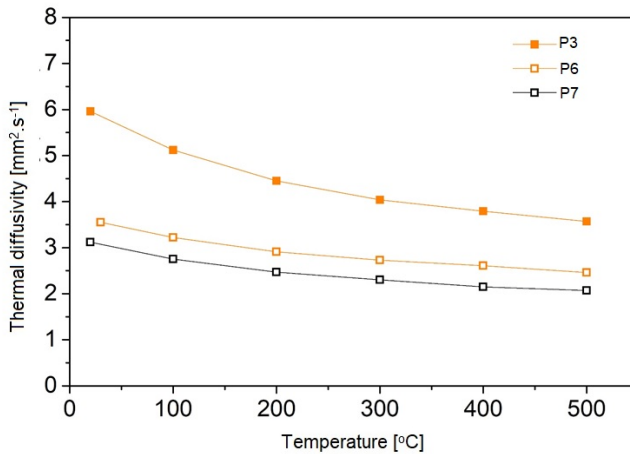
4.3.4   Summary

RHP methodology was shown to be viable to produce, in short periods (15 min holding at 1750 or 1800 ^{o}C), high electrical conductivity materials. P1 and specially P4 being noteworthy examples of this result.

In contrast for the samples obtained through this method after ammonia treatment, conductivity was very low. Similarly outcome found with the "partially" hydroborated samples. This demonstrates the capacity of boron to alter grain boundaries, turning the SIC grains interface much closer during densification and thus increasing electrical conductivity. Also it was shown that aminolysis interferes on the formation of Si-C, probably due to the formation of B-N and Si-N, creating grain boundaries that hinder electrical conductivity.

Therefore, it can be expected that density, which is deeply linked with these factors (electrical conductivity and thermal diffusivity), should be higher for samples P1 and P4, which was the case. It is curious that despite being the third highest density of this work, P7 samples (pre-treated at 450 ^{o}C in ammonia), showed the lowest electrical conductivity. This can be explained by a disorientation of the structure that hinders the mobility of the charge carriers of materials.

These materials with low conductivity can be considered electrical insulators, while the ones with low diffusivity can be described as thermal insulators (such as the ones that underwent ammonia pre-treated).

4.4 The design of macroporous Si(B)C ceramics

In the following sections of this work it will be presented and discussed the results regarding the production of macroporous ceramics (foams) using the hydroborated compound PCS_B30 as a preceramic precursor and PMMA spheres as the sacrificial agent.

Firstly, the results of the synthesis of silver functionalized PMMA spheres will open this section, which were used to produce foams in this work. Commercial PMMA were also applied in the foam produced here.

This will be followed by the presentation of the evaluation of block copolymers (SBS) and their application to obtain, through dip coating, a mesoporous coating for macroporous ceramics.

4.4.1 Silver functionalized PMMA nanospheres

350 nm PMMA (PAg350) synthesis through emulsifier-free emulsion polymerization (EFE) was performed to obtain particles with a narrow size distribution. This way this polymer could act as a sacrificial agent for controlled porosity generation with smaller pore size during pyrolysis in conjuction with 25 μm PMMA microspheres.

In the SEM image shown in Figure 90, it is possible to observe a small variation of the nanoparticle size from the PMMA nanosphere synthesis via EFE. The granulometric distribution graph, Figure 91, indicate an average diameter of 360 nm.

TEM analysis was performed to evaluate if the produced nanospheres were effectively functionalized with silver. This image is presented in Figure 92.

In Figure 92, it is possible to see characteristic silver nanoparticles black spots (Ag Np), as it was previously reported in the work by Sun et al. (2018), when synthesizing Ag Np.

The goal of adding silver was to create spaces surrounded by metal, during the formation of pores through pyrolysis, that would add silver's bactericide potential in filtration applications.

Figure 90: SEM of silver functionalized PMMA nanoparticles.
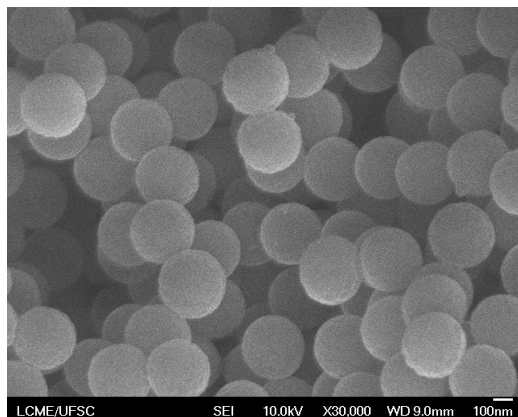
Figure 91: Granulometric distribution of silver functionalized PMMA nanoparticles, showing the narrow size distribution around 360 nm.
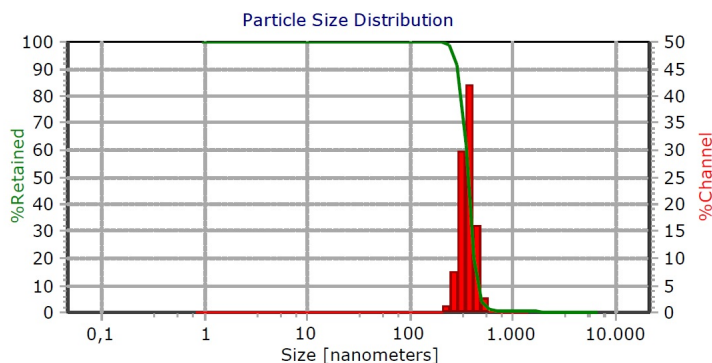
The results confirm the presence of silver nanoparticles, thus demonstrating that it is possible to produce PMMA with high particle size precision through EFE technique using AIBA and AIBN as water phase and oil phase initiators, respectively. It also demonstrated that it is possible to insert silver in its structure, specially close to the surface, as it was desired.

Figure 92:   TEM acquisition of silver functionalized PMMA nanoparticles.
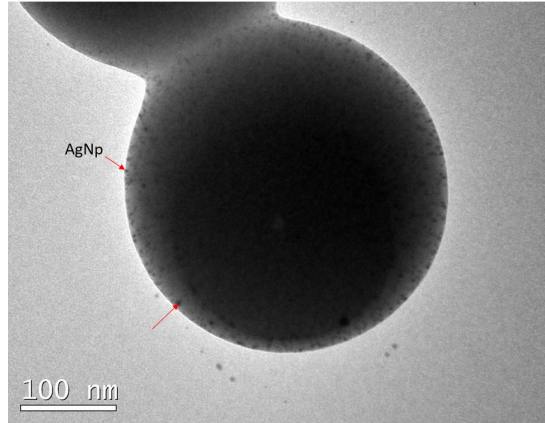
4.4.2   Silver functionalized PMMA microspheres

For the 25 μm sphere synthesis (PAg25), Figure 93 shows its particle size distribution analysis. The average particle size found for these spheres was 26.42 μm.

Figure 93: PAg25 particle size distribution analysis
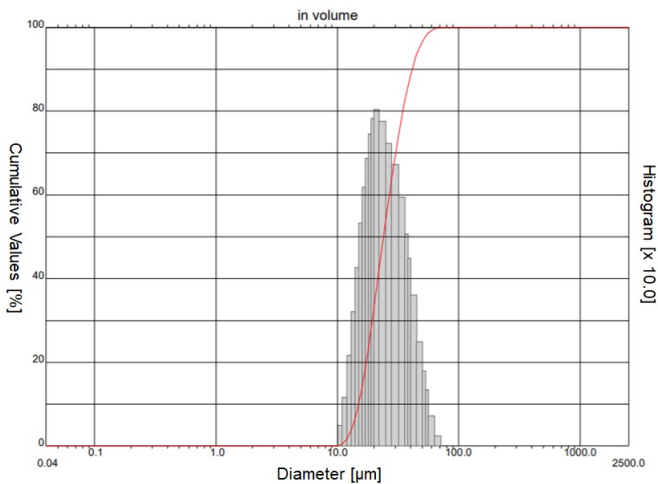
TEM analysis demonstrated that the sample possess a wide range of particle sizes, which is quite a common result when W/O/W emulsion is used. This is due to particle collision during the stages of this method and particle size control being harder in this very specific granulometric distribution range.

In Figure 94 it is observed the TEM image of the sample. Unlike PAg350 nanospheres, it was not possible to verify through this analysis the presence of silver nanoparticles.

Figure 94: TEM microscopy for PAg25 sample.
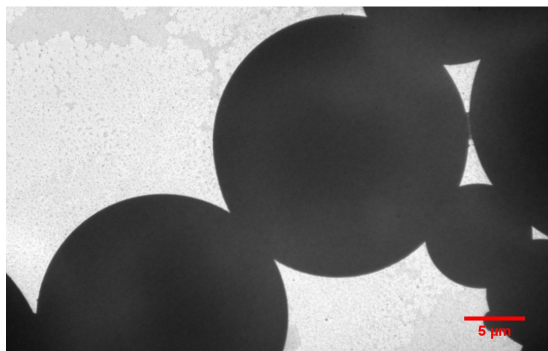
This does not necessarily mean that PAg25 does not contain silver in its structure, the quantity of added particles was very low and more profound analysis is needed to assess with certainty their presence in this sample.

To compare the particle size behavior of the PAg25 sample, it is shown in Figure 95 the P25 image, which is the commercial PMMA of 25 μm used in this work.

4.4.3   Production of foams by warm pressing

Given the results from PMMA synthesis with two different particle sizes, now it is followed by the results obtained using these particles to produce porous structures. Thus, in this work, three types of porous structures were fabricated, all using PCS_B30 as a precursor, albeit with different PMMA compositions (P25, PAg25 and PAg350).

Figure 95: Commercial 25 μ size PMMA's (P25) SEM image, which was used in this work.
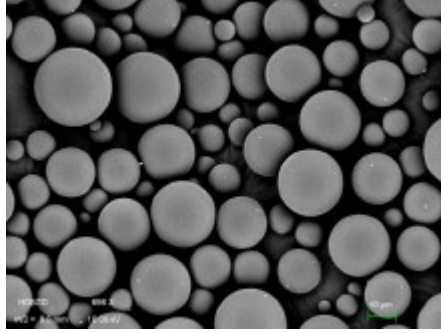
Source: Durif (2017)

The results for each formulation utilizing these different types of PMMA and different molds follow on the next items, starting by the formation of foams with P25 and PAg25 that were initially produced. This follows by having PAg350 mixed with P25, as it will be discussed further on.

4.4.3.1   Foams by 28.5 mm $\varnothing$mold using commercial PMMA as sacrificial agent

Two attempts were performed in the 28.5 mm diameter mold to averiguate the possibility to produce foams with bigger diameters and the results are shown in Figures 96 and 97. It was established as the standard to use 80 wt% of P25 and 20 wt% PCS_B30 in both attempts using this mold.

As it can be see in Figure 96, the structure broke after pyrolysis and was brittle afterwards. This was probably due excessive lost of compounds during the green body's thermal treatment. As, previously mentioned, all foams in this work were pyrolysed with these following settings: heating ramp of 0.5 ^{o}C.min^{-1}, up to 450 ^{o}C dwell time of 2 h and then 1000 ^{o}C and also dwell time of 2 h.

Figure 96: Warm pressing of P25 (3.2 g) + PCS_B20 (0.8 g) at 80 ^{o}C, holding time 30 min, 5 tons. On the left side of the image is the green body and on the right side the foam which broke during pyrolysis at 1000 ^{o}C.
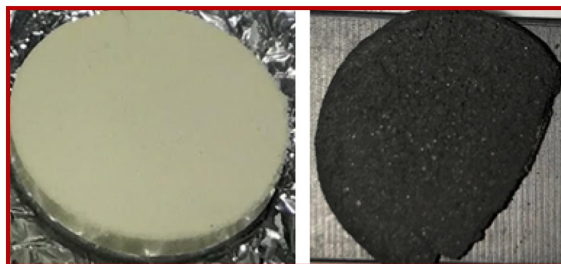
These heavy losses may have been caused by low compaction of the reagents during heating, which was performed at a lower (80 ^{o}C) than usual temperature used in this work for pressing (120 ^{o}C). When the pressing temperature was modified to 100 ^{o}C, using the same strategy as on the previous experiment (30 min, 5 tons, same reagent amount), there was another outcome. After pyrsolysis a foam with very visible cracks was obtained, as shown on Figure 97.

Therefore, a higher temperature during warm pressing resulted in a more compact, albeit cracked foam. More tests are required to establish the optimal procedure to obtain a crack-free foam using this mold.

Interestingly, when compared to the dense pellets from PCS_B30 developed in this work, foams with P25 were shown possible to be created, with the appropriate adaptations, which did not happen with the dense ceramics. Therefore PMMA is considered an important agent that will conduct pore formation, facilitating gas exhaustion during pyrolysis. The gas exhaustion process is quite complicated when there is only preceramic polymer in the formulation as in dense ceramics produced here. Also, a lower preceramic polymer amount also contribute towards foam fabrication.

In fact, usually it is very difficult to control the polymer-

Figure 97: Warm pressing of P25 (3.2 g) + PCS_B20 (0.8 g) at 100 ^{o}C, holding time 30 min, 5 tons. On the left side of the image is the green body and on the right side the cracked foam after pyrolysis at 1000 ^{o}C.

to-ceramic transformation, as during this process cracking can be induced and it is necessary to control crosslinking and thermolysis techniques. However, shape stabilization can also be achieved through the insertion of sacrificial agents during the production of larger size ceramic foams.

4.4.3.2 Foams by 25.6 mm ⌀ mold using commercial and synthesized PMMA (25 μm)

For warm pressing in this section, using the 25.6 mm diameter mold, it was established through previous tests the use of 2 g of the sample, as demonstrated with experimental procedures, being 80 wt% P25 or PAg25. The pressing settings were defined as 120 ^{o}C, 5 tons for 30 minutes.

In Figure 98 are shown the foams produced with PAg25 and PCS_B30, named F25A.

The weight loss for the F25A sample was of 73 wt%. This value was already expected, given that 80 wt% of the sample was PMMA, which suffers total thermal degradation. Degradation of PMMA beads starts approximately at 220 ^{o}C and completes at around 420 ^{o}C (VAKIFAHMETOGLU et al., 2009). The shrink-

Figure 98: Green body from the mixture of PAg25 and PCS_B30 with heating slope of 10 $^oC.min^{-1}$ up to 120 ^oC maintained for 30 minutes using 5 tons powder compression, on the left. On the right the resulting foam after 1000 ^oC pyrolysis.
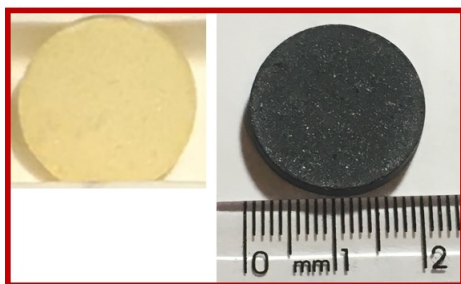
age of the structure was of approximately 45.48 vol%.

F25A was also analyzed by SEM, shown in Figure 99a, which due to its easy degasification lead to an open surface pore structure, where the PMMA particles are in contact with each other. There is also high inter-connectivity (Figure 99b), important for porous materials as it allows free diffusion of liquids.

Figure 99: SEM images- a. F25A surface shown open and in contact pores; b. pore amplification and its inter-connectivity.
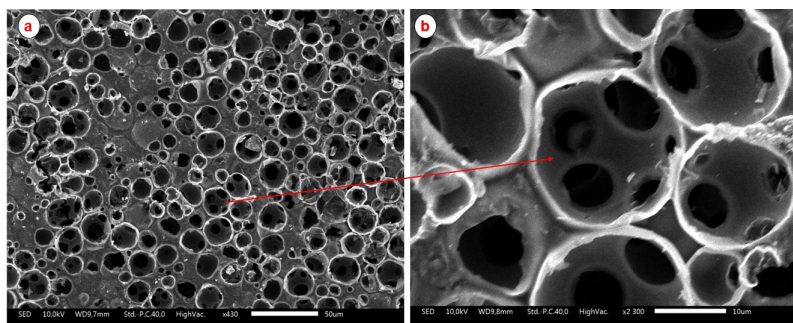
Due to wearing of the mold caused by repetitive use, tiny defects were observed in the obtained ceramics. There was a smaller amount of processing defects in this foams, which due

to the mold design, through the green body removal action after compaction and experiment repetition the mold wear became more pronounced. Nonetheless, these small defects do not affect the final foam structure, as they are just minuscule breakages on the borders of the piece or tiny variations on the surface flatness. Yet, no cracks were seen on the surface.

For the production using commercial PMMA (P25), the same strategy was applied and yielding similar results were found, which are shown in the next images. On the first one, Figure 100, the green body is shown on the left side and the final formed ceramic (named F25) on the right side.

Figure 100: On the left, the green body from the P25 (commercial PMMA) and PCS_B30 mixture. On the right, post-pyrolysis (at 1000 ^{o}C).
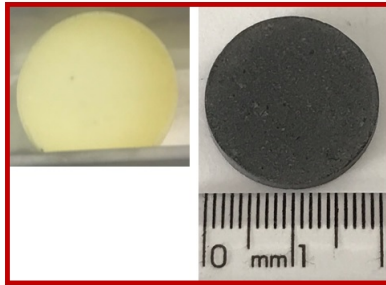
Weight loss and shrinkage values obtained for foam F25 were similar, albeit higher, than F25A . These results were respectively of 76.2 wt% and 47.4 vol%.

It is possible that silver synthesized PMMA (PAg25) has a more efficient packaging than commercial PMMA. Alternatively, it could be that the presence of silver provides a small compensation to the weight loss and volume, but it would require further analysis to identify the definite reason for this behavior.

Naturally, there is a variation in ceramic production and the differences are too small to infer an improvement by using synthesized PMMA based on these results. When compared, the SEM photographs are almost the same. In Figure 101 is

shown F25's internal structure, displaying high porosity and the
formation of interconnected pores.

Figure 101: Internal foam SEM image (commercial PMMA and
PCS_B30).
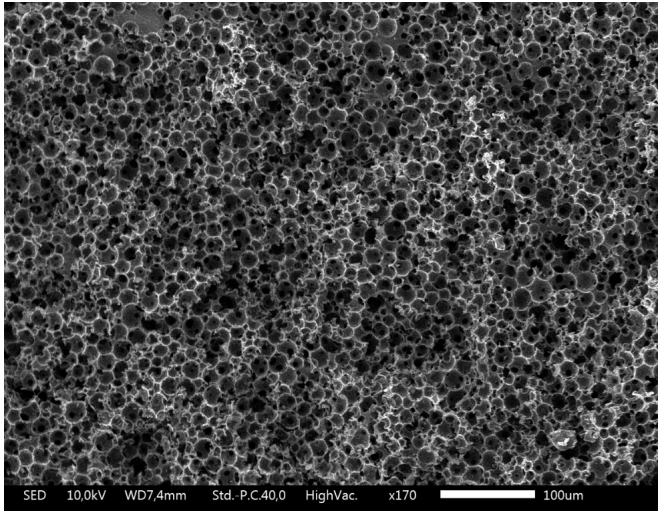
Pores in both foam had a large variation of size, which is
mostly due to the PMMA particle size distribution which had a
wide range, as previously discussed. The size varied, including
interconnections from 2 to 23 μm.

According to Gibson e Ashby (1999), the presence of cells
with a non-homogeneous size distribution is not necessarily a
problem, as many of the important porous ceramic properties
(such as thermal diffusivity, electrical conductivity, hardness,
etc.) are not directly linked to the cells themselves and are more
directly related to the density. This, in turn, as previously dis-
cussed, is affected by the total porosity.

Also, cell shape and size were slightly different to the ones
from PMMA sphere due to shrinkage during pyrolysis.

Some mechanical properties of the F25 sample were tests:
for hardness, the maximum value was 2.46 GPa, and the Young's
Modulus (E) found was of 25.77 GPa (40.065 mN load), as shown

in Figure 102.

Figure 102: Indentation test graphic for the F25 sample, showing its Hardness (H) and Elastic Modulus (E)
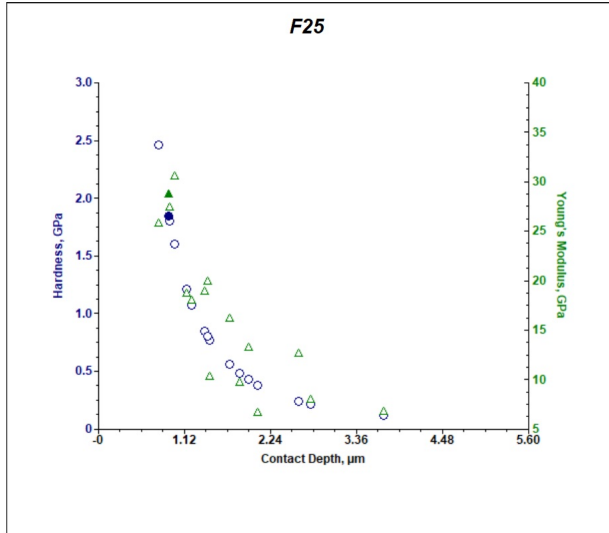
An Elastic Modulus of 16 GPa was found by Shibuya, Takahashi e Koyama (2007) when producing micro cellular silicon oxycarbides by pyrolysis of methylsilicone resin and sacrificial microbeads of polymethyl methacrylate (PMMA), this result was obtained when the PMMA addition was 50 wt%. The PMMA microbeads were added in the range from 0 to 80 wt%, and the pyrolysis was performed at 800 – 1200 °C. The PMMA used in this article had an average particle size of 4.7 μm and the shrinkage value reaches about 60 vol% by a PMMA addition of 80 wt%.

Due to the fact that most porous ceramic production with PMMA use oxide preceramic polymer, which forms SiOC (silicon oxycarbide), there are few comparative works in the literature.

For example, in the work by Colombo e Bernardo (2003) where macrocellular and microcellular SiOC open cell ceramic foams were fabricated from a preceramic polymer. Macrocellular foams (cell size ranging from 50 μm to few millimeters) were

producing using precursors for polyurethane in dichloromethane (with the addition of surfactants and catalysts), a more complex and costly process. Microcellular ceramics (cell size below 50 μm, which can have a cell density higher than 10^9 cells per cm^3), were produced using PMMA as sacrificial agent by uniaxial pressing at room temperature with a silicone resin (COLOMBO, 2010; COLOMBO; BERNARDO, 2003).

In another work (KOTANI et al., 2011), foams were obtained by incorporating sacrificial pore-forming plastic powder, PMMA microbeads, into AHPCS, without critical crack initiation. PMMA of the following sizes were used: 1.5, 10, 40, 90, and 180 μm. The AHPCS polymer and the PMMA were mixed together by stirring for several minutes in the atmosphere, the slurry was then formed into a disk (warm pressing was not used) and heated up without pressure. For some of the tested ratios, the powder could not be mixed uniformly due to insufficient fluidity even if a solvent was used and with the excessive use of pore-forming particles the ceramic cracked. Foam was successfully produced under the conditions of 90 μm m, 68 vol% and 900 ^{o}C, however closed pores were found and no sample characterization was performed. The volume shrinkage of the sample was approximately 65 vol%.

4.4.3.3   Foams by 25.6 mm $\varnothing$ mold using P25 and PMMA nanoparticles (PAg350)

The same methodology used for 25.6 mm $\varnothing$ with P25 (F25) was used for the productions of PAg350 added foams. The only difference was on the sample quantity, that in spite of keeping the 80:20 PMMA:PCS_B30 ratio also had the addition of PMMA nanoparticles (360 nm average size, as described in the sample characterization).

Thus, the total weight was set to 2 g, divided in: 0.4 g PCS_B30, 1.2 g P25 and 0.4 g PAg350. The warm pressing yield of this sample, as well as its ceramization are displayed in Figure 103. The obtained foam was labeled F350.

Figure 103: On the left, green body from P25, PCS_B30 and PAg350 mixture. On the right, the foam after pyrolysis at 1000 ^{o}C.
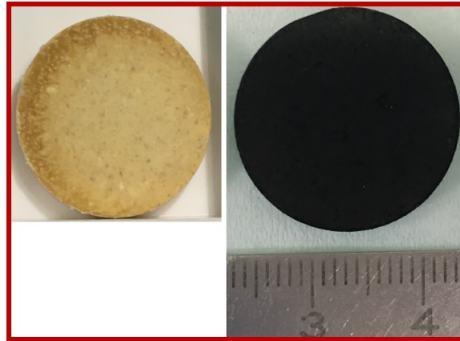
The green body, as shown in Figure 103, possesses a different color to the other green bodies produced in this work. This is due to the silver added 350 nm PMMA used in this experiment. Silver, in colloidal state and with low molecule aggregation does present this "mustard" color (DINESH; KARTHIKEYAN; ARUMUGAM, 2012). Hence, PMMA acquires this tonality when blended with the yellow powder and after warm pressing this color difference to the other samples becomes even more pronounced.

With the insertion of PAg350, the foam became more porous, visible to the naked eye, as it was expect, and both free of cracks and breaks. Weight loss was of approximately 72 wt% while 40 vol% shrinkage was measured. Thus, this ceramic showed a lower volume retraction and weight loss, which may be an indicator that, even though porosity was increased, the nanometric PMMA effect was of maintaining the shape. As a lower amount of P25 was added, there was a lower weight loss than other foams, despite PAg350 weight compensation. As previously hypothesized for the F25A sample, the addition of silver may also have contributed to these figures being lower.

Electronic microscopy (SEM) results from this sample are presented in Figures 104 and 105.

Figure 104: SEM images- a. F350 surface showing open and in contact pores; b. internal view of the structure through a transverse cut of the sample.
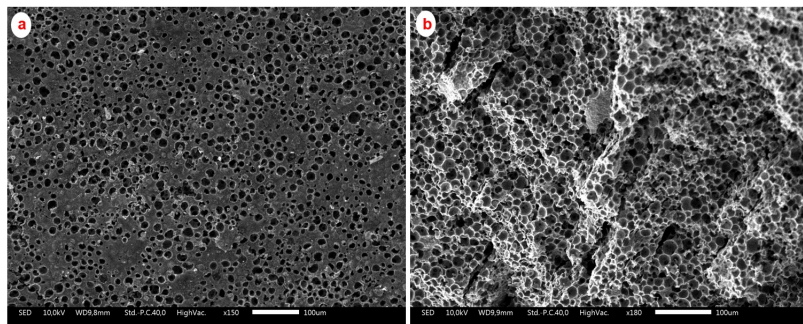
Figure 105: SEM images- a) zoom of F350's internal structure highlighting the interconnected porosity; b) magnification of the pore in image showing nanometric pores and c) amplified pores from image "b" with marked dimensions.
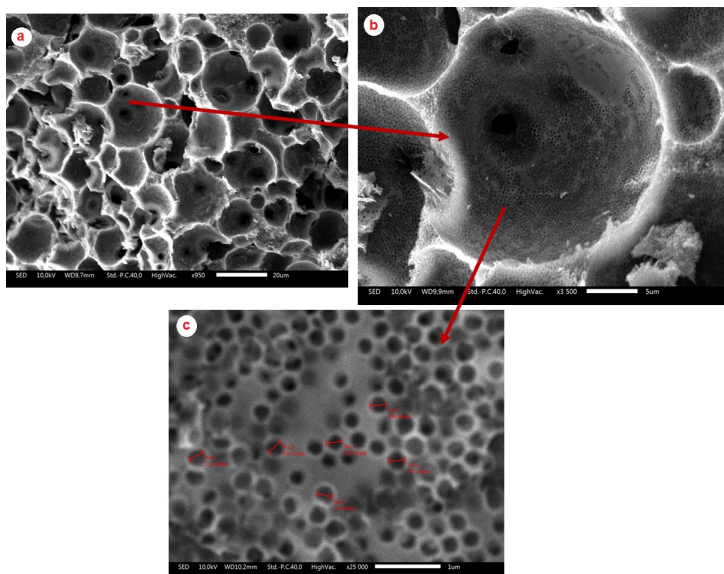
Therefore, in Figure 104a it is possible to view the F350's surface. In Figure 104 its internal structure can be observed. In all images, a high pore connectivity was identified, showing a very similar outcome to the previous experiments (F25 and F25A).

In Figure 105 the main difference of using PAg350 can be observed: the formation of high interconnectivity of pores throughout the whole structure with average size of 240 nm. This is a particularly interesting result as there were reports of such outcome in other structures produced in this research or in similar works found in the literature.

This porosity difference, with much small pores than the ones obtained by solely using 25 μm PMMA, can be useful for various filtration processes, where it can be applied for molecular scale filtration, for example. Thus, the pore size obtained with F25 and F25A can be used to filter particles, while in the 240 nm range, it may be used to separate molecules.

TEM analysis of this sample was performed to assess the presence of silver after 1000 ^{o}C pyrolysis, as it can be seen in Figure 106. The black spots were considered to be from silver in an amorphous region.

Figure 106: F350 TEM with SAED diffraction technique.
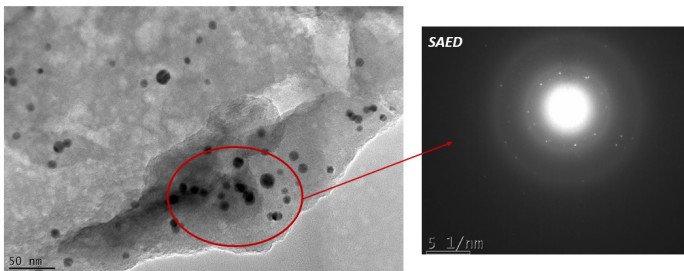
SAED makes evident the fcc structure with clear lattice rings. The crystallographic planes from silver (111), (311) and (220) were found in this image with CrystBox software, using JCPDS, file 04-0783, confirming high resolution TEM image results.

Thermal diffusivities of the dense structure using a 25.6 mold (PSBd$_{25}$) and F25 and F350 porous ceramics were compared. The results are presented in Figure 107.

Figure 107: Thermal diffusivity at room temperature for samples PSBd$_{25}$, F25 and F350.
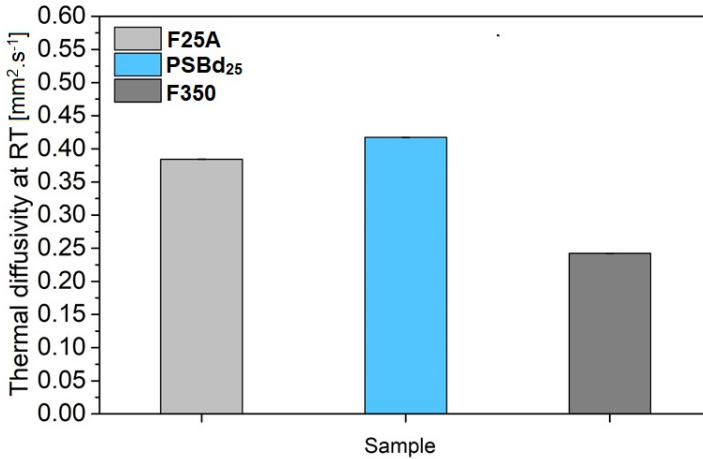
F350 showed the lowest thermal diffusivity, which was expected due to its visibly more porous structure. Porous ceramics are known to be good thermal insulators, as several works have already shown (RHEE, 1975; YU et al., 2018).

4.4.4   Summary

Foams were created using both types of molds, of 28.5 (D28) and 25.6 (D25) mm diameters, that were tested. However, the best resulting structure obtained using the D28 mold was fragile and with many cracks. Hence, even though it showed promise to create macroporous structure, further research and experiments are required to optimize the methods with this mold.

In contrast, the D25 mold was shown to be able to easily succeed to produce porous SiC bodies through the PDC route. This was achieved by a mixture of sacrificial pore former (as

powder), PMMA microbeads created in this work (PAg25 and PAg350) and commercial PMMA (P25), with a solid preceramic polymer, PCS_B30.

PCS_B30-derived porous SiC was reproducibly formed without critical crack initiation. This was only achieved when the preceramic polymer was sufficiently compressed with well distributed PMMA, forming a strong skeletal structure. The porous structured contributes to an efficient gas emission and uniform thermal shrinkage during polymer pyrolysis, thus reducing internal pressure and thermal stress causing cracks.

It is also relevant to highlight the presence of silver in the ceramic sample F350, confirmed by HRTEM, which may reduce weight loss and shrinkage. As for the 25 μm PMMA sample, further analysis are necessary to verify the presence of silver.

Finally, it would be very interesting to obtain data on the compressive strength of the porous ceramics presented in this work and thus understand stress impact on the samples here obtained.

4.5   Functionalization of foams (coatings with Kraton)

Block copolymers based on styrene and butadiene (SBS) were used in this stage. Thus, a description of the results for the creation of a mesoporous layer using these materials as soft templates by self-assembly technique will be discussed.

Before the application by dip coating of the mesoporous layer on the foam, a brief study was conducted to verify SBS's behaviour, as it has a big impact on the final ceramic porosity.

A primary example of this pore modification is the influence on the composition (molecular weight) of copolymers. When polystyrene phase is only a minor part of the total volume, a structure as illustrated in Figure 108, is formed, where there are the cylindrical domains of PS in PB matrix.

Figure 108: Phase structure of SBS.
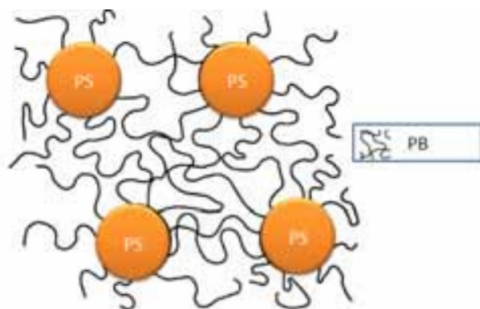
Source: Kennedy e Higginbotham (2011).

Therefore, as is the case of this work, where PS is the part with the least concentration in SBS ($\sim$30 wt%) the expected morphology are of structures where the polystyrene phase consists of separate spherical regions known as domains. This can be seen in Figure 109, where Atomic Force Microscopy (AFM) for each structure formed using the four different studied block

copolymers are found. These structured were obtained by a precipitation-free solution in toluene and solvent evaporation for 24 h at room temperature.

Figure 109: AFM images of ordered microstructure of SBS "A", "B", "C" and "D" after toluene evaporation and a zoom of the SBS structure "D".
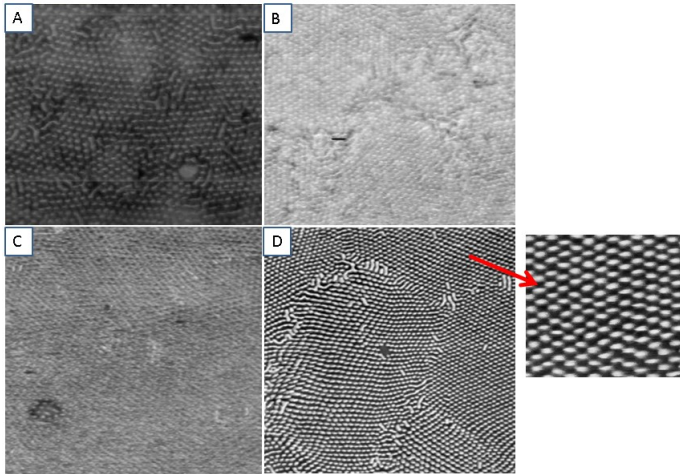
Yet, according to Kennedy e Higginbotham (2011), when SBS is heated, the domains soften and the network loses its strength resulting in the ability of the block copolymer to flow which is one of the main characteristics associated with these types of thermoplastic elastomers. When the heated block copolymer is cooled, the domains become hard and the original properties are regained.

The object formed after solvent evaporation was similar to a very malleable rubber due to the presence of polybutadiene (PB). The lamellar structure, also visible on the images, however in lower quantities is PB, as verified by Kim e Libera (1998), when SBS triblock copolymer microstructures were studied.

The primary structures of all SBS utilized in these work were very similar. Therefore, the choice of a type of block copolymer for the dip coating stage, the following parameters were eval-

uated: (i) the formed structured analysed through AFM and
BET; (ii) some practical tests: the difficulty to coat samples and
solvent solubilization. In some cases, the samples turned into a
viscous gel in solution (as they contained more polybutadiene)
and there fore were discarded given the greater difficulty to apply
a coating without flaws.

Finally, the selected structure was of SBS "A" (SBSa).
With the solution of SBSa and PCS_B30 (in toluene) films with
different ratios were produced. After pyrolyzing these films at
800 ^{o}C (as in Figure 110), their surface area was measured. The
best result or the biggest value for surface area was of 72.95
m^2.g^{-1} from the 1.33 ratio experiment.

Figure 110: On the left side is shown film formed in the PTFE
mold. On the right side is the amorphous film after 800 ^{o}C
pyrolysis.
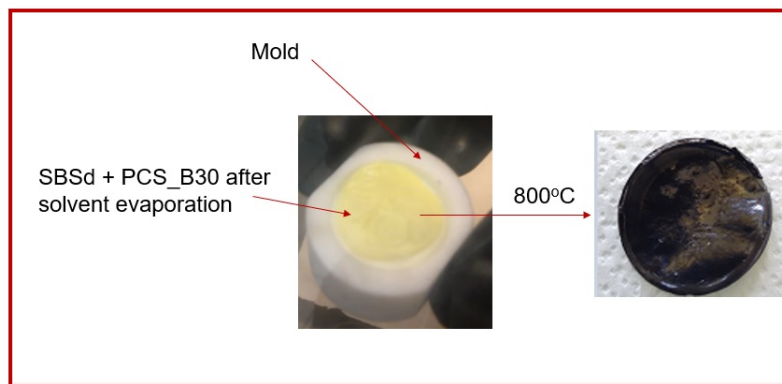
From the 1.33 ratio experiment, the AFM analysis could
show the formation of the structure, when the film was pulled
from the PTFE mold and heat treated at 120 ^{o}C in argon, as
seen in Figure 111.

Therefore, the SBSa and PCS_B30 1.33 ratio solution was
coated on the foam. After solvent evaporation in a glovebox for
24h, it was pyrolyzed at 800 ^{o}C. Figure 112 shows the green body
with a SBSa solution layer and the formed ceramic after pyolysis.

Figure 111: AFM image from 1.33 ratio (SBSa and PCS_B30 (in toluene) film) after treatment in argon at 120 ^{o}C.
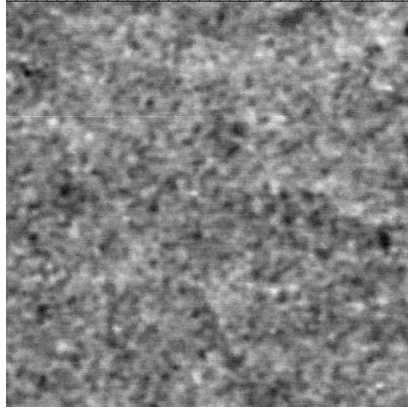
Figure 112: On the left side is the green body with a SBSa and PCS_B30 1.33 solution layer and on the right side the ceramic after 800 ^{o}C pyrolysis.
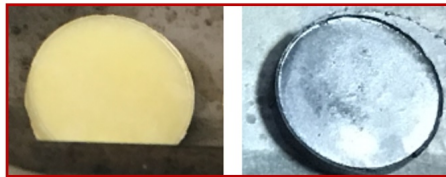
SEM microscopy analysis makes evident the mesoporous structure formed above the macroporous foam structure, as it can be observed in Figure 113.

Therefore, structured constituted of macroporous and mesoporous layers were obtained, more experiments and analysis are required to validate whether the coating technique can produce a flat and crack-free foam surface. For foams with 10 mm of diameter it was possible to observe the absence of cracks, but for larger sizes this has yet to be evaluated.

Figure 113: SEM of yield after 800 ^{o}C pyrolysis. a) macroporous support coated by a mesoporous layer; b) increase of the mesoporous layer with pore size between 10 and 14 nm.

Macroporous SiC support

Mesoporous layer
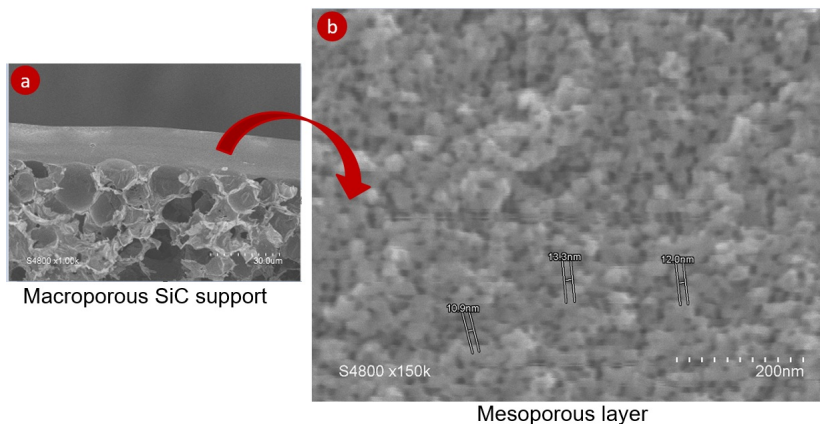
4.6   Results for other methodologies

A mixture of AHPCS and DCP was made for the first technique used in this section to obtain a solid preceramic capable of maintaining its shape during warm pressing. DCP was used as it is a recognized thermal initiator, acting as a crosslinking agent via thermal treatment. Hence, the mixture became solid (labelled as PCSd) at approximately 110 ^{o}C and able to be shaped through warm pressing.

However, during PCSd powder pressing, it was not possible to form a sufficiently compact structure for posterior pyrolysis. In fact, the pressing temperature utilized was of 120 ^{o}C for 30 minutes using 5 tons. The goal of this work was not to utilize high pressing temperatures (above 120 ^{o}C). It was therefore expected that a green body with shape retention would not be formed at this temperature due to low crosslinking. Through TGA analysis (graph shown in Figure 116), the ceramic yield of the PCSd sample was found to be lower than the ones for PCS_B30 and PCS_B60. Therefore, it can be concluded that the sample had a

large loss of volatile oligomers and without having a space holder (such as PMMA) it would be very difficult to achieve an acceptable result.

It is very likely that a structure with a higher crosslinking degree, using more DCP content or higher temperature, both for synthesis and maybe for pressing, would result in the formation of a structure. However, using these methods were not the focus of this work, considering the potentiability that had already been found with the PCS_B30 polymer. Thus, this alternative/production was not continued.

In the second technique, to confirm the hypothesis that PMMA as sacrificial agent could assist in the formation of a structured green body capable to retain the shape due to PMMA "space holder" capacity, AHPCS was used in mixture with DCP for thermal crosslinking and silver benzoate as precursor for silver (sample labeled PCSdAg) and finally, mixed with commercially PMMA (P25).

The warm pressing of this material resulted in a compact green body, which after pyrolysis formed a highly shrinkage ceramic (65 vol%), as well as the weight loss which was also very high (approximately 70 wt%). Figure 114 shows the green body formed after pressing, with the color characteristic of silver, as seen in the foams using PAg350.

Figure 114: Green body from the synthesized material using DCP, silver benzoate, AHPCS (PCSdAg) and P25 after warm pressing.

And, in Figure 115 there is a comparison of the formed ceramic disk (called Fdcp) with the other foams produced in this

work, in order to verify the effect of shrinkage.

Figure 115: Comparison of Fdcp's foam with F350 F25A.
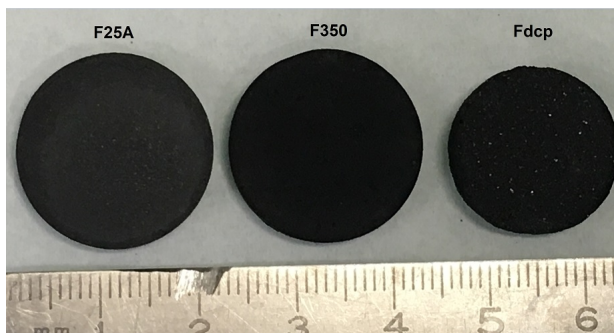
The weight loss was expected since during TGA tests (as in the graph of Figure 116) these samples had a ceramic yield below the other compounds synthesized in this work.

Figure 116: TGA of the samples obtained in this work.
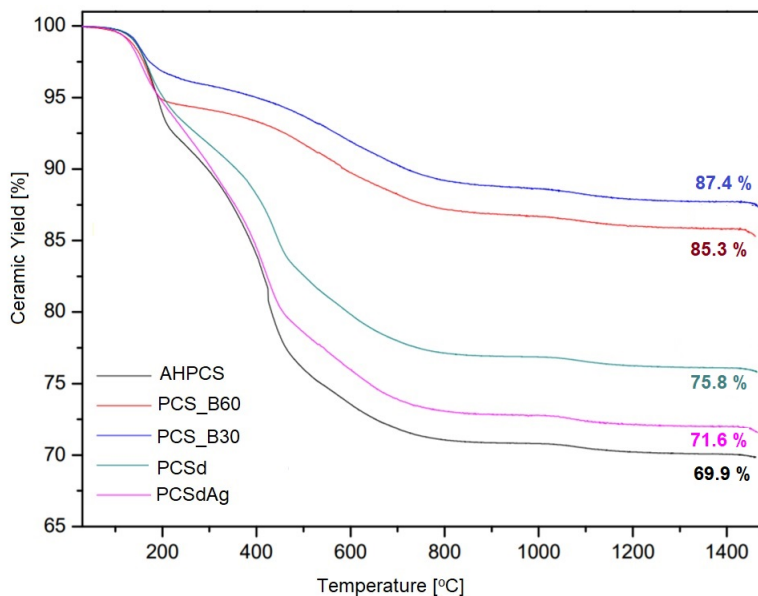
Finally, the purpose of this section was to present different alternatives to the methodology using PCS_B30 as preceramic polymer, however, the most satisfactory results show that dense ceramics and foams are benefited by the addition of boron at the molecular level, not requiring high powder compacting temperatures, as well as it is not necessary to reach high temperatures for a crosslinking that allows to retain the shaping during warm pressing.

5 Conclusions

In this work it was shown that using the PDC route, through a single-source precursor, it is possible to perform the synthesis of Si-(B)-C. These ceramic's microstrucuture may be adapted using this technique. Furthermore, the presented structures reveal the applicability of this preparation technique for the processing of samples with adjustable density and porosity.

Ceramic materials were successfully synthesized by the chemical modification of allylhydridopolycarbosilane (AHPCS) with molecular boron precursor.The obtained hydroborated AHPCS can be attested as promising precursor for the synthesis and processing of ceramic structures with a specific phase compositions and microstructure.

Crack-free dense SiC ceramic's were obtained at 1000 ^{o}C (in argon) through warm pressing, without any further additional treatments. Despite volume loss due to both material change and gas loss during thermal treatment, it was observed that the addition of boron led to a significative improvement of the results and interesting mechanical properties of the 3D dense piece.

Also, dense ceramics were obtained through the Rapid Hot Pressing technique and hydroborated AHPCS with 2.89 g.cm^3 density at 1750 ^{o}C, demonstrating that it is viable to produce, in short periods (15 min holding at 1750 or 1800 ^{o}C), dense strucutures with high electrical conductivity (3096.25 S.m^{-1}).

The use of reactive gases, as was the case for ammonia at relatively low temperatures (450 ^{o}C) before the RHP process, as a material pre nitration stage, led to modifications of the ceramic structure. This effect was even more apparent on the thermal and electrical properties analysis of this material. Despite more analysis being necessary to establish the complete pre-nitrated hydroborated AHPCS behavior, it is evident that different gases will directly influence on the chemical structure and specific ceramic characteristics and, in addition to this, may be an interesting alternative for promoting different class of ceramic materials

without involving more complex synthesis.

Likewise, porous structures (foams) also were obtained through warm-pressing, whereby the employment of PMMA may retain shaping and promote gas exit, leading to a relatively easy production route for this type of material. Also, the use of block copolymer helped towards the formation of a mesoporous structure when mixed with boron modified AHPCS.

Furthermore, it was also confirmed the presence of nanometric silver on the PMMA structure, which was also present on the final ceramic after pyrolysis at 1000 ºC. This may be further researched in future works regarding its application as a bactericide in filtration processes, for example.

5.1   Suggestions for future works

This research work has enabled the elaboration of ceramic structures that in future works might be evaluated in order to measure its density and porosity (through Hg porosimetry), as in the case of porous structures (foams). Other mechanical characterizations common for foams, such as compression strength, also becomes interesting.

Moreover, it becomes necessary to study the behavior of sacrificial agents functionalized with silver, so that it is possible to assess the effect of nanometric silver as bactericidal agent and its impact when applied along with the filtering media in the environment.

It is clear the demand to evaluate the applicability of all 3D ceramics structures obtained by warm-pressing, using PCS_B30 and the different manufactured PMMAs. In addition, in the case of foams functionalization with the solution containing block copolymer.

These foam+mesoporous layer, for its part, might be deeper evaluated, in order to be possible to get improvements to allow the establishment of a coating technique that does not interfere in the foams structure and contributes to the processes to which it will be designated.

The thermal treatments under ammonia applying low tem-

peratures serve of great incentive for future studies, given the technique innovation faced with the existent publications. There are necessary deep characterizations to understand how this gas modifies hydroborated AHPCS properties. Furthermore, as comparative term, the application of AHPCS as ceramic precursor for the RHP process has to be studied, thereby, the boron interference in the material structure when sintered through RHP, will be better evaluated.

Other methods might be developed in the future, aiming the improvement of 3D structures obtained in this work, in order to tailor the technique to obtain greater structures, and, the cost assessment to establish the advantages of using such synthesis precursors.

Bibliography

ABDERRAZAK, H.; HMIDA, E. S. B. H. *Silicon Carbide: Synthesis and Properties.* Rijeka: IntechOpen, 2011. Citado 3 vezes nas páginas 39, 43, and 158.

ACTON, Q. A. *Issues in Structural and Materials Engineering: 2011 Edition.* [S.l.]: ScholarlyEditions, 2012. ISBN 9781464963971. Citado na página 128.

ADHIKARI, S.; FERNANDO, S. Hydrogen membrane separation techniques. *Industrial & Engineering Chemistry Research*, ACS Publications, v. 45, n. 3, p. 875–881, 2006. Citado 2 vezes nas páginas 67 and 68.

ANJOS, V. et al. Thermal lens technique for the determination of sic thermo-optical properties. v. 527, p. 703–706, 2006. Citado na página 160.

ANSALONI, L. M. S.; SOUSA, E. M. B. de. Boron nitride nanostructured: Synthesis, characterization and potential use in cosmetics. *Materials sciences and applications*, Scientific Research Publishing, v. 4, n. 01, p. 22, 2013. Citado na página 148.

ARAYA, N. I. et al. Effect of heat treatments and sic content in the mechanical properties and microstructure of self-lubricating steels. *Materials Research*, SciELO Brasil, v. 21, n. 1, 2018. Citado na página 145.

BERGER, F. et al. Solid-state nmr investigations on si-b-c-n ceramics derived from boron-modified poly (allylmethylsilazane). *Zeitschrift für anorganische und allgemeine Chemie*, Wiley Online Library, v. 631, n. 2-3, p. 355–363, 2005. Citado na página 135.

BERNARD, S.; MIELE, P. Ordered mesoporous polymer-derived ceramics and their processing into hierarchically porous

boron nitride and silicoboron carbonitride monoliths. *New Journal of Chemistry*, Royal Society of Chemistry, v. 38, n. 5, p. 1923–1931, 2014. Citado na página 70.

BERNARD, S.; MIELE, P. Polymer-derived boron nitride: a review on the chemistry, shaping and ceramic conversion of borazine derivatives. *Materials*, Multidisciplinary Digital Publishing Institute, v. 7, n. 11, p. 7436–7459, 2014. Citado na página 45.

BERNARD, S. et al. Boron-modified polysilazane as a novel single-source precursor for SiBCN ceramic fibers: synthesis, melt-spinning, curing and ceramic conversion. *Journal of Materials Chemistry*, v. 15, n. 2, p. 289, 2005. ISSN 0959-9428. Disponível em: <http://xlink.rsc.org/?DOI=b408295h>. Citado na página 52.

BERNARDO, E. et al. Advanced ceramics from preceramic polymers modified at the nano-scale: A review. *Materials*, Multidisciplinary Digital Publishing Institute, v. 7, n. 3, p. 1927–1956, 2014. Citado 2 vezes nas páginas 64 and 67.

BHADURI, S.; BHADURI, S. *Chapter 11 Combustion synthesis*. [S.l.]: Pergamon, 1999. 289 - 309 p. (Pergamon Materials Series, v. 2). ISSN 1470-1804. Citado na página 44.

BLUM, Y. D.; SCHWARTZ, K. B.; LAINE, R. M. Preceramic polymer pyrolysis. *Journal of materials science*, Springer, v. 24, n. 5, p. 1707–1718, 1989. Citado na página 61.

BORCHARDT, L. et al. Preparation and application of cellular and nanoporous carbides. *Chemical Society Reviews*, Royal Society of Chemistry, v. 41, n. 15, p. 5053–5067, 2012. Citado na página 45.

BORDIA, R.; TOMAR, V.; HENAGER, C. Precursor derived nanostructured si-cx materials for nuclear applications. final report, october 2010-september 2014. 2015. Citado 2 vezes nas páginas 60 and 61.

BUONOMENNA, M.; YAVE, W.; GOLEMME, G. Some approaches for high performance polymer based membranes for gas separation: block copolymers, carbon molecular sieves and mixed matrix membranes. *RSC Advances*, Royal Society of Chemistry, v. 2, n. 29, p. 10745–10773, 2012. Citado na página 77.

BURNS, G. T.; CHANDRA, G. Pyrolysis of preceramic polymers in ammonia: preparation of silicon nitride powders. *Journal of the American Ceramic Society*, Wiley Online Library, v. 72, n. 2, p. 333–337, 1989. Citado na página 146.

CHAE, S.-H. et al. Porosity control of porous silicon carbide ceramics. *Journal of the European Ceramic Society*, Elsevier, v. 29, n. 13, p. 2867–2872, 2009. Citado na página 68.

CHEN, L.; GOTO, T.; HIRAI, T. Preparation of silicon carbide powders by chemical vapour deposition of the (ch3)2sicl2-h2 system. *Journal of Materials Science*, v. 25, n. 11, p. 4614–4621, Nov 1990. ISSN 1573-4803. Citado na página 44.

CHEN, Y. Structure and properties of polymer-derived sibcn ceramics. 2012. Citado na página 99.

CHOU, K.-S.; LEE, T.-K.; LIU, F.-J. Sensing mechanism of a porous ceramic as humidity sensor. *Sensors and Actuators B: Chemical*, Elsevier, v. 56, n. 1-2, p. 106–111, 1999. Citado 2 vezes nas páginas 67 and 68.

COLOGNA, M.; RASHKOVA, B.; RAJ, R. Flash sintering of nanograin zirconia in< 5 s at 850 c. *Journal of the American Ceramic Society*, Wiley Online Library, v. 93, n. 11, p. 3556–3559, 2010. Citado na página 63.

COLOMBO, P. Conventional and novel processing methods for cellular ceramics. *Philosophical Transactions of the Royal Society of London A: Mathematical, Physical and Engineering Sciences*, The Royal Society, v. 364, n. 1838, p. 109–124, 2006. Citado na página 83.

COLOMBO, P. *Polymer derived ceramics: from nano-structure to applications.* [S.l.]: DEStech Publications, Inc, 2010. Citado na página 184.

COLOMBO, P.; BERNARDO, E. Macro-and micro-cellular porous ceramics from preceramic polymers. *Composites Science and Technology*, Elsevier, v. 63, n. 16, p. 2353–2359, 2003. Citado 2 vezes nas páginas 183 and 184.

COLOMBO, P. et al. Polymer-Derived Ceramics: 40 Years of Research and Innovation in Advanced Ceramics. *Journal of the American Ceramic Society*, p. no–no, jun 2010. ISSN 00027820. Disponível em: <http://doi.wiley.com/10.1111/j.1551-2916.2010.03876.x>. Citado 3 vezes nas páginas 47, 56, and 61.

COMBUSTION synthesis: an update. *Current Opinion in Solid State and Materials Science*, v. 6, n. 6, p. 507 – 512, 2002. ISSN 1359-0286. Citado na página 44.

DANCER, C. Flash sintering of ceramic materials. *Materials Research Express*, IOP Publishing, v. 3, n. 10, p. 102001, 2016. Citado 2 vezes nas páginas 63 and 64.

DARLING, S. Directing the self-assembly of block copolymers. *Progress in Polymer Science*, Elsevier, v. 32, n. 10, p. 1152–1204, 2007. Citado 2 vezes nas páginas 78 and 79.

DIJEN, F. K. van; METSELAAR, R. The chemistry of the carbothermal synthesis of β-sic : reaction mechanism, reaction rate and grain growth. *Journal of the European Ceramic Society*, Elsevier, v. 7, n. 3, p. 177–184, 1991. ISSN 0955-2219. Citado na página 42.

DINESH, S.; KARTHIKEYAN, S.; ARUMUGAM, P. Biosynthesis of silver nanoparticles from glycyrrhiza glabra root extract. *Archives of Applied Science Research*, v. 4, n. 1, p. 178–187, 2012. Citado na página 185.

DIRE, S. et al. Preparation of dense and porous silicon oxycarbide submicrometer-sized spheres using a modified stöber process. *Journal of the American Ceramic Society*, Wiley Online Library, v. 94, n. 11, p. 3819–3824, 2011. Citado na página 64.

DURIF, C. *Elaboration de membranes non-oxydes de type SiBC pour la maîtrise de la contamination dans les réacteurs à eau pressurisée*. Tese (Doutorado) — Université de Montpellier, 2017. Citado na página 177.

EISENBERG, D. et al. The evolution of hierarchical porosity in self-templated nitrogen-doped carbons and its effect on oxygen reduction electrocatalysis. *RSC Advances*, Royal Society of Chemistry, v. 6, n. 84, p. 80398–80407, 2016. Citado na página 68.

ELASSER, A. et al. A comparative evaluation of new silicon carbide diodes and state of the art silicon diodes for power electronic applications. *IEEE Transactions on Industry Applications*, v. 39, n. 4, p. 915–921, July 2003. ISSN 0093-9994. Citado na página 39.

ELYASSI, B.; SAHIMI, M.; TSOTSIS, T. T. Silicon carbide membranes for gas separation applications". *Journal of Membrane Science*, v. 288, n. 1, p. 290–297, 2007. ISSN 0376-7388. Citado na página 41.

FAN, J.; CHU, P. K. Group iv nanoparticles: Synthesis, properties, and biological applications. *Small*, v. 6, n. 19, p. 2080–2098, 2010. Citado na página 39.

FANG, Y. et al. Synthesis, characterization, and pyrolytic conversion of a novel liquid polycarbosilane. *Journal of the American Ceramic Society*, v. 91, n. 10, p. 3298–3302, 2008. Citado na página 142.

FARD, A. K. et al. Inorganic membranes: Preparation and application for water treatment and desalination. *Materials*, Multidisciplinary Digital Publishing Institute, v. 11, n. 1, p. 74, 2018. Citado na página 41.

FIOCCO, L. *Università degli Studi di Padova Silicate ceramics from preceramic polymers and fillers.* Tese (Doutorado), 2016. Citado 2 vezes nas páginas 48 and 58.

FORELAND, S. *Improved retrospective exposure assessment of dust and selected dust constituents in the Norwegian silicon carbide industry from 1913 to 2005.* Tese (Doutorado) — University of Oslo, Department of Chemistry, Faculty of Mathematics and Natural Sciences, 2012. Citado na página 42.

FRAGA, M. et al. Carbeto de silicio como material base para sensores mems de uso aeroespacial: uma visãoo geral. *Matéria (Rio de Janeiro)*, Rede Latino-Americana de Materiais, 2014. Citado na página 169.

FROEHLING, P. E. Synthesis and properties of a new, branched polyhydridocarbosilane as a precursor for silicon carbide. *Journal of Inorganic and Organometallic Polymers*, v. 3, n. 3, p. 251–258, Sep 1993. ISSN 1572-8870. Disponível em: <https://doi.org/10.1007/BF00683932>. Citado na página 49.

GAO, Y. *Nanodomain Structure and Energetics of Carbon Rich SiCN and SiBCN Polymer-Derived Ceramics.* Tese (Doutorado) — Technische Universität Darmstadt, 2014. Citado 2 vezes nas páginas 57 and 58.

GARCIA, C. B. et al. Synthesis and characterization of block copolymer/ceramic precursor nanocomposites based on a polysilazane. *Journal of Polymer Science Part B: Polymer Physics*, Wiley Online Library, v. 41, n. 24, p. 3346–3350, 2003. Citado na página 76.

GERVAIS, C. et al. Solid-state nmr investigations of the polymer route to sibcn ceramics. *Canadian journal of chemistry*, NRC Research Press, v. 81, n. 11, p. 1359–1369, 2003. Citado na página 136.

GIBSON, L. J.; ASHBY, M. F. *Cellular solids: structure and properties.* [S.l.]: Cambridge university press, 1999. Citado na página 182.

GOELA, J. S.; TAYLOR, R. L. Monolithic material fabrication by chemical vapour deposition. *Journal of Materials Science*, v. 23, n. 12, p. 4331–4339, Dec 1988. ISSN 1573-4803. Disponível em: <https://doi.org/10.1007/BF00551927>. Citado na página 44.

GOTTARDO, L. et al. Chemistry, structure and processability of boron-modified polysilazanes as tailored precursors of ceramic fibers. *Journal of Materials Chemistry*, Royal Society of Chemistry, v. 22, n. 16, p. 7739–7750, 2012. Citado na página 135.

GRASSO, S. et al. Flash spark plasma sintering (fsps) of α and β sic. *Journal of the American Ceramic Society*, Wiley Online Library, v. 99, n. 5, p. 1534–1543, 2016. Citado 2 vezes nas páginas 62 and 63.

GREIL, P. Active-filler-controlled pyrolysis of preceramic polymers. *Journal of the American Ceramic Society*, v. 78, n. 4, p. 835–848, 1995. Disponível em: <https://onlinelibrary.wiley.com/doi/abs/10.1111/j.1151-2916.1995.tb08404.x>. Citado 3 vezes nas páginas 59, 60, and 66.

GREIL, P. Polymer Derived Engineering Ceramics. *Advanced Engineering Materials*, v. 2, n. 6, p. 339–348, jun 2000. ISSN 1438-1656. Citado na página 58.

GREIL, P.; LIFKA, T.; KAINDL, A. Biomorphic cellular silicon carbide ceramics from wood: I. processing and microstructure. *Journal of the European Ceramic Society*, v. 18, n. 14, p. 1961 – 1973, 1998. ISSN 0955-2219. Citado na página 39.

GU, X.; GUNKEL, I.; RUSSELL, T. P. Pattern transfer using block copolymers. *Phil. Trans. R. Soc. A*, The Royal Society, v. 371, n. 2000, p. 20120306, 2013. Citado na página 77.

GUICHELAAR, P. J. *Acheson Process.* Dordrecht: Springer Netherlands, 1997. 115-129 p. ISBN 978-94-009-0071-4. Citado na página 41.

HAUG, R. et al. Plastic forming of preceramic polymers. *Journal of the European Ceramic Society*, Elsevier, v. 19, n. 1, p. 1–6, 1999. Citado na página 66.

HONG, J. et al. Low-temperature chemical vapour curing using iodine for fabrication of continuous silicon carbide fibres from low-molecular-weight polycarbosilane. *J. Mater. Chem. A*, The Royal Society of Chemistry, v. 2, p. 2781–2793, 2014. Disponível em: <http://dx.doi.org/10.1039/C3TA13727A>. Citado na página 126.

INTERRANTE, L. V. et al. High Yield Polycarbosilane Precursors to Stoichiometric SiC. Synthesis, Pyrolysis and Application. *MRS Proceedings*, v. 346, p. 595, jan 1994. ISSN 1946-4274. Citado 2 vezes nas páginas 49 and 50.

INUI, T.; OTOWA, T. Catalytic combustion of benzene-soot captured on ceramic foam matrix. *Applied catalysis*, Elsevier, v. 14, p. 83–93, 1985. Citado 2 vezes nas páginas 67 and 68.

IRMSCHER, K. Electrical properties of sic: characterisation of bulk crystals and epilayers. *Materials Science and Engineering: B*, Elsevier, v. 91, p. 358–366, 2002. Citado na página 169.

IZHEVSKYI, V. et al. silicon carbide. structure, properties and processing. *Cerâmica*, SciELO Brasil, v. 46, n. 297, p. 4–13, 2000. Citado na página 43.

JANAKIRAMAN, N.; ALDINGER, F. Fabrication and characterization of fully dense si–c–n ceramics from a poly (ureamethylvinyl) silazane precursor. *Journal of the European Ceramic Society*, Elsevier, v. 29, n. 1, p. 163–173, 2009. Citado na página 162.

JANG, B.-K.; SAKKA, Y. Thermophysical properties of porous sic ceramics fabricated by pressureless sintering. *Science and Technology of Advanced Materials*, IOP Publishing, v. 8, n. 7-8, p. 655, 2007. Citado na página 160.

KAMINSKI, N. Reliability challenges for sic power devices in systems and the impact on reliability testing. In: *Silicon Carbide and Related Materials 2017*. [S.l.]: Trans Tech Publications, 2018. (Materials Science Forum, v. 924), p. 805–810. Citado na página 39.

KAMPERMAN, M. et al. Morphology control in block copolymer/polymer derived ceramic precursor nanocomposites. *Macromolecules*, 2008. ISSN 00249297. Citado 2 vezes nas páginas 79 and 80.

KAMPERMAN, M. et al. Ordered mesoporous ceramics stable up to 1500 c from diblock copolymer mesophases. *Journal of the American Chemical Society*, ACS Publications, v. 126, n. 45, p. 14708–14709, 2004. Citado 4 vezes nas páginas 75, 76, 77, and 78.

KAUR, S. *Single-Source-Precursor Synthesis of SiC-Based Ceramic Nanocomposites for Energy-Related Applications*. Tese (Doutorado) — Technische Universität Darmstadt, Darmstadt, July 2016. Citado 6 vezes nas páginas 48, 49, 50, 59, 128, and 144.

KAUR, S.; RIEDEL, R.; IONESCU, E. Pressureless fabrication of dense monolithic SiC ceramics from a polycarbosilane. *Journal of the European Ceramic Society*, Elsevier, v. 34, n. 15, p. 3571–3578, dec 2014. ISSN 0955-2219. Citado 3 vezes nas páginas 51, 128, and 156.

KAUR, S.; RIEDEL, R.; IONESCU, E. Pressureless fabrication of dense monolithic sic ceramics from a polycarbosilane. *Journal of the European Ceramic Society*, v. 34, n. 15, p. 3571 – 3578, 2014. ISSN 0955-2219. Citado 6 vezes nas páginas 57, 58, 59, 60, 65, and 66.

KENNEDY, J. E.; HIGGINBOTHAM, C. L. Synthesis and characterisation of styrene butadiene styrene based grafted copolymers for use in potential biomedical applications. InTech, 2011. Citado 2 vezes nas páginas 190 and 191.

KESSEL, H. U. et al. " fast" field assisted sintering technology-a new process for the production of metallic and ceramic sintering materials. *Hennicke, J. Schmidt, T. Weissgarber, BF Kieback, M. Herrmann, J. Rathel*, 2008. Citado na página 62.

KIM, G.; LIBERA, M. Kinetic constraints on the development of surface microstructure in sbs thin films. *Macromolecules*, ACS Publications, v. 31, n. 8, p. 2670–2672, 1998. Citado na página 191.

KIM, Y.-W. et al. Engineering porosity in silicon carbide ceramics. *Journal of materials science*, Springer, v. 45, n. 10, p. 2808–2815, 2010. Citado na página 67.

KöNIG, K. et al. One-step deposition of ultrafiltration sic membranes on macroporous sic supports. *Journal of Membrane Science*, v. 472, p. 232 – 240, 2014. ISSN 0376-7388. Citado na página 40.

KOTANI, M. et al. Processing of polymer-derived porous sic body using allylhydridopolycarbosilane (ahpcs) and pmma microbeads. *Journal of the Ceramic Society of Japan*, The Ceramic Society of Japan, v. 119, n. 1391, p. 563–569, 2011. Citado na página 184.

KUSUNOSE, T.; SEKINO, T. Increasing resistivity of electrically conductive ceramics by insulating grain boundary phase. *ACS applied materials & interfaces*, ACS Publications, v. 6, n. 4, p. 2759–2763, 2014. Citado na página 169.

LAINE, R. M.; BABONNEAU, F. Preceramic polymer routes to silicon carbide. *Chemistry of Materials*, v. 5, n. 3, p. 260–279, mar 1993. ISSN 0897-4756. Disponível em: <http://pubs.acs.org/doi/abs/10.1021/cm00027a007>. Citado na página 49.

LALE, A. et al. Polymer-derived ceramics with engineered mesoporosity: From design to application in catalysis. *Surface and Coatings Technology*, v. 350, p. 569 – 586, 2018. ISSN

0257-8972. Citado 6 vezes nas páginas 67, 68, 70, 73, 74, and 82.

LEE, A.; ELAM, J. W.; DARLING, S. B. Membrane materials for water purification: design, development, and application. *Environmental Science: Water Research & Technology*, Royal Society of Chemistry, v. 2, n. 1, p. 17–42, 2016. Citado na página 40.

LEE, S. et al. Polymer impregnation and pyrolysis process development for improving thermal conductivity of sicp/sic–pip matrix fabrication. *Fusion Engineering and Design*, Elsevier, v. 83, n. 5-6, p. 713–719, 2008. Citado na página 160.

LI, Y. et al. Microstructure, thermal conductivity, and electrical properties of in situ pressureless densified sic–bn composites. *Journal of the American Ceramic Society*, Wiley Online Library, v. 98, n. 3, p. 879–887, 2015. Citado na página 167.

LIEW, L.-A. et al. Fabrication of sicn mems by photopolymerization of pre-ceramic polymer. *Sensors and Actuators A: Physical*, Elsevier, v. 95, n. 2-3, p. 120–134, 2002. Citado na página 99.

LIJUAN, H. et al. Liquid polycarbosilanes: synthesis and evaluation as precursors for sic ceramic. *Polymer International*, v. 64, n. 8, p. 979–985. Citado na página 126.

MAGNANI, G. et al. Sintering and mechanical properties of β-sic powder obtained from waste tires. *Journal of Advanced Ceramics*, v. 5, n. 1, p. 40–46, Mar 2016. ISSN 2227-8508. Citado na página 42.

MAJOULET, O. et al. Ordered mesoporous silicoboron carbonitride ceramics from boron-modified polysilazanes: Polymer synthesis, processing and properties. *Microporous and Mesoporous Materials*, Elsevier, v. 140, n. 1-3, p. 40–50, 2011. Citado na página 136.

MALENFANT, P. R. et al. Self-assembly of an organic–inorganic block copolymer for nano-ordered ceramics. *Nature nanotechnology*, Nature Publishing Group, v. 2, n. 1, p. 43, 2007. Citado na página 74.

MALIK, R. et al. Grain-growth-induced high electrical conductivity in sic–bn composites. *Ceramics International*, Elsevier, 2018. Citado na página 170.

MANIÈRE, C.; LEE, G.; OLEVSKY, E. A. All-materials-inclusive flash spark plasma sintering. *Scientific reports*, Nature Publishing Group, v. 7, n. 1, p. 15071, 2017. Citado na página 62.

MATSEN, M. W.; BATES, F. S. Origins of complex self-assembly in block copolymers. *Macromolecules*, ACS Publications, v. 29, n. 23, p. 7641–7644, 1996. Citado na página 78.

MCNAUGHTON, A. L. *High Temperature Compression Testing of Monolithic Silicon Carbide (SiC)*. Tese (Doutorado), 2007. Citado na página 59.

MERA, G. et al. Ceramic nanocomposites from tailor-made preceramic polymers. *Nanomaterials*, Multidisciplinary Digital Publishing Institute, v. 5, n. 2, p. 468–540, 2015. Citado 4 vezes nas páginas 58, 59, 74, and 75.

MOGSTAD, K. *A study on commercial SiC-powders sintered by hot pressing*. Tese (Doutorado) — NTNU, 2016. Citado na página 167.

MOREIRA, E.; INNOCENTINI, M.; COURY, J. Permeability of ceramic foams to compressible and incompressible flow. *Journal of the European Ceramic Society*, Elsevier, v. 24, n. 10-11, p. 3209–3218, 2004. Citado 2 vezes nas páginas 10 and 37.

MORI, Y.; SUGAHARA, Y. Pyrolytic organic-to-inorganic conversion of precursors into aln-a review. *Journal of the*

Ceramic Society of Japan, v. 114, n. 1330, p. 461–472, 2006. Citado na página 48.

MUHE, H. et al. Synthesis and properties of liquid polycarbosilanes with hyperbranched structures. *Journal of Applied Polymer Science*, v. 113, n. 3, p. 1611–1618, 2009. Disponível em: <https://onlinelibrary.wiley.com/doi/abs/10.1002/app.30071>. Citado na página 126.

MUNIR, Z.; ANSELMI-TAMBURINI, U.; OHYANAGI, M. The effect of electric field and pressure on the synthesis and consolidation of materials: A review of the spark plasma sintering method. *Journal of Materials Science*, Springer, v. 41, n. 3, p. 763–777, 2006. Citado na página 62.

NAKANO, H. et al. Microstructural characterization of high-thermal-conductivity sic ceramics. *Journal of the European Ceramic Society*, Elsevier, v. 24, n. 14, p. 3685–3690, 2004. Citado na página 160.

NETTLESHIP, I. Applications of porous ceramics. In: TRANS TECH PUBL. *Key Engineering Materials*. [S.l.], 1996. v. 122, p. 305–324. Citado 2 vezes nas páginas 67 and 68.

NIU, B. et al. Ultra-fast densification of boron carbide by flash spark plasma sintering. *Scripta Materialia*, Elsevier, v. 116, p. 127–130, 2016. Citado na página 62.

OLEVSKY, E. A.; ROLFING, S. M.; MAXIMENKO, A. L. Flash (ultra-rapid) spark-plasma sintering of silicon carbide. *Scientific reports*, Nature Publishing Group, v. 6, p. 33408, 2016. Citado na página 62.

OLIVER, W. C.; PHARR, G. M. An improved technique for determining hardness and elastic modulus using load and displacement sensing indentation experiments. *Journal of materials research*, Cambridge University Press, v. 7, n. 6, p. 1564–1583, 1992. Citado na página 116.

ORTEGA, F. et al. Alternative gelling agents for the gelcasting of ceramic foams. *Journal of the European Ceramic Society*, Elsevier, v. 23, n. 1, p. 75–80, 2003. Citado 2 vezes nas páginas 10 and 37.

PARCIANELLO, G. Advanced ceramics from preceramic polymers and fillers. 2012. Citado na página 47.

PARK, K.-H.; SUNG, I.-K.; KIM, D.-P. A facile route to prepare high surface area mesoporous sic from sio2 sphere templates. *J. Mater. Chem.*, The Royal Society of Chemistry, v. 14, p. 3436–3439, 2004. Disponível em: <http://dx.doi.org/10.1039/B410841H>. Citado na página 72.

PARKER, W. et al. Flash method of determining thermal diffusivity, heat capacity, and thermal conductivity. *Journal of applied physics*, AIP, v. 32, n. 9, p. 1679–1684, 1961. Citado na página 117.

PUERTA, A. R. et al. Synthesis and ceramic conversion reactions of 9-BBN-modified allylhydridopolycarbosilane: A new single-source precursor to boron-modified silicon carbide. *Chemistry of Materials*, 2003. ISSN 08974756. Citado 7 vezes nas páginas 52, 53, 54, 61, 137, 138, and 150.

RAHMAN, A. et al. Mechanical characterization of fine grained silicon carbide consolidated using polymer pyrolysis and spark plasma sintering. *Ceramics International*, Elsevier, v. 40, n. 8, p. 12081–12091, 2014. Citado na página 62.

RAJ, R.; RIEDEL, R.; SORARU, G. D. Introduction to the special topical issue on ultrahigh-temperature polymer-derived ceramics. *Journal of the American Ceramic Society*, v. 84, n. 10, p. 2158–2159, 2001. Citado na página 45.

RHEE, S. Porosity—thermal conductivity correlations for ceramic materials. *Materials Science and Engineering*, Elsevier, v. 20, p. 89–93, 1975. Citado na página 188.

RIEDEL, R. et al. Synthesis of dense silicon-based ceramics at low temperatures. *Nature*, Nature Publishing Group, v. 355, n. 6362, p. 714, 1992. Citado na página 64.

ROMAN-MANSO, B. et al. Enhanced electrical conductivity of silicon carbide ceramics by addition of graphene nanoplatelets. *Journal of the European Ceramic Society*, Elsevier, v. 35, n. 10, p. 2723–2731, 2015. Citado na página 169.

ROSENBLOOM, A. et al. Nanoporous sic: A candidate semi-permeable material for biomedical applications. *Biomedical microdevices*, Springer, v. 6, n. 4, p. 261–267, 2004. Citado na página 39.

RUH, R.; BENTSEN, L. D.; HASSELMAN, D. Thermal diffusivity anisotropy of sic/bn composites. *Journal of the American Ceramic Society*, Wiley Online Library, v. 67, n. 5, p. c83–c84, 1984. Citado na página 170.

SAHU, S. et al. Formation of boron nitride thin films on β-si3n4 whiskers and α-sic platelets by dip-coating. *Journal of the European Ceramic Society*, Elsevier, v. 18, n. 8, p. 1037–1043, 1998. Citado na página 148.

SALAZAR, J. G. de et al. Compression strength and wear resistance of ceramic foams–polymer composites. *Materials Letters*, Elsevier, v. 60, n. 13-14, p. 1687–1692, 2006. Citado 4 vezes nas páginas 10, 37, 67, and 68.

SARKAR, S. The fabrication of polymer-derived sicn/sibcn ceramic nanostructures and investigation of their structure-property relationship. 2010. Citado 2 vezes nas páginas 48 and 49.

SCARLETE, M. et al. Poly (methylsilane) and poly (hydrazinomethylsilane) as precursors for silicon-containing ceramics. In: *Applications of Organometallic Chemistry in the Preparation and Processing of Advanced Materials*. [S.l.]: Springer, 1995. p. 125–140. Citado na página 148.

SCHMIDT, M. et al. Molecular-Level Processing of Si-
(B)-C Materials with Tailored Nano/Microstructures.
Chemistry - A European Journal, v. 23, n. 67, p.
17103–17117, dec 2017. ISSN 09476539. Disponível em:
<http://doi.wiley.com/10.1002/chem.201703674>.   Citado 18
vezes nas páginas 10, 36, 52, 54, 56, 59, 60, 64, 65, 97, 126, 134,
135, 136, 137, 140, 144, and 153.

SEA, B.-K. et al. Separation of hydrogen from steam using a
sic-based membrane formed by chemical vapor deposition of
triisopropylsilane. *Journal of Membrane Science*, v. 146, n. 1, p.
73 – 82, 1998. ISSN 0376-7388.   Citado na página 40.

SHAH, S. R.; RAJ, R. Mechanical properties of a fully dense
polymer derived ceramic made by a novel pressure casting
process. *Acta Materialia*, v. 50, n. 16, p. 4093 – 4103, 2002.
ISSN 1359-6454.   Citado na página 64.

SHE, J.; OHJI, T.; DENG, Z.-Y. Thermal shock behavior
of porous silicon carbide ceramics. *Journal of the American
Ceramic Society*, Wiley Online Library, v. 85, n. 8, p. 2125–2127,
2002.   Citado 2 vezes nas páginas 10 and 37.

SHI, Y.; WAN, Y.; ZHAO, D. Ordered mesoporous non-oxide
materials. *Chemical Society Reviews*, Royal Society of
Chemistry, v. 40, n. 7, p. 3854–3878, 2011.   Citado 3 vezes nas
páginas 74, 75, and 76.

SHIBUYA, M.; TAKAHASHI, T.; KOYAMA, K. Microcellular
ceramics by using silicone preceramic polymer and pmma
polymer sacrificial microbeads. *Composites Science and
Technology*, v. 67, n. 1, p. 119–124, 2007.   Citado na página 183.

SMART, T. et al. Block copolymer nanostructures. *Nano Today*,
Elsevier, v. 3, n. 3-4, p. 38–46, 2008.   Citado na página 78.

SOMIYA, S.; INOMATA, Y. *Silicon Carbide Ceramics—1:
Fundamental and Solid Reaction*. [S.l.]: Springer Netherlands,
2012. (Ceramic research and development in Japan). ISBN
9789401138420.   Citado na página 41.

SPEARING, S. Materials issues in microelectromechanical systems (mems). *Acta materialia*, Elsevier, v. 48, n. 1, p. 179–196, 2000. Citado na página 169.

STOBIERSKI, L.; GUBERNAT, A. Sintering of silicon carbide ii. effect of boron. *Ceramics international*, Elsevier, v. 29, n. 4, p. 355–361, 2003. Citado na página 166.

SUGIMOTO, M. et al. Reaction mechanisms of silicon carbide fiber synthesis by heat treatment of polycarbosilane fibers cured by radiation: I, evolved gas analysis. *Journal of the American Ceramic Society*, Wiley Online Library, v. 78, n. 4, p. 1013–1017, 1995. Citado na página 48.

SUN, L. et al. Green synthesis of silver nanoparticles using wolfberry fruits extract and their photocatalytic performance. v. 292, n. 1, p. 012017, 2018. Citado na página 173.

SUNG, I.-K. et al. Fabrication of macroporous sic from templated preceramic polymers. *Chemical Communications*, Royal Society of Chemistry, n. 14, p. 1480–1481, 2002. Citado 2 vezes nas páginas 70 and 71.

SWEET, M.; SINGLETON, I. Silver nanoparticles: a microbial perspective. In: *Advances in applied microbiology.* [S.l.]: Elsevier, 2011. v. 77, p. 115–133. Citado na página 101.

VAKIFAHMETOGLU, C. et al. Highly porous macro-and micro-cellular ceramics from a polysilazane precursor. *Ceramics International*, Elsevier, v. 35, n. 8, p. 3281–3290, 2009. Citado 3 vezes nas páginas 84, 85, and 179.

VAKIFAHMETOGLU, C.; ZEYDANLI, D.; COLOMBO, P. Porous polymer derived ceramics. *Materials Science and Engineering: R: Reports*, v. 106, p. 1 – 30, 2016. ISSN 0927-796X. Citado 4 vezes nas páginas 67, 70, 82, and 83.

VIARD, A. et al. Molecular Chemistry and Engineering of Boron-Modified Polyorganosilazanes as New Processable and Functional SiBCN Precursors. *Chemistry - A European Journal*,

v. 23, n. 38, p. 9076–9090, jul 2017. ISSN 09476539. Disponível em: <http://doi.wiley.com/10.1002/chem.201700623>. Citado 2 vezes nas páginas 51 and 52.

WAN, J. et al. Nanostructured non-oxide ceramics templated via block copolymer self-assembly. *Chemistry of materials*, ACS Publications, v. 17, n. 23, p. 5613–5617, 2005. Citado 2 vezes nas páginas 81 and 82.

WAN, J.; GASCH, M. J.; MUKHERJEE, A. K. Effect of ammonia treatment on the crystallization of amorphous silicon–carbon–nitrogen ceramics derived from polymer precursor pyrolysis. *Journal of the American Ceramic Society*, Wiley Online Library, v. 85, n. 3, p. 554–564, 2002. Citado 2 vezes nas páginas 147 and 148.

WEI, Y. et al. Design and synthesis of 3d ordered macroporous ceo2-supported pt@ ceo2-δ core–shell nanoparticle materials for enhanced catalytic activity of soot oxidation. *Small*, Wiley Online Library, v. 9, n. 23, p. 3957–3963, 2013. Citado 2 vezes nas páginas 101 and 103.

WHITESIDES, G. M.; GRZYBOWSKI, B. Self-assembly at all scales. *Science*, American Association for the Advancement of Science, v. 295, n. 5564, p. 2418–2421, 2002. Citado na página 73.

WHITMARSH, C. K.; INTERRANTE, L. V. Synthesis and structure of a highly branched polycarbosilane derived from (chloromethyl)trichlorosilane. *Organometallics*, American Chemical Society, v. 10, n. 5, p. 1336–1344, may 1991. ISSN 0276-7333. Disponível em: <http://pubs.acs.org/doi/abs/10.1021/om00051a025>. Citado na página 50.

WIELIGOR, M.; WANG, Y.; ZERDA, T. Raman spectra of silicon carbide small particles and nanowires. *Journal of Physics: Condensed Matter*, IOP Publishing, v. 17, n. 15, p. 2387, 2005. Citado na página 145.

WU, L. et al. Liquid phase sintering of silicon carbide with aln-re2o3 additives. InTech, 2011. Citado na página 43.

YAKIMOVA, R. et al. Surface functionalization and biomedical applications based on sic. *Journal of Physics D: Applied Physics*, v. 40, n. 20, p. 6435, 2007. Disponível em: <http://stacks.iop.org/0022-3727/40/i=20/a=S20>. Citado na página 39.

YANG, Z.; ZHANG, Y.; SCHNEPP, Z. Soft and hard templating of graphitic carbon nitride. *Journal of Materials Chemistry A*, Royal Society of Chemistry, v. 3, n. 27, p. 14081–14092, 2015. Citado 2 vezes nas páginas 70 and 71.

YOON, T.-H.; HONG, L.-Y.; KIM, D.-P. Fabrication of sic-based ceramic microstructures from preceramic polymers with sacrificial templates and softlithography techniques. In: *Lithography.* [S.l.]: InTech, 2010. Citado 2 vezes nas páginas 72 and 73.

YU, J. et al. A novel highly porous ceramic foam with efficient thermal insulation and high temperature resistance properties fabricated by gel-casting process. In: IOP PUBLISHING. *IOP Conference Series: Earth and Environmental Science.* [S.l.], 2018. v. 108, n. 2, p. 022043. Citado na página 188.

YU, Z. et al. Modification of a liquid polycarbosilane with 9-BBN as a high-ceramic-yield precursor for SiC. *Reactive and Functional Polymers*, Elsevier, v. 70, n. 6, p. 334–339, jun 2010. ISSN 1381-5148. Citado 5 vezes nas páginas 52, 59, 126, 137, and 139.

YU, Z. et al. Single-source-precursor synthesis of high temperature stable sic/c/fe nanocomposites from a processable hyperbranched polyferrocenylcarbosilane with high ceramic yield. *J. Mater. Chem. C*, The Royal Society of Chemistry, v. 2, p. 1057–1067, 2014. Disponível em: <http://dx.doi.org/10.1039/C3TC32088J>. Citado na página 126.

ZAPATA-SOLVAS, E. et al. Ultra-fast and energy-efficient sintering of ceramics by electric current concentration. *Scientific reports*, Nature Publishing Group, v. 5, p. 8513, 2015. Citado 2 vezes nas páginas 62 and 64.

ZETTERLING, C. Present and future applications of silicon carbide devices and circuits. In: *Proceedings of the IEEE 2012 Custom Integrated Circuits Conference*. [S.l.: s.n.], 2012. p. 1–8. ISSN 2152-3630. Citado na página 39.

ZETTERLING, C.; ENGINEERS, I. of E. *Process Technology for Silicon Carbide Devices*. [S.l.]: INSPEC, 2002. (EMIS processing series). ISBN 9780852969984. Citado na página 41.

ZEUNER, B. et al. Immobilization of alcohol dehydrogenase on ceramic silicon carbide membranes for enzymatic ch3oh production. *Journal of Chemical Technology & Biotechnology*, v. 93, n. 10, p. 2952–2961, 2018. Disponível em: <https://onlinelibrary.wiley.com/doi/abs/10.1002/jctb.5653>. Citado na página 39.

ZHONG, X. et al. Accelerating the crosslinking process of hyperbranched polycarbosilane by UV irradiation. *Journal of the European Ceramic Society*, Elsevier Ltd, v. 37, n. 10, p. 3263–3270, 2017. ISSN 1873619X. Citado 2 vezes nas páginas 49 and 59.

ZHU, X.; JIANG, D.; TAN, S. Preparation of silicon carbide reticulated porous ceramics. *Materials Science and Engineering: A*, Elsevier, v. 323, n. 1-2, p. 232–238, 2002. Citado 2 vezes nas páginas 67 and 68.

ZSIRAI, T. et al. Ceramic membrane filtration of produced water: Impact of membrane module. *Separation and Purification Technology*, v. 165, p. 214 – 221, 2016. ISSN 1383-5866. Citado na página 40.

ZUNJARRAO, S. C. *Polymer Derived Ceramics: Processing –Structure–Property Relationships*. 142 p. Tese (Doutorado), 2008. Citado na página 44.

ZUNJARRAO, S. C.; RAHMAN, A.; SINGH, R. P. Characterization of the evolution and properties of silicon carbide derived from a preceramic polymer precursor. *Journal of the American Ceramic Society*, Wiley Online Library, v. 96, n. 6, p. 1869–1876, 2013. Citado na página 158.

ZUNJARRAO, S. C.; SINGH, A. K.; SINGH, R. P. Structure-Property Relationships in Polymer Derived Amorphous/Nano-Crystalline Silicon Carbide for Nuclear Applications. In: *Volume 3: Structural Integrity; Nuclear Engineering Advances; Next Generation Systems; Near Term Deployment and Promotion of Nuclear Energy.* [S.l.]: ASME, 2006. v. 2006, p. 419–425. ISBN 0-7918-4244-4. Citado na página 51.